ANALYSIS OF STRESSES AND DEFLECTIONS IN FRAME SUPPORTED TENTS

Paul J. Remington, et al

Bolt Beranek and Newman, Incorporated

Prepared for:

Army Natick Laboratories

April 1974

AD

TECHNICAL REPORT
75-31

ANALYSIS OF STRESSES AND DEFLECTIONS IN FRAME SUPPORTED TENTS

by
Paul J. Remington
John C. O'Callahan
and
Richard Madden

Bolt, Beranek and Newman Inc.
50 Moulton Street
Cambridge, Massachusetts 02138

Contract No. DAAG17-73-C-0107

April 1974

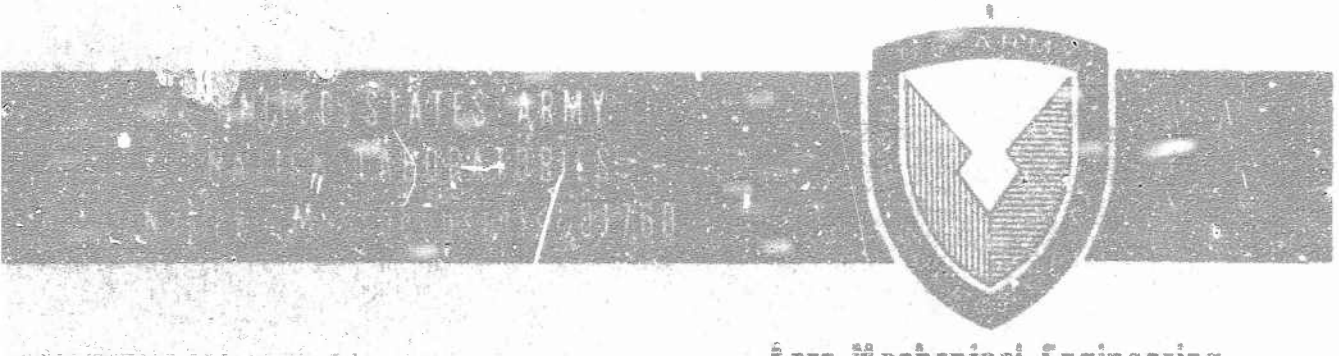

Aero-Mechanical Engineering
Laboratory

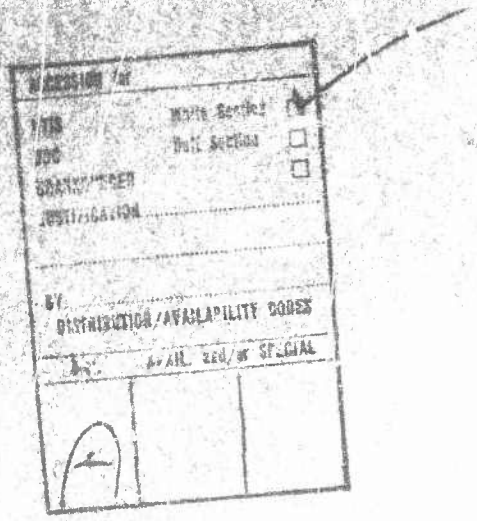

Approved for public release; distribution unlimited.

Citation of trade names in this report does not constitute an official indorsement or approval of the use of such items.

Destroy this report when no longer needed. Do not return it to the originator.

ANALYSIS OF STRESSES AND DEFLECTIONS IN FRAME SUPPORTED TENTS

by

Paul J. Remington
John C. O'Callahan
Richard Madden

Bolt Beranek and Newman Inc.
50 Moulton Street
Cambridge, Massachusetts 02138

Contract No. DAAG17-73-C-0107

April 1974

Submitted to:

U. S. Army Natick Laboratories
Natick, Massachusetts 01760

FOREWORD

This report was prepared by Bolt Beranek and Newman Inc. under U.S. Army Contract No. DAAG17-73-C-0107. The work was carried out under the direction of Drs. Constantin J. Monego and Earl Steeves of the U.S. Army Natick Laboratories acting as project engineers.

TABLE OF CONTENTS

TABLE OF CONTENTS *(Cont'd.)*

LIST OF FIGURES

LIST OF FIGURES *(Cont'd.)*

LIST OF FIGURES *(Cont'd.)*

LIST OF FIGURES *(Cont'd.)*

ABSTRACT

A finite element computer code has been developed for predicting the stress and deflection in frame-supported tents under static load. The code can accept geometric nonlinearities due to large deflections and nonlinear biaxial stress/strain fabric properties. The predictions of the computer code are validated by tests performed on two 1/8-scale model tents that approximately model two existing Army tents, the *tent maintenance shelter* and the *Fritche shelter*. The 2.6-oz cotton typewriter ribbon cloth used in the models was tested on a biaxial testing machine to obtain its biaxial stress/strain behavior for input to the computer code. Preliminary comparison of computer predictions and measurements from tests on the deflection and stress in a fabric strip, on the deflections of the tent frames under a point load, and on the deflections and stress in a rectangular fabric membrane in a rigid frame demonstrated the validity of the code predictions. These comparisons also pointed out the need to include joint efficiencies in modeling the frame. Comparison of computer predictions and measurements of the deflections in the tent frame models showed the computer predictions to agree adequately with measurements.

SECURITY CLASSIFICATION OF THIS PAGE (When Data Entered)

AD/A002 072

REPORT DOCUMENTATION PAGE

READ INSTRUCTIONS BEFORE COMPLETING FORM

1. REPORT NUMBER: TR 75-31	2. GOVT ACCESSION NO.
3. RECIPIENT'S CATALOG NUMBER	
4. TITLE (and Subtitle): Analysis of Stresses and Deflections in Frame Supported Tents	5. TYPE OF REPORT & PERIOD COVERED: Final
6. PERFORMING ORG. REPORT NUMBER: BBN Report No. 2802	
7. AUTHOR(s): Paul J. Remington, John C. O'Callahan, Richard Madden	8. CONTRACT OR GRANT NUMBER(s): DAAG17-73-C-01701
9. PERFORMING ORGANIZATION NAME AND ADDRESS: Bolt Beranek and Newman Inc. 50 Moulton St. Cambridge, Mass. 02138	10. PROGRAM ELEMENT, PROJECT, TASK AREA & WORK UNIT NUMBERS: 6.2 Exploratory Dev Project AE 98 Task 16AE
11. CONTROLLING OFFICE NAME AND ADDRESS: Aero-Mechanical Engineering Laboratory (AMEL) Engineering Science Division (ESD) STSNL-UE US Army Natick Laboratories, Natick, MA 01760	12. REPORT DATE: 22 April 1974
	13. NUMBER OF PAGES: ~~117~~ 131
14. MONITORING AGENCY NAME & ADDRESS (if different from Controlling Office): NA	15. SECURITY CLASS. (of this report): Unclassified
	15a. DECLASSIFICATION/DOWNGRADING SCHEDULE

16. DISTRIBUTION STATEMENT (of this Report)

Approved for public release; distribution unlimited.

17. DISTRIBUTION STATEMENT (of the abstract entered in Block 20, if different from Report)

Same

18. SUPPLEMENTARY NOTES: To be released by the Technical Information Service of the Department of Commerce

19. KEY WORDS (Continue on reverse side if necessary and identify by block number)

Tents
Frame Supported Tents
Fabric
Membranes
Biaxial Fabric Testing

20. ABSTRACT (Continue on reverse side if necessary and identify by block number)

A finite element computer code has been developed for predicting the stresses and deflections in frame-supported tents under static load. The code can accept geometric nonlinearities due to large deflections and nonlinear biaxial stress/strain fabric properties. The predictions of the computer code are validated by tests performed on two 1/8 scale model tents that approximately model two existing Army tents, the tent maintenance shelter and the Fritche shelter. The 2.6-oz cotton typewriter ribbon cloth used in the models was tested on a biaxial test-

DD FORM 1 JAN 73 1473 EDITION OF 1 NOV 65 IS OBSOLETE

Unclassified

SECURITY CLASSIFICATION OF THIS PAGE (When Data Entered)

(131)

20. cont'd

ing machine to obtain its biaxial stress/strain behavior for input to the computer code. Preliminary comparison of computer predictions and measurements from tests on the deflection and stress in a fabric strip, on the deflections of the tent frames under a point load, and on the deflections and stress in a rectangular fabric membrane in a rigid frame demonstrated the validity of the code predictions. These comparisons also pointed out the need to include joint efficiencies in modeling the frame. Comparison of computer predictions and measurements of the deflections in the tent frame models showed the computer predictions to agree adequately with measurements.

TABLE FOR CONVERSION FROM BRITISH UNITS TO SI UNITS

Quantity	British Units	SI Units	To Convert British Units to SI Units Multiply By
Mass	pounds mass	Kilograms	0.455
Force	pounds force	Newtons	4.45
Length	inch	meter	0.0254
	foot	meter	0.305
	yard	meter	0.91
Area	square inch	square meters	$6.45 \cdot 10^{-4}$
	square foot	square meters	0.093
Volume	cubic inches	cubic meters	$1.64 \cdot 10^{-5}$
	cubic feet	cubic meters	0.0283
Density	pounds per cubic inch	kilograms per cubic meter	$2.77 \cdot 10^{4}$
	ounces	grams per square meter	34
Tension	pounds per inch	newtons per meter	176
Moment of Inertia	$(\text{inches})^4$	$(\text{meters})^4$	$4.1 \cdot 10^{-7}$
Modulus of Elasticity	pounds per square inch	newtons per square meter	$6.9 \cdot 10^{3}$
Loading	pounds per square foot	newtons per square meter	48

1. INTRODUCTION

One type of shelter extensively used in Army field operations is the frame-supported tent, essentially a metal frame to which is attached one or more layers of fabric. This type of shelter has many attractive features. It is light, easily transportable, and provides a reasonably secure shelter from the weather. Although these tent structures are fairly simple to construct and erect, a good understanding of their static response to snow loads is lacking. Clearly, if lighter, more efficient, structurally sound, frame-supported tents are to be designed, such an understanding must be developed.

The program described in this report has concentrated on the development of a computer code for predicting the stresses and deflections in frame-supported tents under dead weight loads and the verification of that code through comparison of the predictions with measurements on model frame-supported tents. The resulting computer code is a finite element code capable of predicting stresses and deflections in both tent fabric and frame, including the effect of any geometric nonlinearities due to large deflections. The code will accept any configuration for the frame which can be modeled as a number of simple beams and will also accept fairly general nonlinear stress/strain properties for the fabric. A detailed description of the code is given in Sec. 2.

Once the computer code was developed, it was necessary to verify its predictions. To this end, two model 1/8-scale tent frames were constructed and a model fabric was selected so as to simulate approximately the *tent maintenance shelter*, a slant roof tent, and the *Fritche shelter*, an arch roof tent, whose geometries are typical of Army frame-supported tents. It should be emphasized that these model tents were not *exact* scale models of the above-mentioned Army tents. All that was required was to show that the computer code could adequately predict the stresses and deflections in a frame-supported tent. For this reason, any frame-fabric model would have been sufficient. It was felt, though, that the models should roughly scale to existing full-scale tents, so that once it has been demonstrated that the code can deal with a small-model tent, the user will have confidence that the code can also deal with the full-scale tent. Therefore, selection of the model fabric, scaling of the applied loads, and design of the frames were based on the crude scaling laws developed in Sec. 3. These laws result in (1) comparable strains in the model tent fabric and the full-scale tent

fabric and (2) deflections in the fabric of the model in the same proportion to the model frame deflections as in the full-scale.

Section 4 describes the screening process for selecting a model fabric, the ensuing biaxial stress/strain test on the chosen fabric, and the adaptation of a fabric force sensor for measuring the low level loads in the modes. The tent frame design is described in Sec. 5.

Before testing on the model was begun, it was felt that a number of simpler tests would be useful to point up any difficulties in predicting stress or deflections in the fabric or the frame of the model tents. Section 6 compares computer predictions with results from three of these tests: the stresses and deflections in a thin fabric strip, the deflections in the model tent frames under a point load, and the stresses and deflections in a rectangular piece of fabric in a rigid frame.

The final comparison of computer predictions and measurement of deflection in the two model tents is made in Sec. 7. Section 8 presents the conclusions.

2. COMPUTER PROGRAM

In this section a very brief description is given of the computer code developed during this program. No attempt is made in this report to provide detailed information on the code. For such information the reader is referred to the User's Manual.*

2.1 Program Capabilities

The computer code developed to solve problems involving nonlinear geometry and material properties has been named NONFESA (Nonlinear Finite Element Structural Analysis). The code was designed to determine deflections and stresses in frame-supported tents by discretizing the continuous frame and fabric into "finite elements" such that straight beam elements represent the frame and flat triangular membrane elements may be assembled for the fabric.

The beam element is the standard, straight, finite element beam with the ability to include shear deformations. It is considered linear in the code; i.e., it is assumed that structural deformations are small and can be modeled by linear beam theory. Therefore, the stiffness and strain-displacement matrices for the beam elements need be calculated only once.

Because the membrane elements involve large displacements, the program must calculate the nonlinear stiffness matrix by breaking up the full load into small increments or steps and by using an iterative scheme to update the displacements and stresses. The material properties may be linear (stress proportional to strain) or nonlinear (treated as piecewise linear assuming incremental stress proportional to incremental strain).

Loads on the membrane elements may be in the form of local surface tractions, pressure, gravity, or point-concentrated loads. As described above, for dealing with nonlinear problems, the load is divided into small increments, or steps.

---

*O'Callahan, J.C., "NONFESA – Nonlinear Finite Element Structural Analysis Program for the Analysis of Stresses and Deflections in Frame-Supported Tents," BBN Report No. 2803, June 1974.

2.2 Program Organization

The program, a derivative of SAP II,* is very versatile. It is designed such that all subroutines effectively use the common storage arrays without even knowing a fixed dimension for the arrays. This feature allows the user easy assembly of a very large or a very small problem.

The flow of the present program can best be described by the chart given in Fig. 2.1. The program has the potential of mixing many different elements, although, at present, only the beam and membrane element are available.

The solution scheme used in NONFESA is accomplished by a direct reduction technique – i.e., a Gaussian elimination. The algorithm allows for an in-core as well as an out-of-core solution of the linear algebraic equations. The decision about which method to use is made internally and is particularly affected by the user allocation of common block storage. The larger the allocated space, the bigger the block of equations that will be in-core for solution. Input/output processing will be minimized if the blocks are kept as large as possible.

2.3 Program Input and Output

This section contains a brief description of the input data required to run the program and the type of output the program generates. Further details of the input and output may be found in the User's Manual.

2.3.1 Input requirements

The program requires that the user input information which will set maximum parameter conditions, such as number of nodal points, element types, load steps, and convergence criteria. In addition, one must input the fraction of the total load used in the incremental solution technique.

The geometry of the structure is modeled with nodal point cards. These cards also contain pertinent information about the equilibrium equations to be solved. Any zero displacement boundary conditions are set by these cards. Following the nodal cards, sets of element cards are input

---

*Wilson, E.L., "SOLID SAP – A Static Analysis Program for Three-Dimensional Solid Structures," SESM Report 71-19, Dept. of Civil Engineering, Univ. of California, Berkeley, 1971.

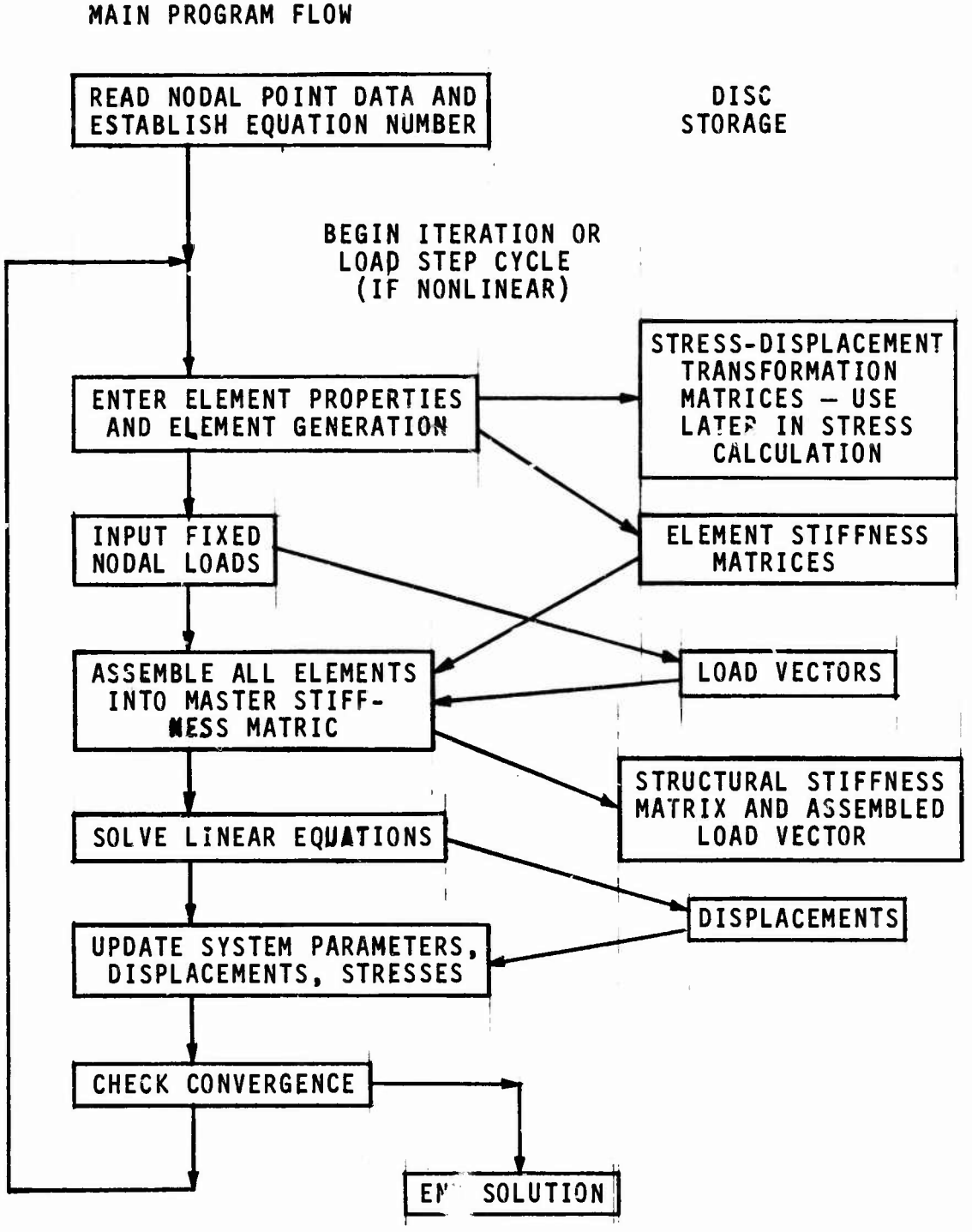

FIG. 2.1. FLOW CHART OF PROGRAM.

to define the element connectivity to the nodal structure and material properties. Presently, the program contains two element types: the linear beam and the nonlinear membrane. From these cards, the element and such properties as stiffness and stress-displacement matrices are calculated and written to disc storage.

The last type of input required is the loading function. If point loads are used in the solution, then the list of cards containing the nodal forces are input to the program and a load vector is generated and placed in disc storage. If distributed loads are used on the elements, the information is calculated and stored with the element information. When assembly occurs, all load vectors are added together.

2.3.2 Output descriptions

The output data calculated in the program is printed for each cycle in the load step.* Information such as incremental nodal displacements and relations, beam and fabric stresses, beam forces and moments, accumulated nodal displacements and rotations, and new nodal global coordinates may be selected in the cycle printout.

The first page contains the start of cycle information: the cycle number, load step number, and load fraction. The second section is a table of incremental nodal displacements and rotations calculated during the given cycle. This table contains all nodes and possible degrees of freedom. If a degree of freedom is fixed or deleted from the solution, a zero is printed.

Next, beam stresses are printed in tabular form. They are listed by element with reference to both ends of the beam. Principal bending and average shear stresses relative to the local axes of the beam are printed. The next section is a table containing the resulting beam forces and moments. This table, which is similar in form to the beam stress table, contains the internal forces and moments at each end of the beam.

The membrane stress resultants are printed next by element number. The resultants are described relative to

---

*As described above, the total applied load is divided into small increments called steps. The iterations within each step are called cycles.

the local axes of the membrane. A table containing the accumulated (all previous steps plus the given cycle) incremental nodal displacements and rotations is then printed.

The new global nodal coordinates of the structure (including deflections) are printed next. This table is helpful when a deformed configuration of the structure is desired.

3. SCALING LAWS FOR FRAME-SUPPORTED TENTS

The primary objective of this study is the development of a computer program to predict deflections and stresses in frame-supported tents under static loads. The purpose of the model tent test program is simply to verify the validity of the computer program. Strictly speaking, then, accurate scaling of the model tents with full-scale tents is not necessary, because agreement of the computer program and test results is all that is required to verify the computer model. In fact, though, we have approximately scaled the tent models with real tents so as to obtain realistic fabric strain and frame deflections in proper proportion with fabric deflections.

3.1 Fabric Scaling

If the relevant partial differential equations governing the deflection and stress in the membrane and frame are known, development of the scaling laws is almost a trivial problem. Referring to Appendix A, we find approximate equations for the deflection and stress of a strip membrane. We can use these equations for developing the scaling laws for two-dimensional membranes, if we recognize that certain conditions must be satisfied. First, the models must be geometrically similar to full-scale tents; i.e., the length and width of the membrane must be in the same ratio for the model and the full-scale tent. Second, shear stresses in the fabric must be negligible. Last, the stiffness matrix relating tension and strain in the real tent fabric must be proportional to the same matrix for the model fabric. Taking these conditions to be valid, we find from the equations of equilibrium that

$$\frac{\partial T}{\partial x} = 0 \ , \tag{3.1a}$$

$$\frac{\partial}{\partial x}\left(T \frac{\partial w}{\partial x}\right) = f \ , \tag{3.1b}$$

where T is the tension per unit length, f is the load per unit area, w is the membrane deflection perpendicular to a plane connecting the end supports, and x is a spatial coordinate. From the strain displacement relationship, we find

$$\varepsilon = \frac{\partial u}{\partial x} + \frac{1}{2}\left(\frac{\partial w}{\partial x}\right)^2 , \qquad (3.2)$$

where ε is the strain and u is the displacement in the membrane parallel to the plane connecting the end supports. Assuming a linear stress/strain relationship, which is approximately true for cotton fabrics*, we find that

$$T = \kappa\varepsilon \qquad (3.3)$$

where κ, a constant, is the slope of the fabric stress/strain curve.

From the equilibrium equations, we can show that at geometrically similar points in the model and full-scale tents

$$\left(\frac{Tw}{fL^2}\right)_m = \left(\frac{Tw}{fL^2}\right)_{FS} \qquad (3.4)$$

where L is the distance between membrane supports and the subscripts m and FS refer to model and full scale, respectively. From the strain displacement relationship and the equilibrium equation, it is easy to see that at geometrically similar points in the model and the full-scale tent

$$\left(\frac{\varepsilon L^2}{w^2}\right)_m = \left(\frac{\varepsilon L^2}{w^2}\right)_{FS} . \qquad (3.5)$$

Since we want the strain in the model tent and full-scale tent to be the same, we can show from Eq. 3.5 that

$$\left(\frac{w}{L}\right)_m = \left(\frac{w}{L}\right)_{FS} , \qquad (3.6)$$

*As will be seen later, at very low stress levels cotton fabrics exhibit a stiffening character. Under increasing levels of stress, the stress/strain relationship eventually becomes linear.

and from this equation, and Eqs. 3.3 and 3.4 that

$$\left(\frac{\kappa}{fL}\right)_m = \left(\frac{\kappa}{fL}\right)_{FS} . \tag{3.7}$$

Equation 3.7 tells us that if we make the model 1/10 full scale and choose a fabric with 1/10 the stiffness, then we must load the model with the same load per unit area as the real tent to obtain the same strains. Once a model fabric is selected, then Eq. 3.7 can be used to choose an appropriately scaled load.

3.2 Frame Scaling

We follow a similar procedure to the one above to scale the frame. By modeling the tent frame as a beam in bending*, we can show that

$$\frac{\partial^2}{\partial x^2}\left(EI\,\frac{\partial^2 w_B}{\partial x^2}\right) = T , \tag{3.8}$$

where E is the modulus of the beam material, I is the moment of inertia, w_B is the bending deflection of the beam, and T is the tension per unit length in the fabric. From Eq. 3.8, we can show that a geometrically similar points in the model and full-scale tent frame

$$\left(\frac{EIw_B}{TL^4}\right)_m = \left(\frac{EIw_B}{TL^4}\right)_{FS} . \tag{3.9}$$

To ensure that the deflections in the model and full-scale tent are geometrically similar, we must have

---

*If the fabric is mounted to the beam in such a way that the force on the beam due to the fabric acts through the axis of the beam, there will be no torsional deformation of the beam.

$$\left(\frac{w_B}{w}\right)_m = \left(\frac{w_B}{w}\right)_{FS} .$$

Comoination of this equation and Eqs. 3.3 and 3.6 yields

$$\left(\frac{EI}{\kappa L^3}\right)_m = \left(\frac{EI}{\kappa L^3}\right)_{FS} . \qquad (3.10)$$

By using Eq. 3.10, we can select the frame material and frame beam cross section such that the ratio of fabric deflection to frame deflection is the same in both model and full-scale tents. We will use this scaling law in a later section to design the model tent frames.

4. MODEL FABRIC

In this section we describe the process for selection of a model test fabric to be used in the model tents, the testing of the biaxial properties of that fabric, and the development of a sensor to measure fabric stress.

4.1 Screening

There is a wide variety of light fabrics available for use as a model fabric in scale model tents. We decided to limit our search to cotton fabrics, since most existing Army frame-supported tents presently use 9.85-oz cotton duck or 8.5-oz cotton sateen. Also (as the scaling equations in Sec. 3.1 show), the stiffer the fabric, the higher will be the required load applied to model to scale with the full-scale load. Therefore, we decided to search for as compliant a fabric as possible so as to keep the model loads small and manageable.

Ideally, one would like to base fabric selection on the biaxial stress/strain properties of the candidate fabrics, but selection by that means is prohibitively expensive. Instead, we limited ourselves to uniaxial fabric stress/strain tests on the candidate fabrics in both the warp and fill directions and compared these results with similar tests on 9.85-oz cotton duck.* To simplify the comparison further, we considered only the fabric stiffness κ in the region where stress and strain are linearly related. κ is defined in that region by

$$\kappa = \frac{\Delta T}{\Delta \varepsilon} ,$$

where ΔT is the change in tension per unit length of the fabric and $\Delta \varepsilon$ is the change in the strain.

The uniaxial test setup is shown schematically in Fig. 4.1. The fabric is held by clamps that consist of two aluminum plates with grooves on their inside surfaces. The grooves accept two strips of 1/8-in. diameter drill rod.

---

*We could also have used 8.5-oz cotton sateen for comparison, but cotton duck is used in the *tent maintenance shelter* and the *Fritche shelter*, which are the tents we model in later sections of this report.

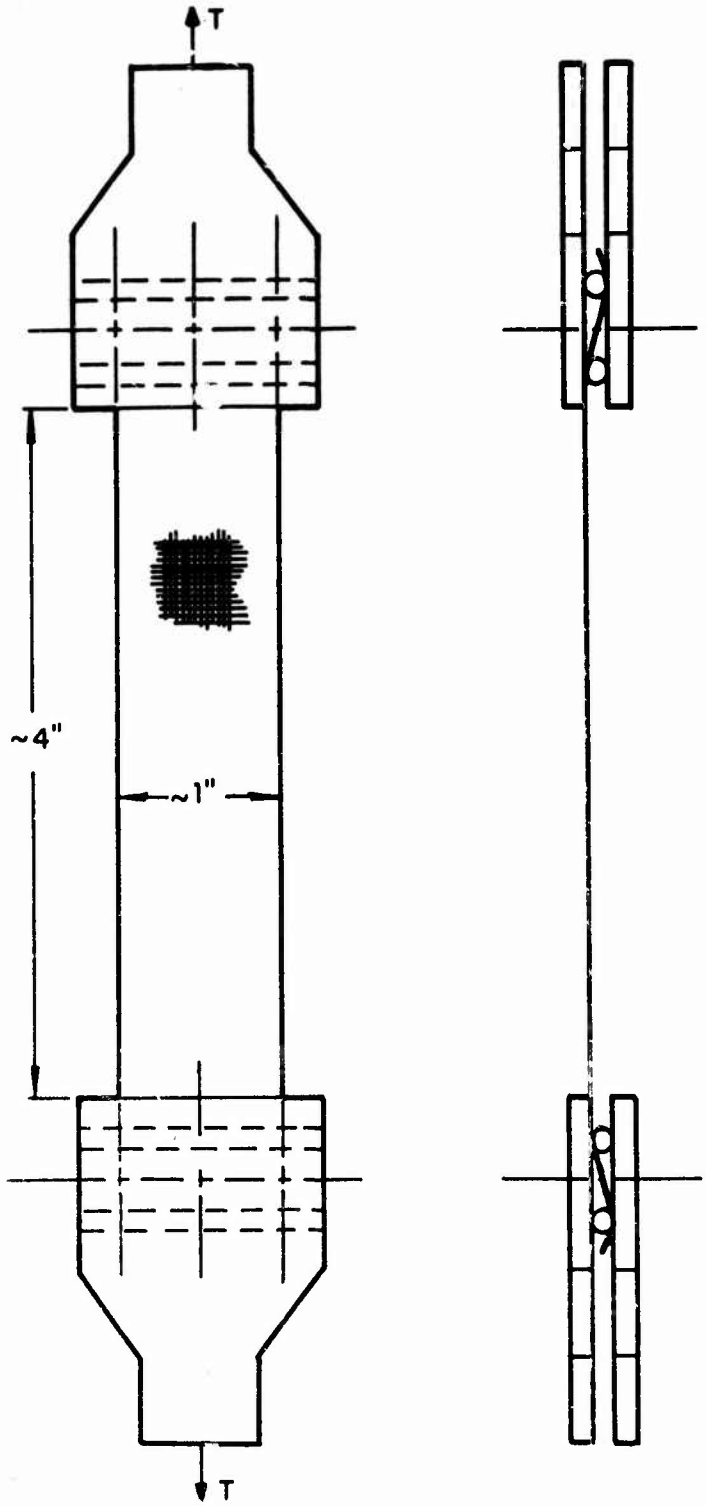

FIG. 4.1. UNIAXIAL TEST APPARATUS.

Three bolts (shown as center lines) clamp the fabric between the rods and the aluminum plates. This holding method is excellent for light loads but does lead to some reduction in breaking strength (10 to 20%) at high loads.

We applied loads to the fabric simply by hanging weights for light loads (up to about 20 lb) or by placing the holding brackets in a tensile testing machine. In general, creep with the cotton fabric tested here was not a serious problem. Deflections were measured using vernier calipers having accuracy to within a few thousandths of an inch. The 4-in. by 1-in. fabric specimen size was found to be convenient for both loading and deflection measurement.

Cotton duck (9.85-oz) and a number of candidate model fabrics were tested in this manner in both warp and fill directions. Among the most promising were 3.1-oz cotton muslin (78/78), 2.6-oz cotton typewriter ribbon cloth, and 2-oz cotton balloon cloth.

All of the fabrics tested required repeated loadings before reproducible stress/strain data could be obtained. Since it was anticipated that repeated loadings would be required during the tent model tests, we based our comparison of fabric stiffness on the repeatable values; i.e., we loaded each candidate fabric a sufficient number of times such that additional loadings produced no change in the stress/strain behavior.

The stress/strain properties of 9.85-oz cotton duck in the fill direction are shown in Fig. 4.2. After loading the fabric up to 70 lb/in. five times, we found that the fabric stress/strain properties were essentially repeatable. Note that the second loading of the fabric is not shown as the data was not properly taken. Fitting a straight line through the points from the last three loadings, we find a fabric stiffness of 1800 lb/in. in the fill direction, a value which we will use in future calculations.

Figure 4.3 shows that, after about five loadings, the stiffness in the linear range for 9.85-oz cotton duck in the warp direction is about 1900 lb/in., giving a warp-to-fill stiffness ratio of 1.05. We wanted not only to have a very compliant model fabric but also to have the same warp-to-fill ratio as the cotton duck. With these two criteria in mind, we examined the stress/strain behavior of the candidate model fabrics.

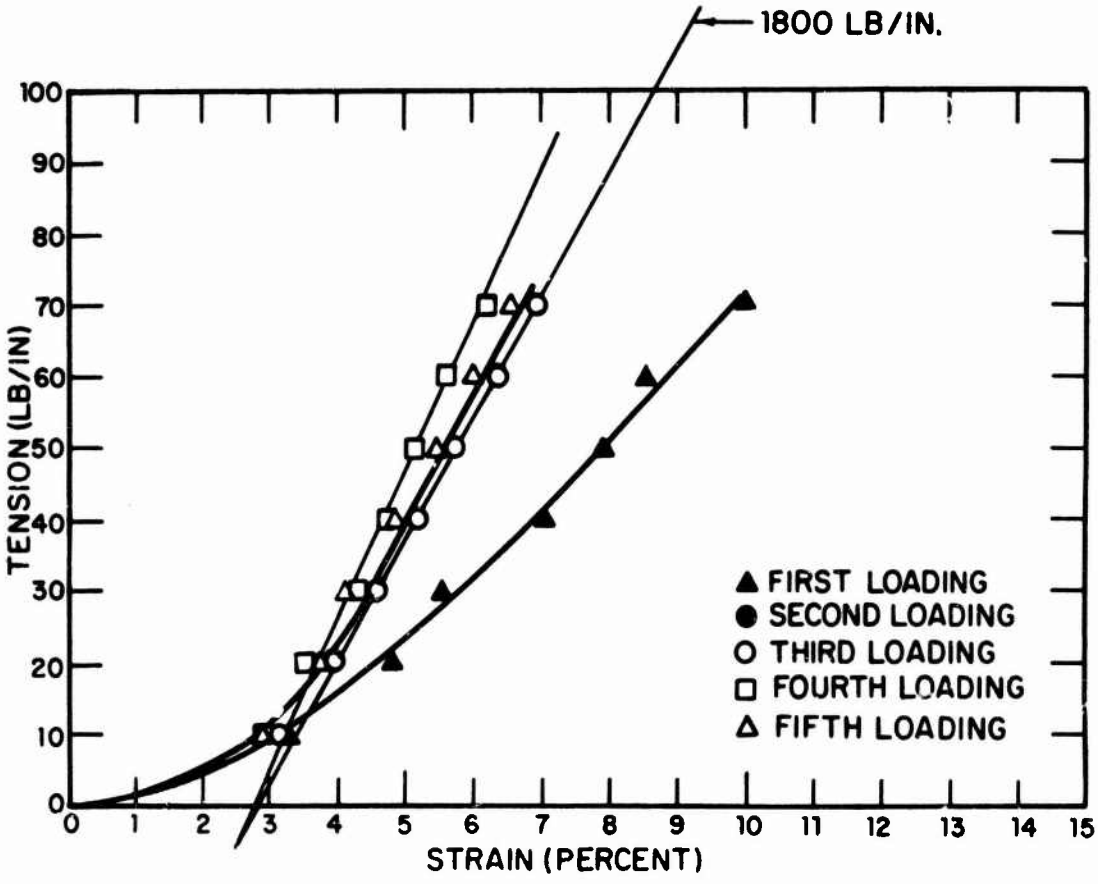

FIG. 4.2. STRESS/STRAIN PROPERTIES OF 9.85-OZ COTTON DUCK (FILL DIRECTION).

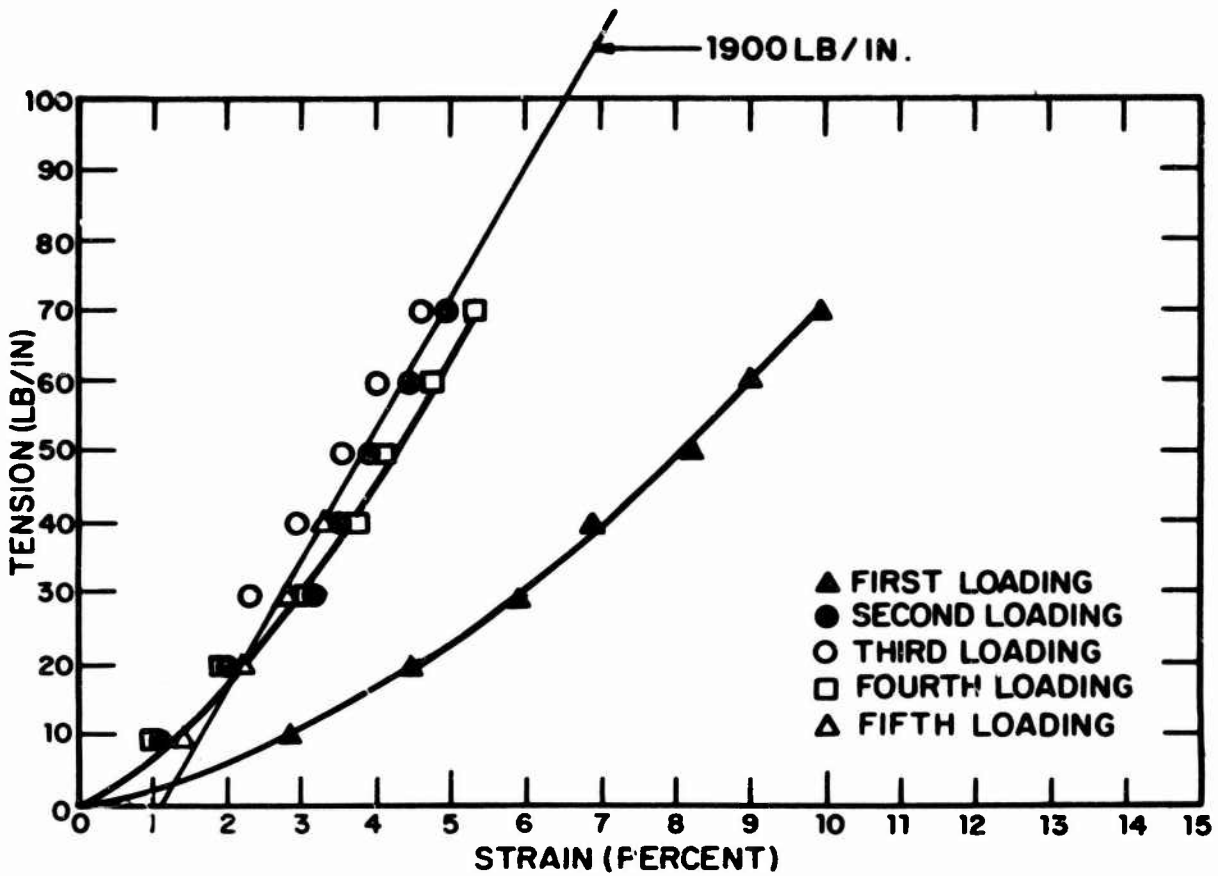

FIG. 4.3. STRESS/STRAIN PROPERTIES OF 9.85-OZ COTTON DUCK (WARP DIRECTION).

The first candidate fabric shown is 3.1-oz (78/78) bleached cotton muslin. Four loadings showed that its stiffness in the fill direction is 370 lb/in. (see Fig. 4.4). Three subsequent loadings (see Fig. 4.5) showed that the stiffness in the warp direction is 620 lb/in. Thus, the muslin's warp-to-fill ratio of ~1.7 is considerably different from that of cotton duck. Figures 4.6 and 4.7 show the stress/strain behavior of 2.6-oz cotton typewriter ribbon cloth in the fill and warp directions, respectively. Three loadings on this fabric showed the fill stiffness to be about 320 lb/in. and the warp stiffness to be about 400 lb/in., giving a warp-to-fill ratio of 1.25 – very nearly the same as cotton duck.

The last fabric to be tested was 2-oz cotton balloon cloth. Its stress/strain behavior in the fill and warp directions is shown in Figs. 4.8 and 4.9, respectively. The fill stiffness of 435 lb/in. and warp stiffness of 830 lb/in. gives a warp-to-fill ratio of 1.9. The results of the fabric testing are summarized in Table 4.1.

TABLE 4.1. FABRIC SCREENING SUMMARY.

Fabric	Warp Stiffness	Fill Stiffness	Warp/Fill Ratio
9.85-oz Cotton Duck	1900 lb/in.	1800 lb/in.	1.05
3.1 -oz Muslin	620 lb/in.	370 lb/in.	1.7
2.6 -oz Typewriter Ribbon Cloth	400 lb/in.	320 lb/in.	1.25
2 -oz Balloon Cloth	830 lb/in.	435 lb/in.	1.9

Based on the ratio of stiffness in the warp and fill directions in the linear region of stress/strain behavior, the 2.6-oz typewriter ribbon cloth is most similar to cotton duck. Also, the typewriter ribbon cloth is the most compliant of the fabrics tested.

Looking for further similarities, we decided to compare the stress/strain behavior of the 2.6-oz fabric with that of cotton duck. For example, if the 2.6-oz cloth were five times stiffer (i.e., if five times the stress were required

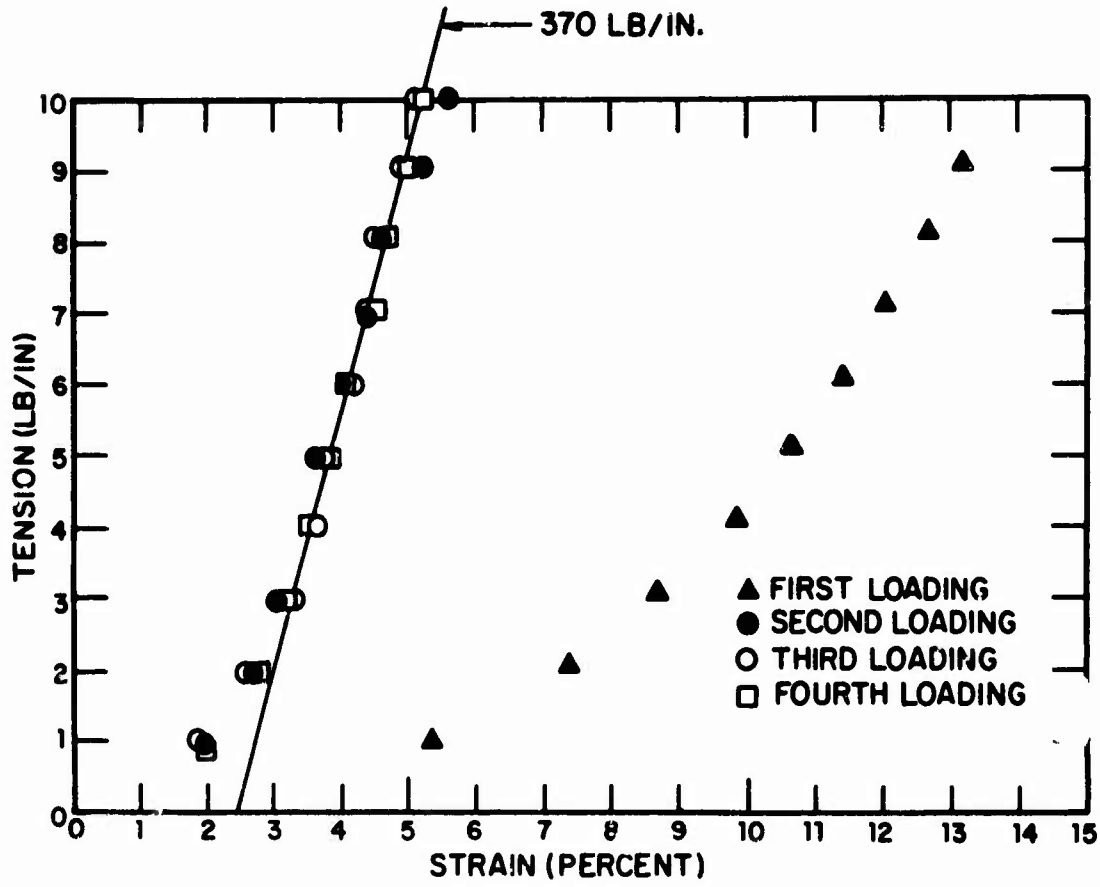

FIG. 4.4. STRESS/STRAIN PROPERTIES OF 3.1-OZ (78/78) BLEACHED COTTON MUSLIN (FILL DIRECTION).

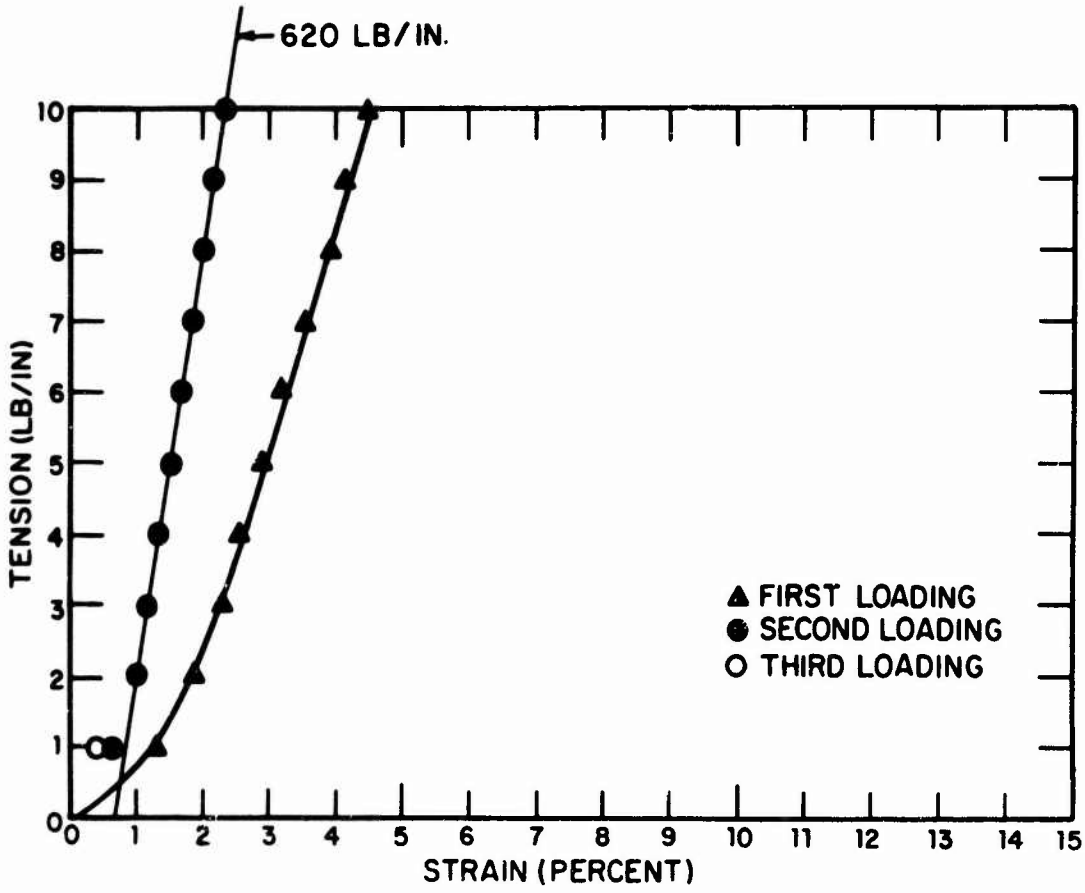

FIG. 4.5. STRESS/STRAIN BEHAVIOR OF 3.1-OZ COTTON MUSLIN (WARP DIRECTION).

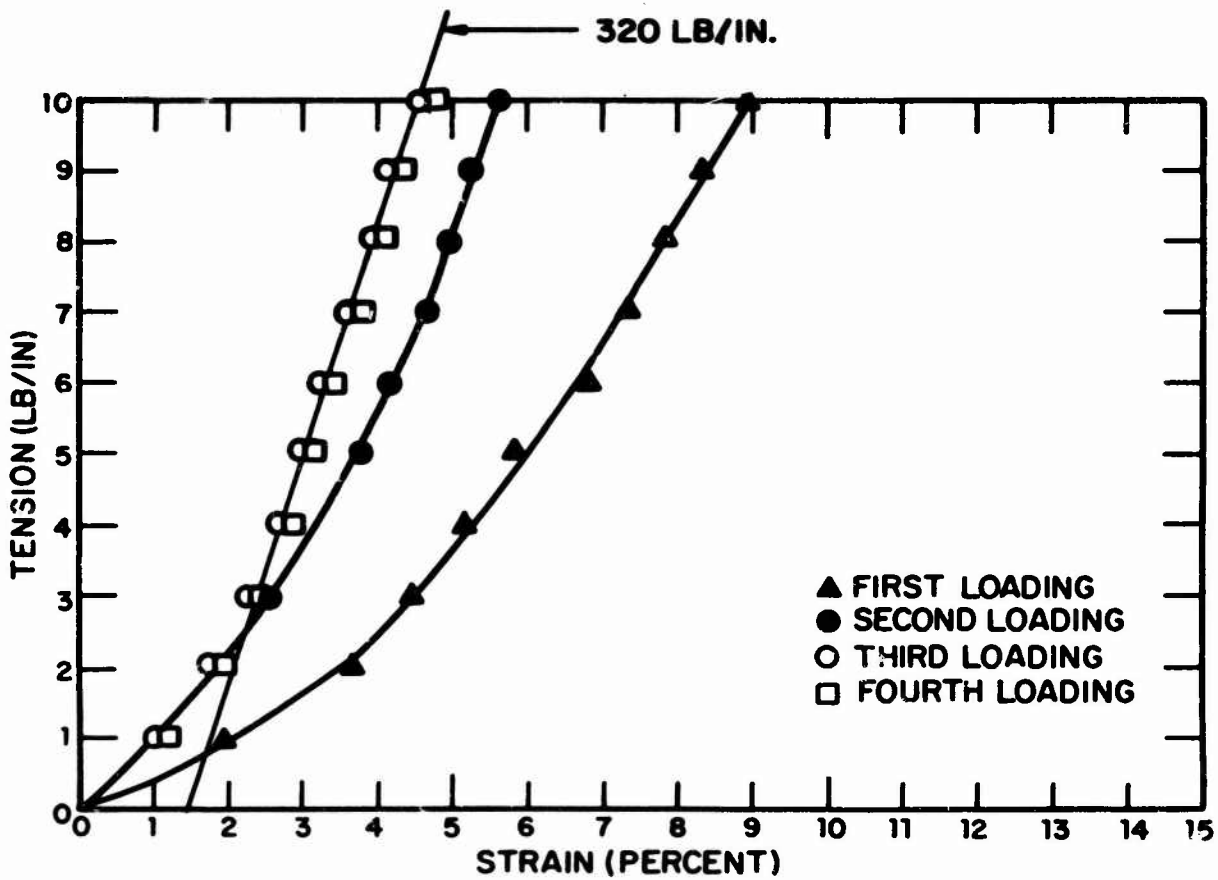

FIG. 4.6. STRESS/STRAIN BEHAVIOR OF 2.6-OZ TYPEWRITER RIBBON CLOTH (FILL DIRECTION).

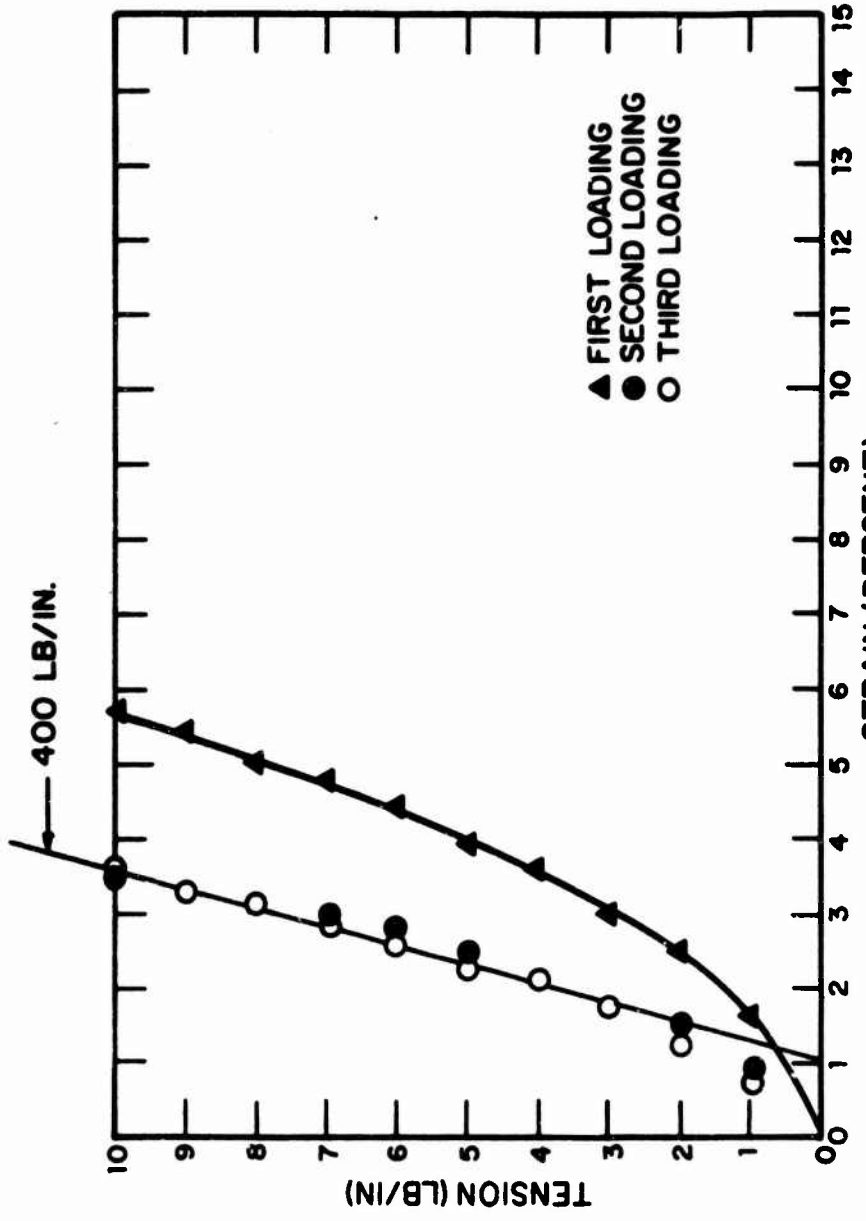

FIG. 4.7. STRESS/STRAIN BEHAVIOR OF 2.6-OZ COTTON TYPEWRITER RIBBON CLOTH (WARP DIRECTION).

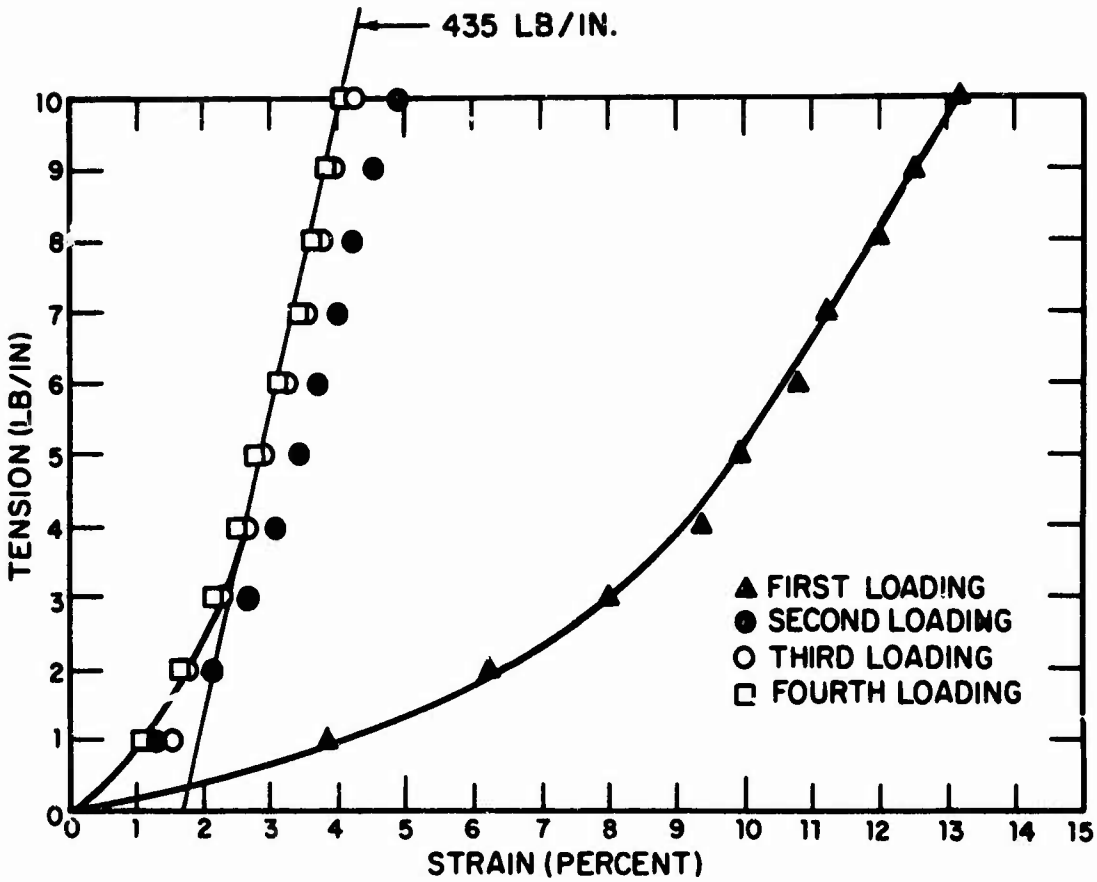

FIG. 4.8. STRESS/STRAIN BEHAVIOR OF 2-OZ BALLOON CLOTH (FILL DIRECTION).

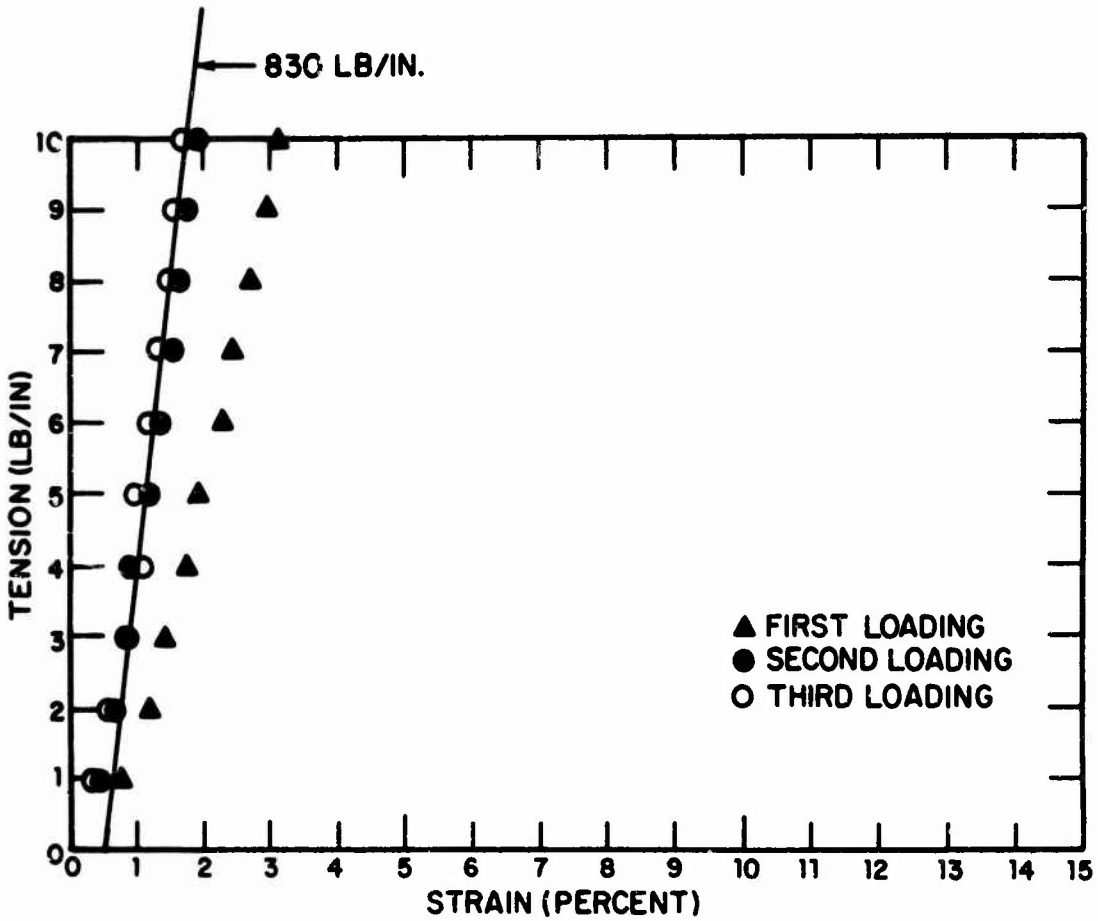

FIG. 4.9. STRESS/STRAIN BEHAVIOR OF 2-OZ COTTON BALLOON CLOTH (WARP DIRECTION).

to produce the same strain), the stress/strain behavior of the two fabrics would be as shown in Fig. 4.10. Clearly, even the nonlinear behavior of the two fabrics in uniaxial strain is quite similar, although the cotton duck is somewhat more compliant in the fill direction.

We should emphasize that the selection criterion used here is a very approximate one. For example, we have made no real effort to match the nonlinear behavior of the model fabric to the equivalent behavior of cotton duck, although the two are actually quite similar. In addition, selecting a fabric based on uniaxial properties (an economic necessity) when it is biaxial properties that we want to match has some drawbacks. However, the problem is not to develop an accurate tent model but rather to provide a means for validating the computer model predictions.

4.2 Biaxial Fabric Testing

In this section, we discuss the design and construction of a device for measuring the stress/strain behavior of fabrics under biaxial load as well as the results of tests on specimens of 2.6-oz cotton typewriter ribbon cloth, the model test fabric.

4.2.1 Biaxial testing apparatus

The apparatus for obtaining the stress/strain properties of fabric under biaxial load is shown in Fig. 4.11. The device consists of two aluminum channels (3 in. × 1½ in.) welded together to form a cross. Two adjacent arms of the cross have ball-bearing pulleys mounted at their ends. The other two adjacent arms have angle blocks through which eyebolts are passed. By adjusting the nuts which hold the eyebolts to the angle blocks, we could vary the length of eyebolt protruding through the block and align the fabric with the cross.

A cruciform of fabric approximately 3 ft square in which each arm is 4-in. wide (one arm parallel to the fill direction and the other parallel to the warp direction) was tested in the apparatus. Clamps similar to those used in the uniaxial fabric tests (see Sec. 4.1) were attached to each arm of the cross. Nylon lines were attached to the clamps on two adjacent arms and passed over the pulleys. Steel wire was attached to the clamps on the other two adjacent arms and connected to the eyebolts.

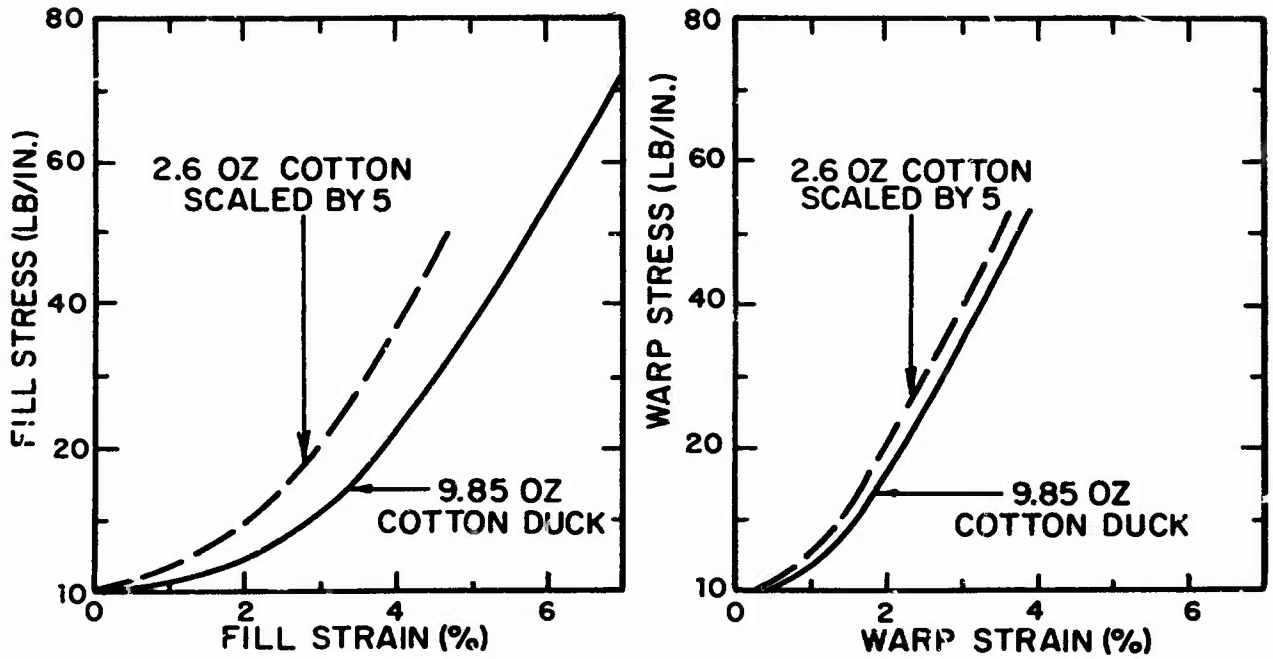

FIG. 4.10. COMPARISON OF SCALED 2.6-OZ COTTON TYPEWRITER RIBBON CLOTH AND 9.85-OZ COTTON DUCK.

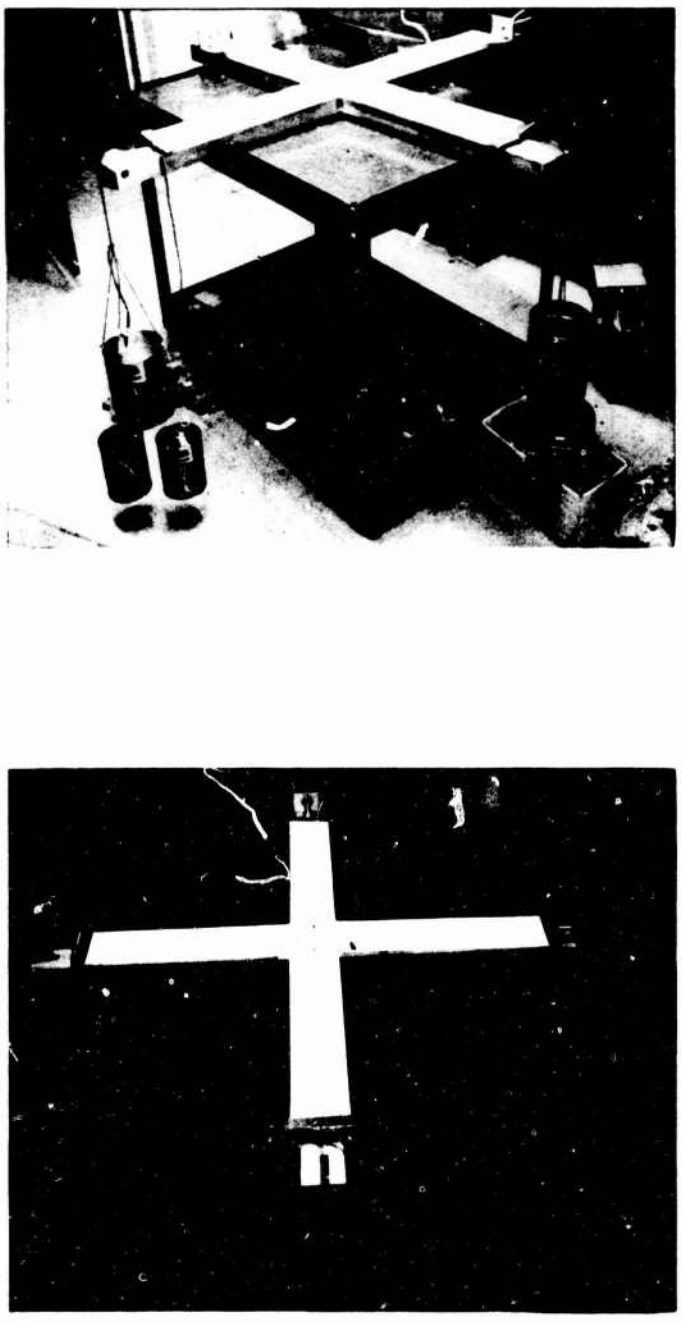

FIG. 4.11. BIAXIAL FABRIC TESTING MACHINE.

Small buckets were connected to the nylon lines passed over the pulleys. Weights (small bags containing 1/2 or 1 lb of sand) were placed in the buckets. In general, the load was increased in 2- or 3-lb increments on that arm of the cross carrying the major load. The load on the other arm was increased simultaneously in the proper ratio. Each 1-lb load generates a fabric stress of 1/4 lb/in.* Tests were conducted in which the ratio of warp-to-fill load was 1/6, 1/2, 1, 2, and 6. After applying each load increment, we adjusted the eyebolts so that the arms of the cross would remain straight and perpendicular.

The fabric deflection was measured in a 3-in. × 3-in. section of fabric in the center of the cross. Small hardened steel tabs with a cross scribed on each were glued to the fabric in the test section as shown in Fig. 4.12. By using a vernier caliper with pins glued to the jaws, we were able to measure the distance between the scribed lines on opposite tabs to about 1 mil.† Knowing the gauge length between the tabs (3 in.) and the change in spacing between the tabs as the load was applied, we were able to calculate the strain in both the warp and fill directions.

4.2.2 Biaxial properties of the model fabric

To characterize the mechanical properties of 2.6-oz cotton typewriter ribbon cloth, we tested it in the apparatus described in the previous section at stress levels up to 4 lb/in. As discussed in Secs. 6 and 7, this load is somewhat above the maximum levels to be encountered in later testing. In general, the first time the fabric was loaded, its stress/strain behavior was different from subsequent loadings. As a result, we loaded the fabric a number of times at each stress ratio until the deflections obtained were reproducible (within 1 or 2 mils). The first time a piece of fabric was mounted in the apparatus, ten repeated loadings were required for reproducibility. Generally, after

---

*Tests with a spring scale showed that passing the line over the pulley resulted in no change in applied load; i.e., the load in the buckets was the load applied to the fabric. There was essentially no difference in reading if the load was directly supported by the scale or if the load was attached to a line and passed over the pulley and then the line was attached to the scale (with the scale parallel to the ground plane).

†Measurements of this distance by two different technicians were never more than 1 mil apart.

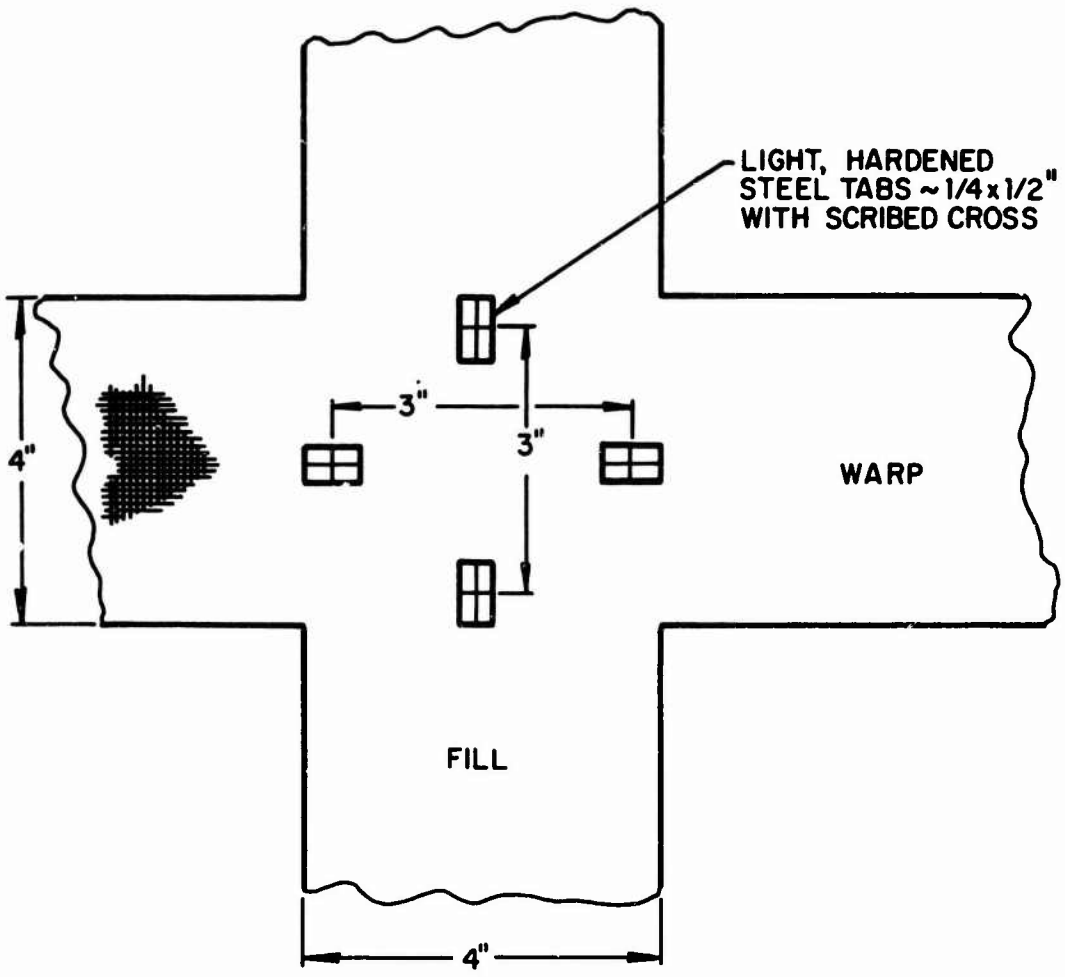

FIG. 4.12. FABRIC CROSS TEST SECTION.

this first cycling of the loading, it would only require a few repeated loads (at most three) to get reproducible deflections at other stress ratios.

Data were obtained on three separate pieces of fabric, all from the same bolt. Unfortunately, the fabric was subject to breaking at the higher loads. The breaking usually occurred after repeated loads and usually at the center of the cross. As a result, we do not have three complete sets of data.

Figures 4.13 and 4.14 present the results of the biaxial fabric tests. Comparison between two specimens of fabric are included when available. The solid lines are the mathematical models of the stress/strain data (described in the next section). The circles, triangles, and squares (either open or closed)* refer to the first, second, and third specimen of fabric, respectively. There is some inevitable scatter in the data, but, in general, the consistency is satisfactory.

4.2.3 Mathematical model of the biaxial stress/strain data

In this section, we discuss a mathematical model of the biaxial stress/strain properties of the fabric for use in the computer code. The model is based simply on a curve fitted to the data rather than on any theoretical model of yarn interaction. A very simple model matches the data quite well. We found that at a stress ratio of 1 ($T_W/T_F = \alpha = 1$), functions of the following form fit the data in Figs. 4.13 and 4.14 quite well:

$$\varepsilon_W = C_W T_W^{P_W} , \qquad (4.1)$$

$$\varepsilon_F = C_F T_F^{P_F} , \qquad (4.2)$$

*To prevent confusion the open symbols refer to the stress ratio $T_W/T_F = 2$ in Fig. 4.13 and to the stress ratio $T_W/T_F = 1/6$ in Fig. 4.14.

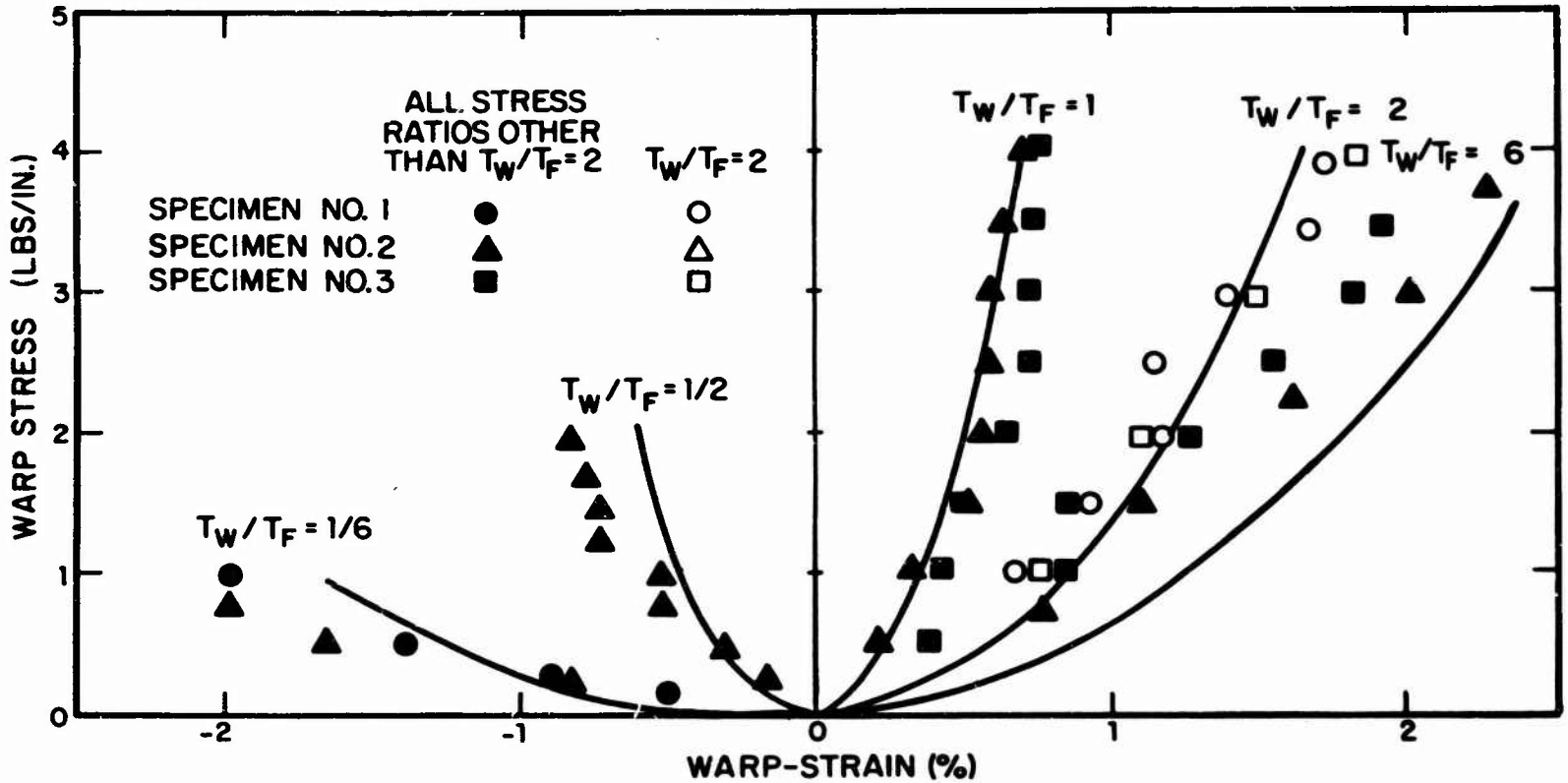

FIG. 4.13. BIAXIAL FABRIC TEST DATA FOR 2.6-OZ COTTON TYPEWRITER RIBBON CLOTH.

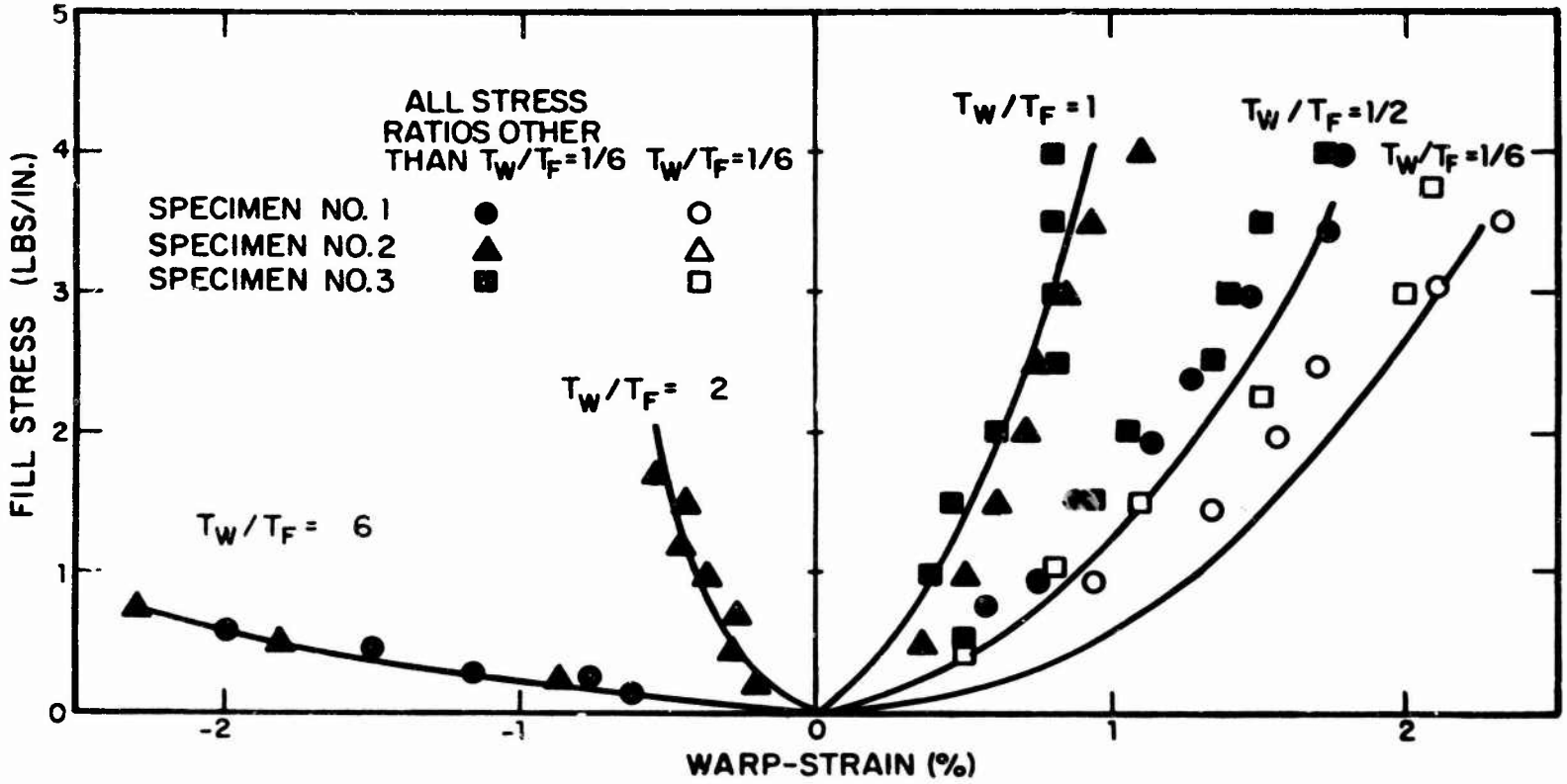

FIG. 4.14. BIAXIAL FABRIC TEST DATA ON 2.6-OZ COTTON TYPEWRITER RIBBON CLOTH.

where ϵ is the strain, T the stress, C and P are constants, and the subscripts W and F refer to the warp and fill directions, respectively. At other stress ratios, we found, quite surprisingly, that Eqs. 4.1 and 4.2 would still be valid if one simply multiplied them by a constant that depended only on the stress ratio α. The resulting biaxial stress/strain model that emerges is of the form

$$\epsilon_W = C_W T_W^{P_W} G_W(\alpha) \ , \tag{4.3}$$

$$\epsilon_F = C_F T_F^{P_F} G_F(\alpha) \ , \tag{4.4}$$

where one must now select the four constants C_W, C_F, P_W, and P_F and the two functions $G_W(\alpha)$ and $G_F(\alpha)$ by fitting Eqs. 4.3 and 4.4 to the data points in Figs. 4.13 and 4.14. Before doing this, however, we need to examine a number of other requirements that will constrain the allowable values of the constants and the allowable forms of the functions.

The finite element computer code described in Sec. 2 requires at least piecewise linear material properties. In particular, we require a stress/strain law of the form

$$\epsilon_W = B_{WW} T_W + B_{WF} T_F$$

$$\epsilon_F = B_{FW} T_W + B_{FF} T_F \ , \tag{4.5}$$

where the B's are material constants that may be a function of the fabric tensions T.*

---

*Note that we have neglected shear. In general, this approach is reasonable because uncoated fabrics are very weak in shear. The computer code is capable of accepting some shear stiffness in the fabric and, at present, a value of 5 lb/in. shear stiffness is used in the program. This value has very little effect on the fabric deflections but does help the code to converge. Using a shear stiffness of zero causes considerable problems with convergence.

We can put our fabric model into this form on a piecewise linear basis by expanding Eqs. 4.3 and 4.4 in a Taylor series about a given stress operating point (T_{WO}, T_{FO}). The resulting equation takes on the form

$$\varepsilon_W = \varepsilon_W(T_{WO},T_{FO}) + \frac{\partial \varepsilon_W}{\partial T_W}(T_W-T_{WO}) + \frac{\partial \varepsilon_W}{\partial T_F}(T_F-T_{FO}) , \quad (4.6)$$

$$\varepsilon_F = \varepsilon_F(T_{WO},T_{FO}) + \frac{\partial \varepsilon_F}{\partial T_W}(T_W-T_{WO}) + \frac{\partial \varepsilon_F}{\partial T_F}(T_F-T_{FO}) . \quad (4.7)$$

Since $\varepsilon_W(T_{WO},T_{FO})$ and $\varepsilon_F(T_{WO},T_{FO})$ are the warp and fill strain, respectively, at the operating point (T_{WO},T_{FO}), we can rewrite the above equations as

$$\Delta\varepsilon_W = \frac{\partial \varepsilon_W}{\partial T_W}\Delta T_W + \frac{\partial \varepsilon_W}{\partial T_F}\Delta T_F , \quad (4.8)$$

$$\Delta\varepsilon_F = \frac{\partial \varepsilon_F}{\partial T_W}\Delta T_W + \frac{\partial \varepsilon_F}{\partial T_F}\Delta T_F . \quad (4.9)$$

Equations 4.8 and 4.9 agree with the form of Eq. 4.5, but now the $\Delta\varepsilon$'s and ΔT's mean *increments* in strain and stress, respectively, relative to the chosen operating point. Calculating the derivatives called for in Eqs. 4.8 and 4.9, we can express the fabric material properties called for in Eq. 4.5 as

$$B_{WW} = C_W\left[P_W G_W(\alpha) + \alpha\frac{\partial G_W}{\partial \alpha}\right] T_W^{(P_W-1)}$$

$$B_{FF} = C_F\left[P_F G_F(\alpha) - \alpha\frac{\partial G_F}{\partial \alpha}\right] T_F^{(P_F-1)}$$

$$B_{WF} = -C_W T_W^{P_W-1}\frac{\partial G_W}{\partial \alpha}\alpha^2$$

$$B_{FW} = C_F T_F^{P_F-1} \frac{\partial G_F}{\partial \alpha} . \qquad (4.10)$$

The major difficulty with implementing this model in the computer code is that most existing finite element "solvers" require symmetry in the material property matrix; i.e., $B_{WF} = B_{FW}$. As a result, we need to examine what constraints the requirement that $B_{WF} = B_{FW}$ places on Eqs. 4.3 and 4.4 and then try to fit those equations to the data in Figs. 4.13 and 4.14. Symmetry in the material property matrix requires that

$$-C_W T_W^{(P_W-1)} \frac{\partial G_W}{\partial \alpha} \alpha^2 = C_F T_F^{(P_F-1)} \frac{\partial G_F}{\partial \alpha} . \qquad (4.11)$$

As described above, the G's can be approximated as being functions only of α. One means of satisfying this condition in Eq. 4.11 is to take $P_W = P_F = P$, which gives

$$\frac{\partial G_W}{\partial \alpha} = - \frac{C_F}{C_W} \alpha^{-(1+P)} \frac{\partial G_F}{\partial \alpha} . \qquad (4.12)$$

In earlier attempts at fitting Eqs. 4.3 and 4.4 to the data in Figs. 4.13 and 4.14, it was found that $G_F(\alpha)$ was approximately a linear function of α; i.e.,

$$G_F(\alpha) \cong a(\alpha-1) + 1 . \qquad (4.13)$$

where a is a constant obtained from linear regression. Substituting Eq. 4.13 into Eq. 4.12 and integrating the result, one obtains

$$G_W(\alpha) = \frac{C_F}{C_W} \frac{a}{P} \left(\frac{1}{\alpha}\right)^P + \left(1 - \frac{C_F}{C_W} \frac{a}{P}\right) . \qquad (4.14)$$

Using a trial-and-error process, we have fitted the data in Eqs. 4.3 and 4.4 to the data in Figs. 4.13 and 4.14 subject to the restrictions that $P_W = P_F$ and that $G_W(\alpha)$ and

$G_F(\alpha)$ have the mathematical form shown in Eqs. 4.13 and 4.14. The resulting values of the constants (for T_W and T_F in lb/in.) have been chosen to be

$$C_W = 3.5 \cdot 10^{-3}$$

$$C_F = 4.6 \cdot 10^{-3}$$

$$P = 0.5$$

$$a = -1.54 \ ,$$

which gives

$$\varepsilon_W = 3.5 \cdot 10^{-3} \ T_W^{\frac{1}{2}} \ G_W(\alpha)$$

$$\varepsilon_F = 4.6 \cdot 10^{-3} \ T_F^{\frac{1}{2}} \ G_F(\alpha) \ , \qquad (4.15)$$

where

$$G_W = -4.06 \ \frac{1}{\alpha^{\frac{1}{2}}} + 5.06$$

$$G_F = -1.54\alpha + 2.55 \ . \qquad (4.16)$$

Equation 4.15 is plotted as the solid curves in Figs. 4.13 and 4.14. The curves match the biaxial stress/strain data quite well at most stress ratios. However, as is apparent in Fig. 4.13, Eq. 4.15 overestimates the warp strain for $T_W/T_F = 6$ and underestimates these strains for $T_W/T_F = 1/2$. In addition, from Fig. 4.14 one can also see that Eq. 4.15 tends to overestimate the fill strain (at least at low stress) for $T_W/T_F = 1/6$. Using Eqs. 4.15 and 4.16 to predict the stress/strain relationship for uniaxial stress yields quite good agreement with measurement for uniaxial stress in the fill direction; i.e., $G_F = 2.55$ for $\alpha = 0$ and $\varepsilon_F = 1.75 \cdot 10^{-3} T_F^{\frac{1}{2}}$ (see Fig. 4.15). For uniaxial stress in

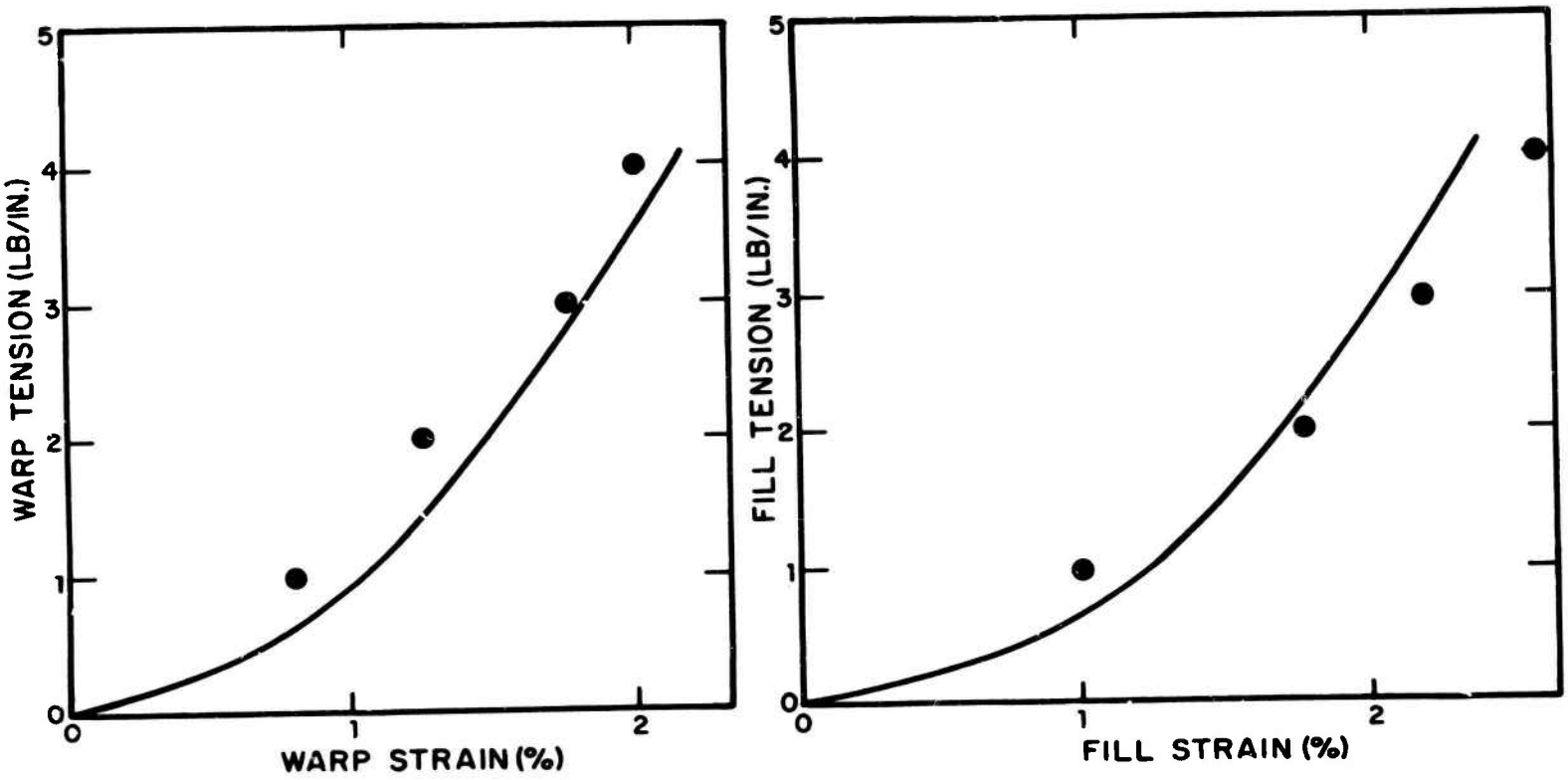

FIG. 4.15. COMPARISON OF UNIAXIAL DATA WITH THE BIAXIAL STRESS/STRAIN MATHEMATICAL MODEL.

the warp direction ($\alpha \to \infty$), Eqs. 4.15 and 4.16 predict excessively high strains. However, if we limit $G_W(\alpha)$ to the largest value measured (i.e., 3.2 at $\alpha = 6$), then quite good agreement with uniaxial data is obtained, as shown in Fig. 4.15.

In general, though, with the above exceptions, Eq. 4.15 agrees well with the measured biaxial stress/strain data and will constitute our mathematical model for the biaxial stress/strain behavior of 2.6-oz cotton typewriter ribbon cloth.*

Equation 4.16 requires some special treatment, because it is clearly in error not only for predicting uniaxial warp strain under stress in the warp direction but also for predicting the Poisson effect under uniaxial stress (i.e., warp strain due to fill stress or fill strain due to warp stress). Equation 4.16 as presently constituted would predict infinite warp strain under uniaxial fill stress ($G_W \to -\infty$ as $\alpha \to 0$) and infinite fill strain under uniaxial warp stress ($G_F \to -\infty$ as $\alpha \to \infty$). To avoid this problem, we have limited the value of G_W and G_F in the computer code to those values obtained for the range of α over which we have biaxial stress/strain data (i.e., $\alpha = 1/6 \to 6$).** This approach results in

$$-6.2 < G_W < 3.2 ,$$

$$-7 < G_F < 2.25 ,$$

which yields good agreement with uniaxial stress data.

---

*The mathematical model in Eqs. 4.15 and 4.16 was used in the computer code to model the biaxial stress/strain tests of typewriter ribbon cloth as a check on the code. The resulting predictions of the biaxial stress/strain behavior were in good agreement with the solid curves of Figs. 4.14 and 4.15.

**In effect the computer code does not allow α to go out of the range 1/6 to 6 when G_W or G_F is being calculated.

4.3 Fabric Force Sensor

4.3.1 General description

The sensor for measuring the tension forces in fabrics was developed at BBN and was designed to measure those forces independently of the fabric's properties. During this program, the sensor was refined so that it could measure small loads. Such measurements are distinct from strain gauge measurements in that one must know the usually nonlinear biaxial stress/strain properties of the fabric to translate strain measurements into tension forces. The sensor is much stiffer than the fabric and, as a result, carries all the load in the yarns to which it is attached. This is analogous to a soft spring and a hard spring attached in parallel; the hard spring carries all the load. The disadvantage of the enlargement is that the sensor is a rigid inclusion in the fabric which distorts the strain field. This distortion can be minimized by making the sensor as small as possible.

The sensor used in this program has two stainless steel load links like those shown in Fig. 4.16. The load links are fastened (one above and one below the fabric) to ~0.25-in. diameter stainless steel buttons, which are glued to the fabric (shown actual size in Fig. 4.17). The load links consist of a measuring beam (see Fig. 4.16), to which a strain gauge is attached, and flexures, which tend to decouple the measuring beam from all but axial deformations of the load link. A second, dummy, strain gauge is attached to a nondeforming surface of each load link for temperature compensation. The four sensor strain gauges are then wired together into a full bridge. The resulting instrument is a rugged, reasonably stable device whose one disadvantage is low sensitivity.

4.3.2 Calibration

A number of fabric force sensors have been constructed from a variety of materials. In general, we have found the invar sensors to be the most sensitive and the least subject to drift. Figure 4.18 is a typical calibration curve showing a sensitivity of 10 μV/2V/(lb/in.); the scatter is caused primarily by drift at these extremely low voltages. The most reliable means that we have found for calibrating these sensors is to assemble the load links with no fabric between them, apply a known load, and measure the output voltage of the strain gauge bridge. Since the gauges are attached to 1/4-in.-diameter "buttons" on the fabric, a 1-lb load in the

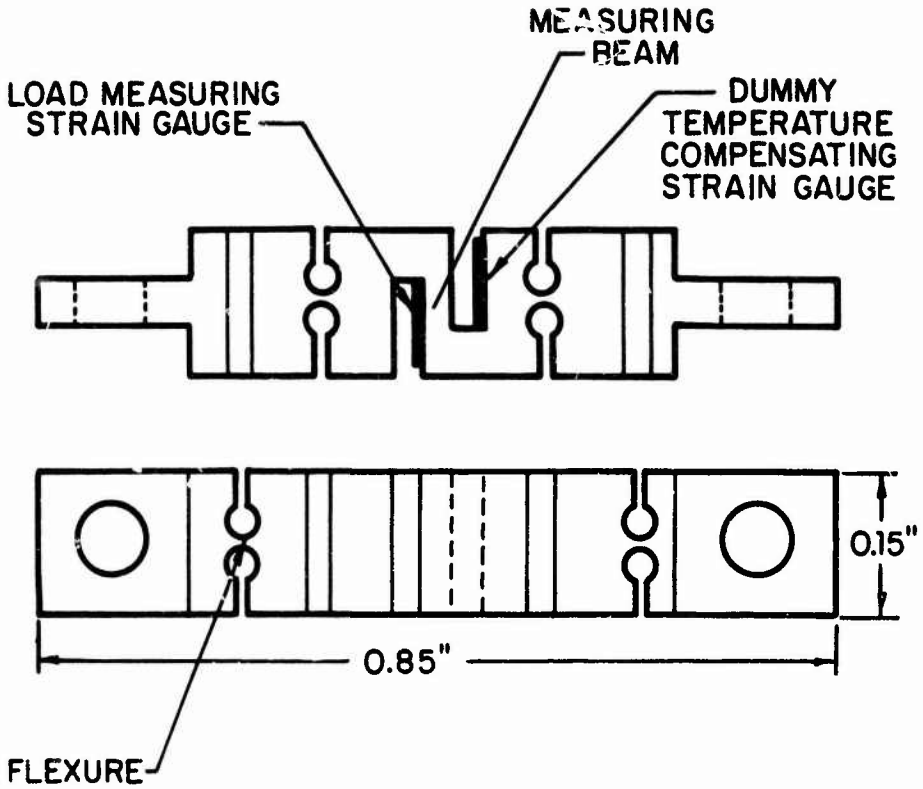

FIG. 4.16. LOAD LINK IN THE FABRIC FORCE SENSOR.

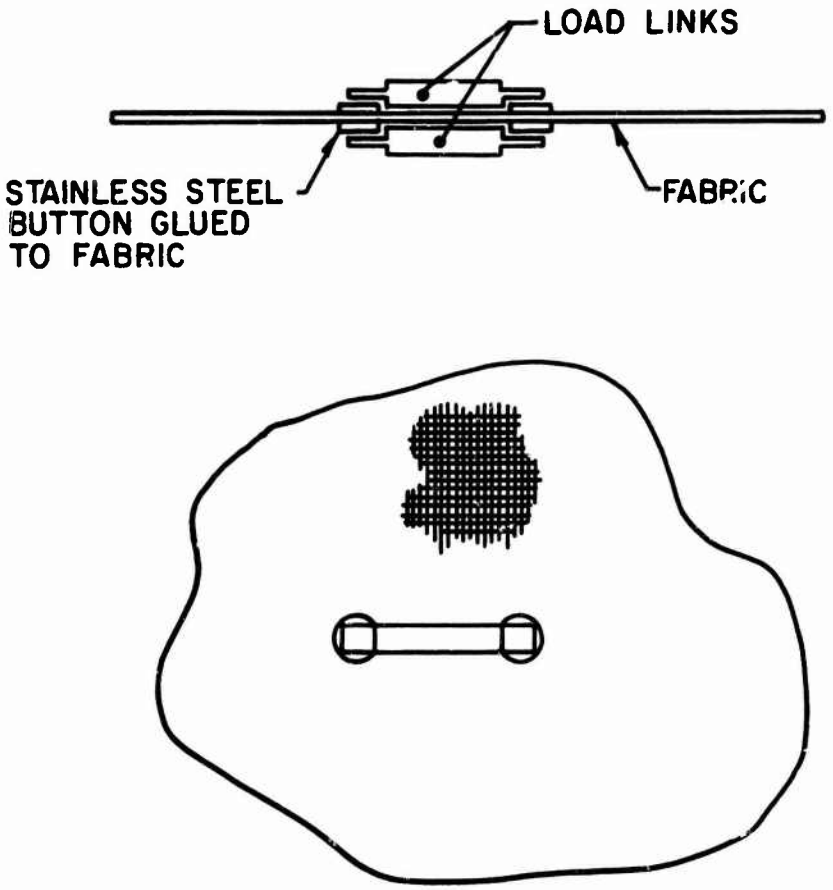

FIG. 4.17. FABRIC FORCE SENSOR DRAWN ACTUAL SIZE.

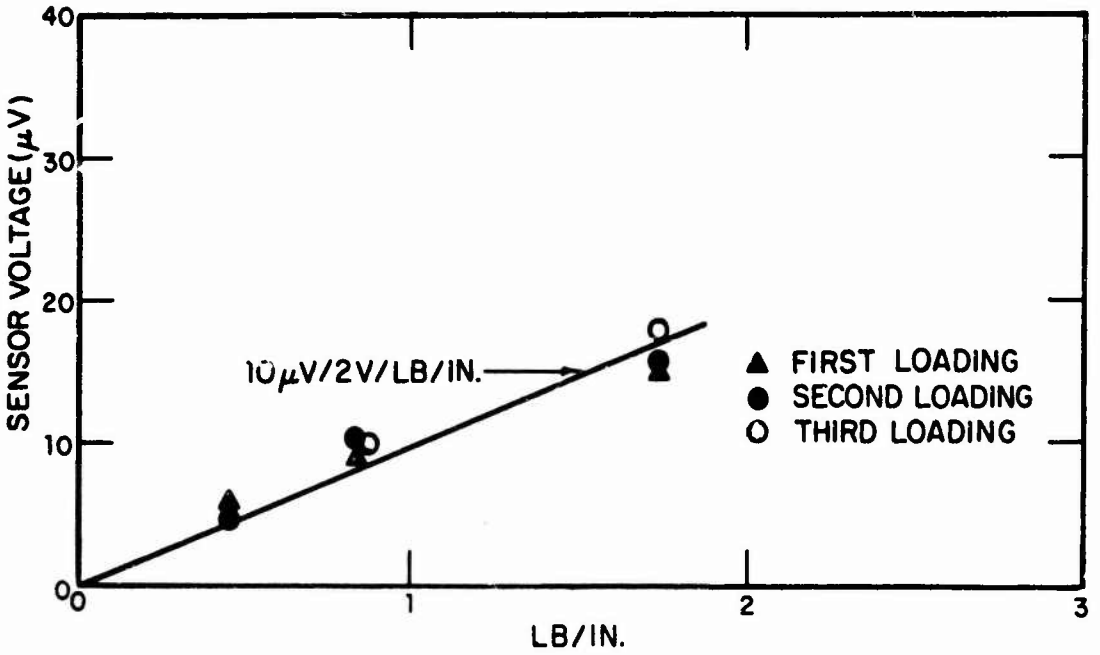

FIG. 4.18. FABRIC FORCE GAUGE CALIBRATION CURVE.

calibration procedure corresponds to a fabric stress of approximately 4 lb/in.* when the gauge is attached to the fabric.

*Because of the low shear stiffness of most fabrics, nearby threads may be thought to act independently. Thus, the only threads applying load to the sensor are those attached to the buttons.

5. MODEL TENT FRAMES

In this section we discuss the design of two model tent frames based on the scaling laws of Sec. 3 and the model fabric properties of Sec. 4. The two full-scale shelters to be modeled are a slant-roof frame tent and an arch-roof frame tent.

5.1 Slant Roof Frame

The slant-roof frame model is based on, but by no means is an exact scale model of, the *tent maintenance shelter (TMS)*. The frame has been chosen to deflect in approximately the same ratio to the model fabric deflections as the full-scale frame does to the full-scale fabric. We have selected a scale factor (based on a convenient model size) of 1/8. All of the arches and frames in the full scale TMS are constructed from steel box beams whose cross section is shown in Fig. 5.1. The bending stiffness of our model beam should be related to the bending stiffness of this box beam by (see Sec. 3.2)

$$\frac{(EI)_m}{(EI)_{FS}} = \frac{\kappa_m}{\kappa_{FS}} \left(\frac{L_m}{L_{FS}} \right)^3 \qquad (5.1)$$

where E is Young's modulus, I is the bending moment of inertia, κ is the fabric uniaxial stiffness, L is a characteristic length, the subscript m refers to the model tent, and the subscript FS refers to the full-scale tent. The model cloth is 2.6-oz cotton typewriter ribbon. From uniaxial load tests on the model fabric and on the full-scale fabric (9.85-oz cotton duck), we have shown the ratio κ_m/κ_{FS} to be 1/5 (see Sec. 4, Fig. 4.10). This value, along with the scale factor of 1/8, gives a ratio of bending stiffnesses

$$\frac{(EI)_m}{(EI)_{FS}} = 3.9 \cdot 10^{-4} \ . \qquad (5.2)$$

Modeling the full-scale beam as a box beam, we find that $I_{FS} = 0.4$ in.^{4} A 1/4-in. square aluminum beam, which very closely satisfies the above ratio, is used in our model frame. A drawing of the model is shown in Fig. 5.2. The model is scaled to one section of the TMS (in reality there

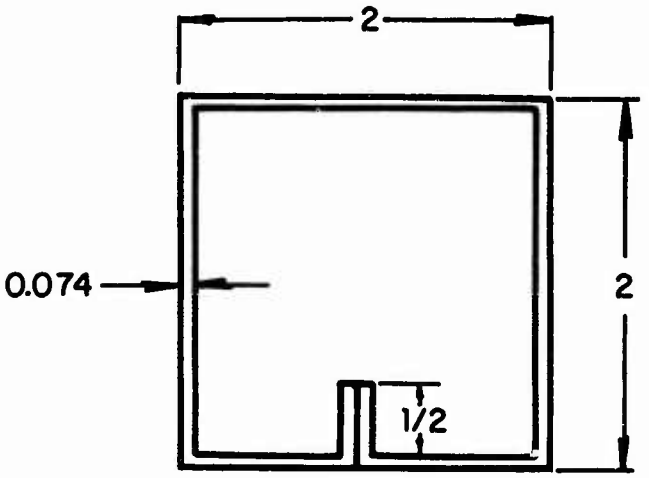

FIG. 5.1. TENT MAINTENANCE SHELTER BEAM CROSS SECTION.

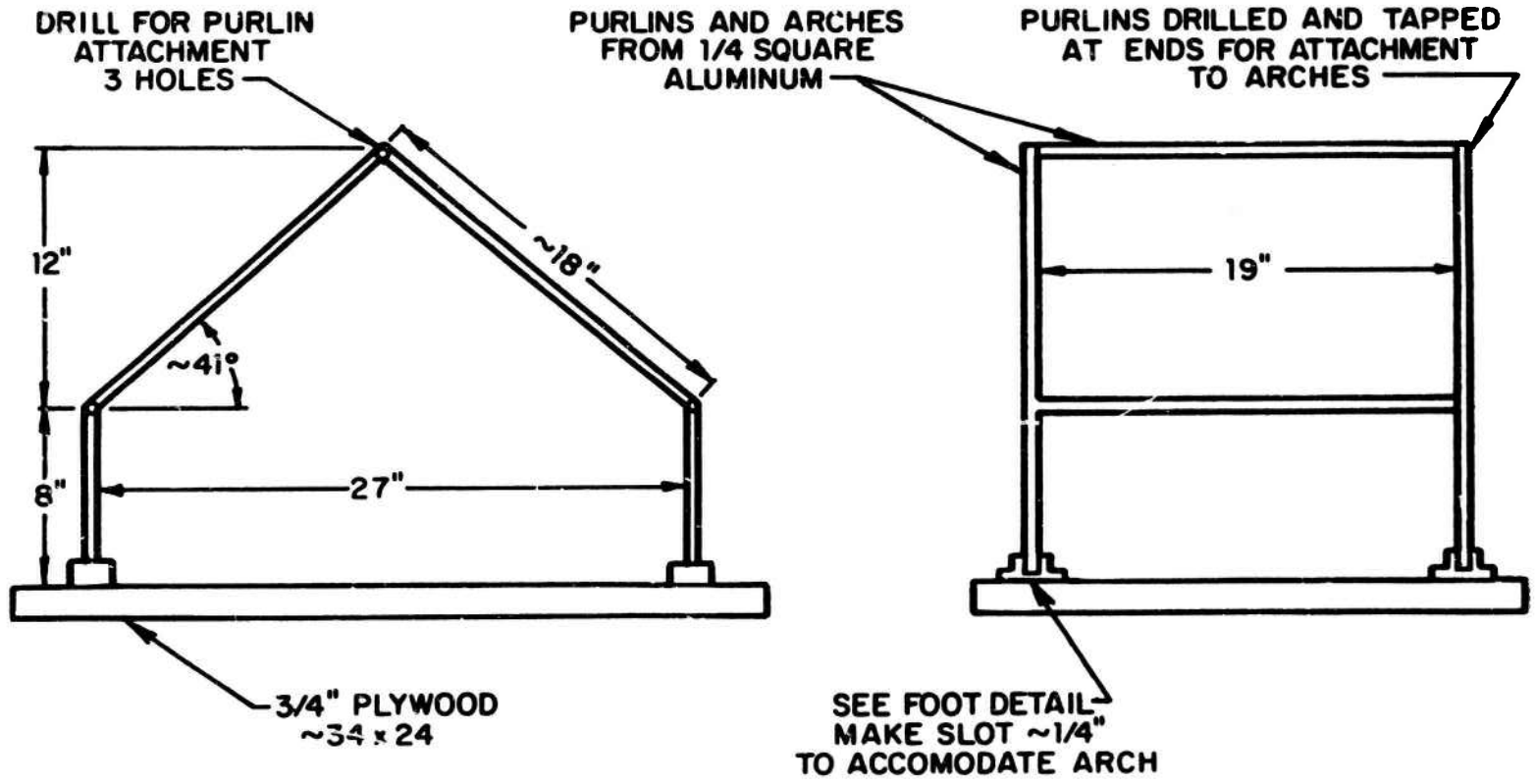

FIG. 5.2. ONE-EIGHTH SCALE APPROXIMATE MODEL OF TMS.

are three arches) and models primarily the bending stiffness of the arch and purlins and their relative lengths. Little effort has been made to scale the interconnection between beams* or the bending stiffness of the ridge pole. This additional complexity is not justified as these details vary greatly for different designs of slant roof tents. Note, however, that the connection between the model frames and the ground (a hinge joint, see Fig. 5.3), has been modeled, because this is a fairly common geometry in existing Army frame-supported tents.

5.2 Arch Roof Frame

The arch roof frame model is based on one section of the Fritche Shelter (FrS) and models two arches with their respective purlins. (The actual shelter contains up to eight arches.) We again selected a scale factor of 1/8 to give a convenient model size. Again, the model fabric is 2.6-oz cotton typewriter ribbon cloth. Since the full-scale cloth is 9.85-oz cotton duck, the ratio κ_m/κ_{FS} remains 1/5, and Eq. 5.2 applies to this frame also.

Unlike the TMS, the FrS has different cross sections for the arch beams and the purlins. These cross sections are shown in Fig. 5.4. Since the arch cross section is not square, we need to match the stiffness for bending about the two possible axes of the beams. The purlins are square and, hence, one bending stiffness is sufficient to characterize them. The full-scale moments of inertia are given below.

Arches	
I_{xx}	2.42 in.^{4}
I_{yy}	0.63 in.^{4}
Purlins	
$I_{xx} = I_{yy}$	0.30 in.^{4}

*All connections between arches and purlins, except at the ridge pole, are drilled and tapped (for ease of assembly and disassembly) to model a rigid interconnection similar to the full-scale interconnections.

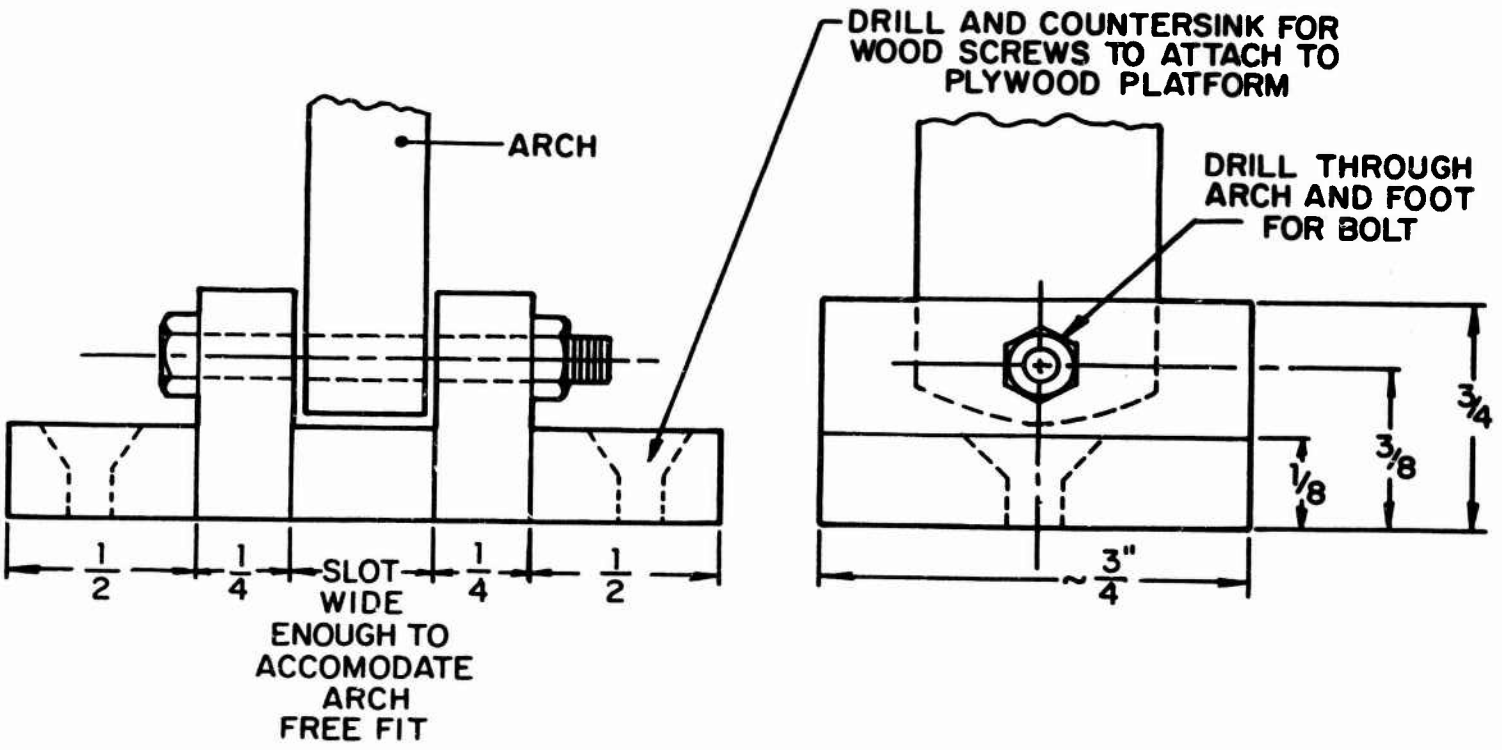

FIG. 5.3. TENT FRAME MODEL FOOT DETAIL.

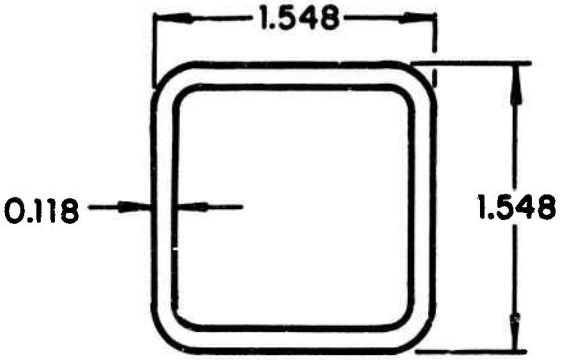

PURLINS

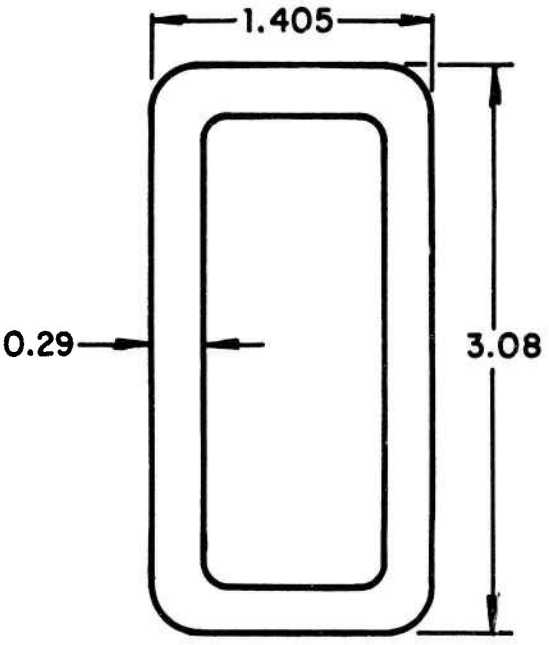

ARCHES

FIG. 5.4. FRITCHE SHELTER FRAME MEMBERS.

Both purlins and arches are magnesium ($E = 6 \cdot 10^6$ lb/in.^{2}). We find that a 3/16-in. square aluminum beam satisfies the criterion in Eq. 5.2 for the purlins and that 5/16 in. × 0.34 in. aluminum beam satisfies Eq. 5.2 for the arches. The latter beam can be readily machined from a standard 5/16 in. × 1/2 in. aluminum bar.

A drawing of the resulting model frame is shown in Fig. 5.5. Again, the primary objective was to model lengths and bending stiffnesses of the arches and the purlins. For this particular model frame, the interconnections between the purlins and arches are quite representative of the full-scale tent. In both cases, the purlins are connected to the arches by "bolts" that run through the arches. Again, the hinge-like connection in the full-scale tent between the arches and the ground is also used in the model. Photographs of the model frames are shown in Fig. 5.6.

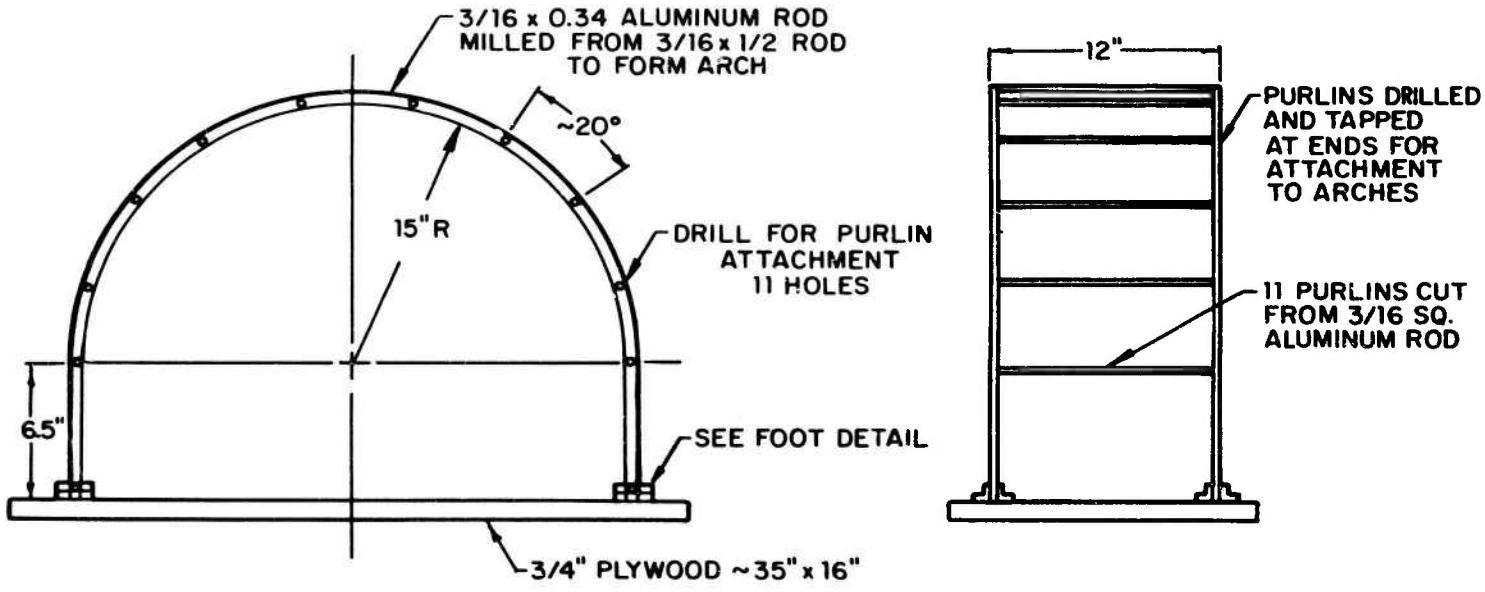

FIG. 5.5. ONE-EIGHTH SCALE APPROXIMATE MODEL OF THE FrS.

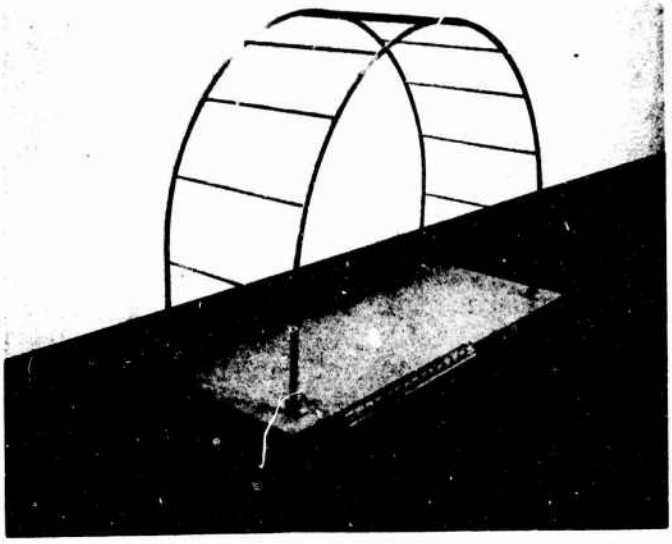

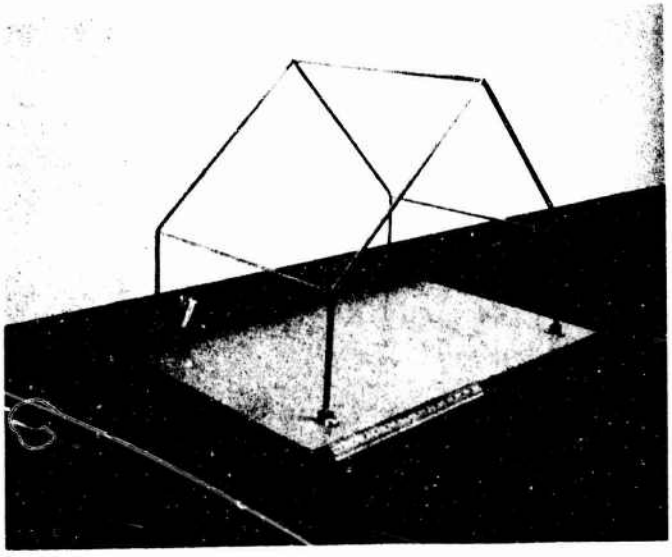

FIG. 5.6. MODEL TENT FRAMES.

6. PRELIMINARY VERIFICATION OF THE COMPUTER CODE

Before beginning detailed measurements on the model tents, we decided to check the performance of the computer code by comparing the code predictions with the results of some simple tests. Three tests were performed: the stress and deflection of a thin strip of fabric uniformly loaded perpendicular to its plane, the deflections of the two tent frames under a point load, and the stress and deflection of a two-dimensional fabric membrane rigidly supported at its boundaries. We next describe the results of those tests.

6.1 Fabric Strip Membrane

Measuring the deflection of a strip of fabric uniformly loaded perpendicular to its plane is a particularly useful problem, because it can be solved analytically (see the Appendix) as well as experimentally; both calculated and measured results can then be compared to the computer code.

6.1.1 Test set-up

A 24-in. long by 5-in. wide strip of 1.8-oz coated dacron fabric* was mounted in a rigid wood frame attached to the bed of a milling machine. By moving the bed up and down, we were able to measure the deflection of a point on the fabric strip from a fixed reference. Also, we could select any point on the fabric for testing by moving the milling machine bed from side to side and from front to back. We applied the load at five discrete points along the 24-in. length of the strip, as shown in Fig. 6.1. Each of the loads was attached to a 5-in.-long rigid wooden strip, which in turn rested on the fabric so as to distribute the load evenly across the 5-in. fabric width. Deflections were measured near each of the loading points. Two configurations were considered: (1) an initially flat membrane and (2) a membrane with some initial deflection (i.e., free hanging deflection).

Uniaxial stress/strain tests of the 1.8-oz coated dacron fabric were performed to provide the fabric data required for the computer code. The results of these measurements are shown in Fig. 6.2. At low load, the fabric behaves approximately linearly with a stiffness of 50 lb/in.

---

*These tests were performed early in the program before the 2.6-oz cotton typewriter ribbon cloth was available.

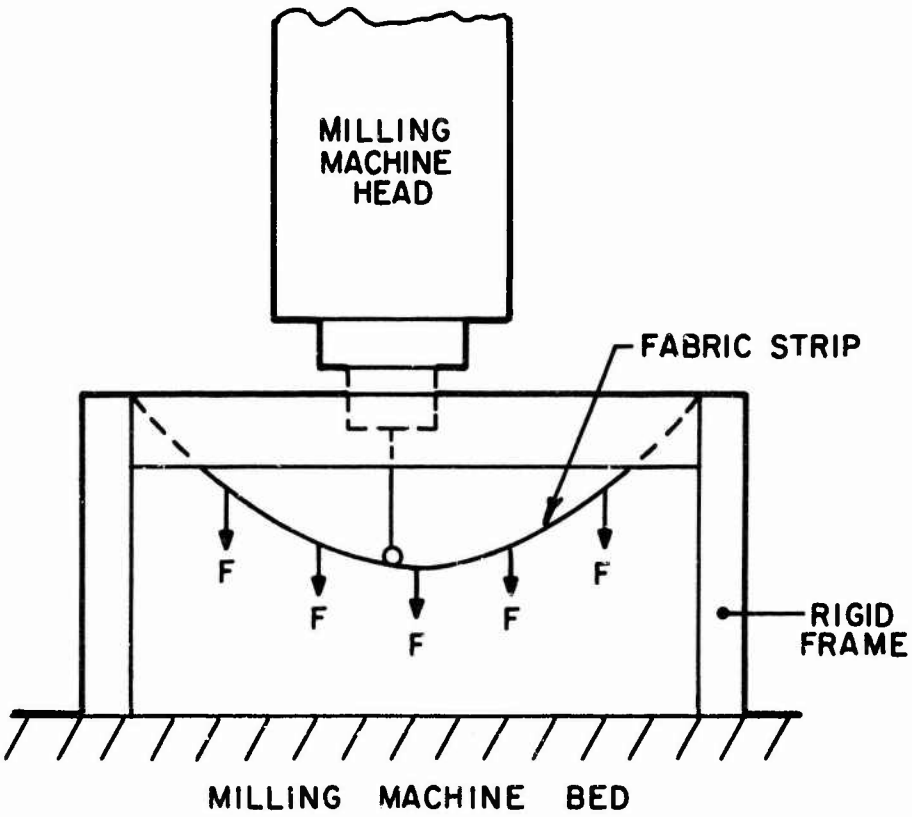

FIG. 6.1. TEST CONFIGURATION.

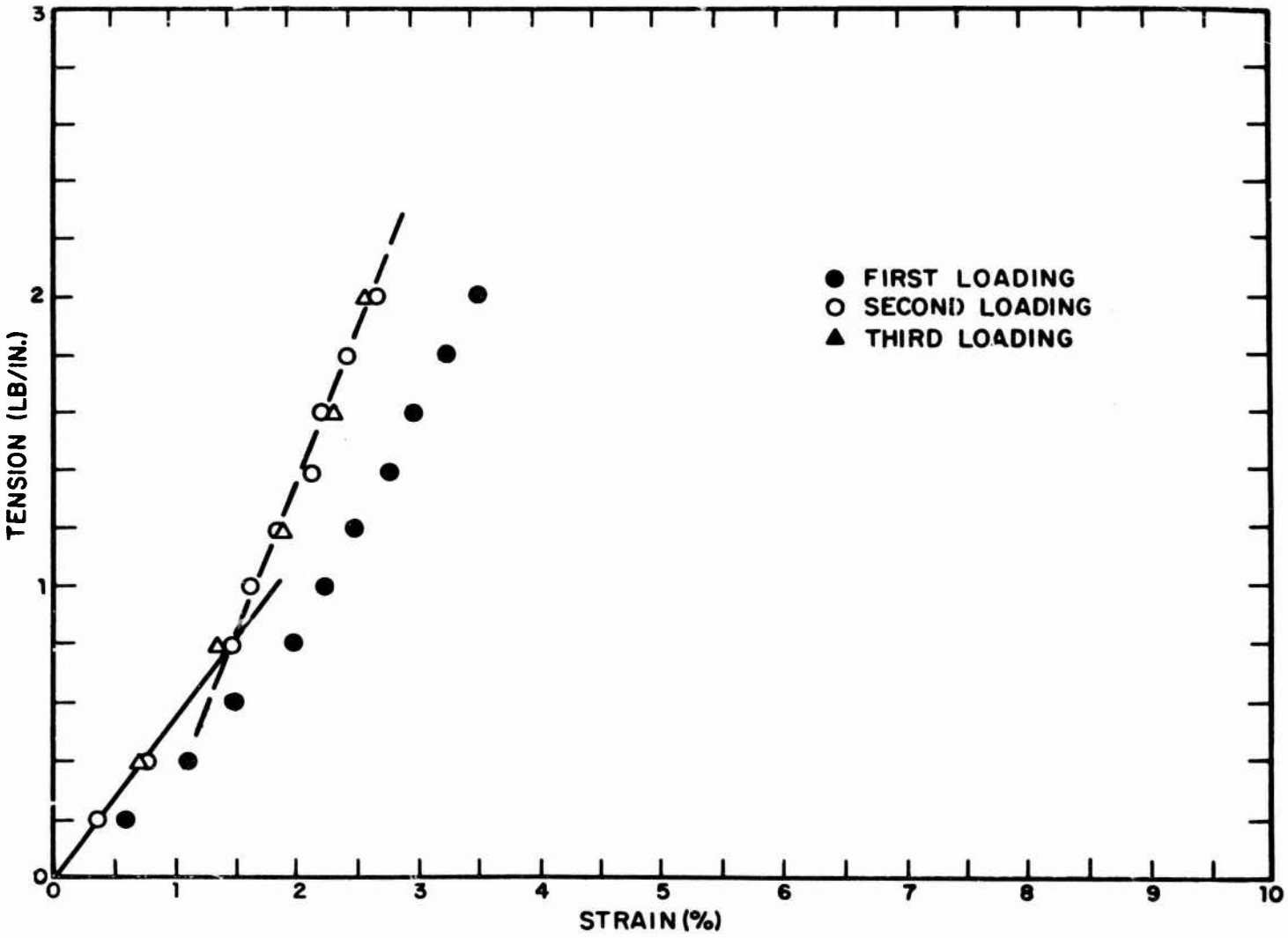

FIG. 6.2. STRESS/STRAIN DATA FOR 1.8-OZ DACRON (COATED) IN THE FILL DIRECTION.

6.1.2 Computer program model

The computer program was exercised using the models of the fabric membrane strip shown in Fig. 6.3. Two sets of input were used: one for an initially flat membrane and the second for a membrane with an initial displacement. If the x and y membrane curvatures are zero, the computer program will predict, at the first iteration, very large displacements. The program will then try to reach an equilibrium state from this first iteration but will take a very long time to converge. Therefore, in both models, a slight y curvature was introduced, and in the initially flat membrane model, a slight x curvature was used as shown in Fig. 6.3.

The x,y grid of the strip model is shown in Fig. 6.3, where the numbers at the triangular vertices represent the global nodal numbers and the circled numbers represent the element numbers. Since the model and loading are symmetric, only one-half the model had to be used. The loading is uniform and is applied in the z-direction. The boundary conditions are that

- nodes 1, 2 and 3 are fully restrained,
- all nodes are restrained in the y-direction, and
- nodes 10, 11, and 12 are restrained in the x-direction (symmetry condition).

The membrane material was taken to be isotropic with a fabric stiffness of 50 lb/in. Although the fabric is, in fact, orthotropic, the fabric strip is in uniaxial strain; as a result, the isotropic assumption and the initial curvatures are simply means of initializing the computer code so that it will run efficiently. The results of the computer calculations are described below.

6.1.3 Test results

The initially flat membrane deflections are shown in Fig. 6.4. The theoretical results, calculated as described in the Appendix with no initial tension, agree poorly with the measured results. Note, however, that the computer results and theoretical results agree well, indicating that the computer program is performing satisfactorily and that the discrepancy between theory and measurement is some uncontrolled factor in the measurement. A possible explanation for the discrepancy might be the tension required in the fabric to make the strip initially flat. We did not

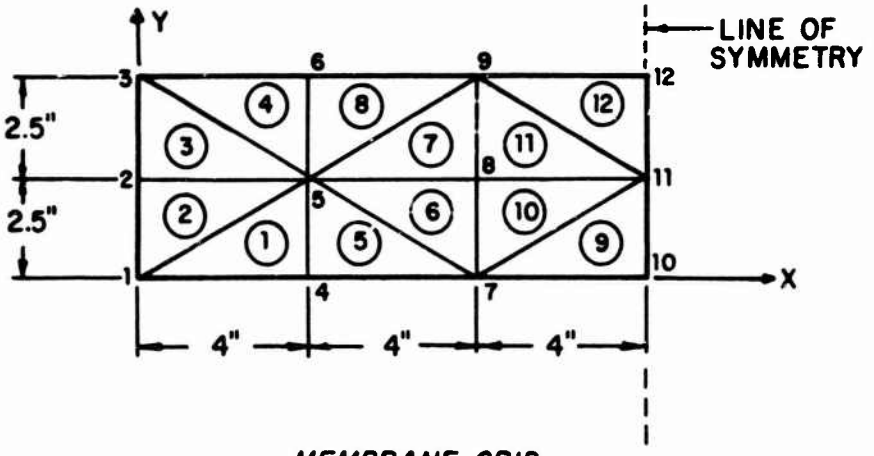

MEMBRANE GRID

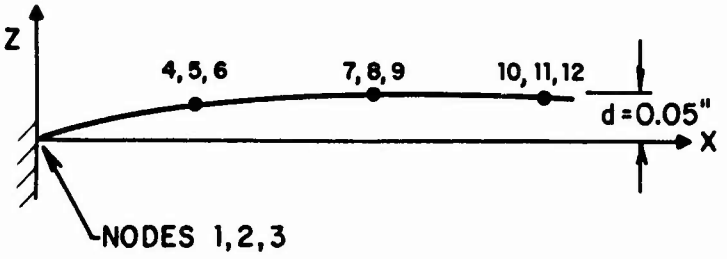

INITIALLY FLAT MEMBRANE

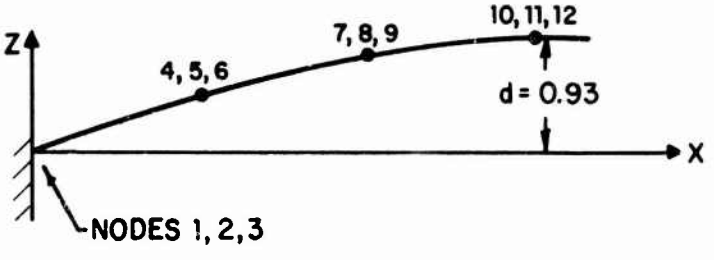

INITIALLY DISPLACED MEMBRANE

FIG. 6.3. FABRIC STRIP COMPUTER MODEL.

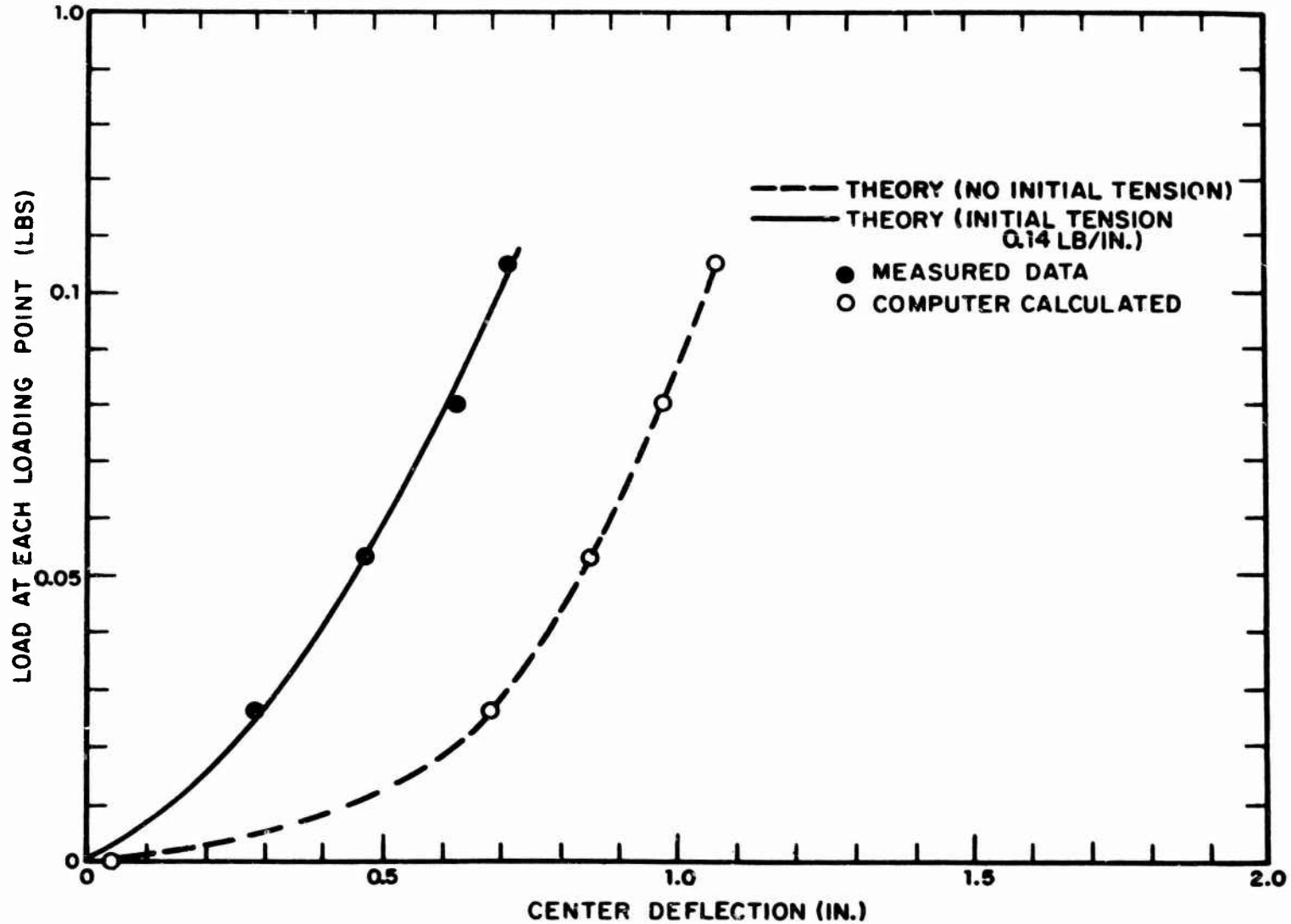

FIG. 6.4. DEFLECTION OF INITIALLY FLAT MEMBRANE.

measure the tension in the fabric for the initially flat case, but if we make a guess of 0.14 lb/in. and use that value in the theory of Sec. 2, we obtain the solid curve of Fig. 6.4, which agrees quite well with the data points. The deflection then appears to be quite sensitive to initial tension and the large discrepancy between measurement and theory appears to be due to neglect of that tension.

Also of interest is the deflection as a function of position in the membrane. Plotting the measured deflection divided by the measured center deflection in Fig. 6.5, we find that theory, computer program, and data all agree quite well.

The results of tests on an initially deflected membrane are shown in Fig. 6.6. The membrane's initial shape was nearly parabolic (in theory, it should be catenary) with a center deflection of 0.93 in. Note that the loads applied here are somewhat higher than in the undeflected membrane tests. The agreement between theory (see the Appendix) and measurement is not bad, although the measured points appear to be consistently higher. This may be due partly to creep. We noticed that after unloading the strip, the center deflection was ~100 mils greater than before loading, but that this deflection rapidly decreased to its original value with time. Again, the computer calculations agree closely with the simplified theory.

For the initially deflected membrane, we also measured the stresses in the fabric strip at two locations – at 1½ in. from the support (position No. 1) and at 8 in. from the support (position No. 2). Both sensors were mounted in the center of the width of the strip.

The comparison of predicted (see the Appendix) and measured fabric stresses is shown in Fig. 6.7. Theoretically, the fabric tension should be the same at positions 1 and 2. In fact, the fabric was supported only over 4¼ in. of its 5-in. width at the end supports. Since the fabric is coated and can be expected to have some shear strength, proper distribution of the load requires the tension per unit width at the center of the span of the strip (position 2) to be lower than that near the end supports. The dotted line in Fig. 6.7 corrects for this "apparent" width change by increasing the tension per unit width by a factor of $5/4.25 \approx 1.2$.* The open circle (position 1) should coincide

*Note that the measured tension at position 1 (rear supports) is a factor of ~1.3 larger than the tension at position 2 (near the center of the strip span), which agrees fairly well with this number.

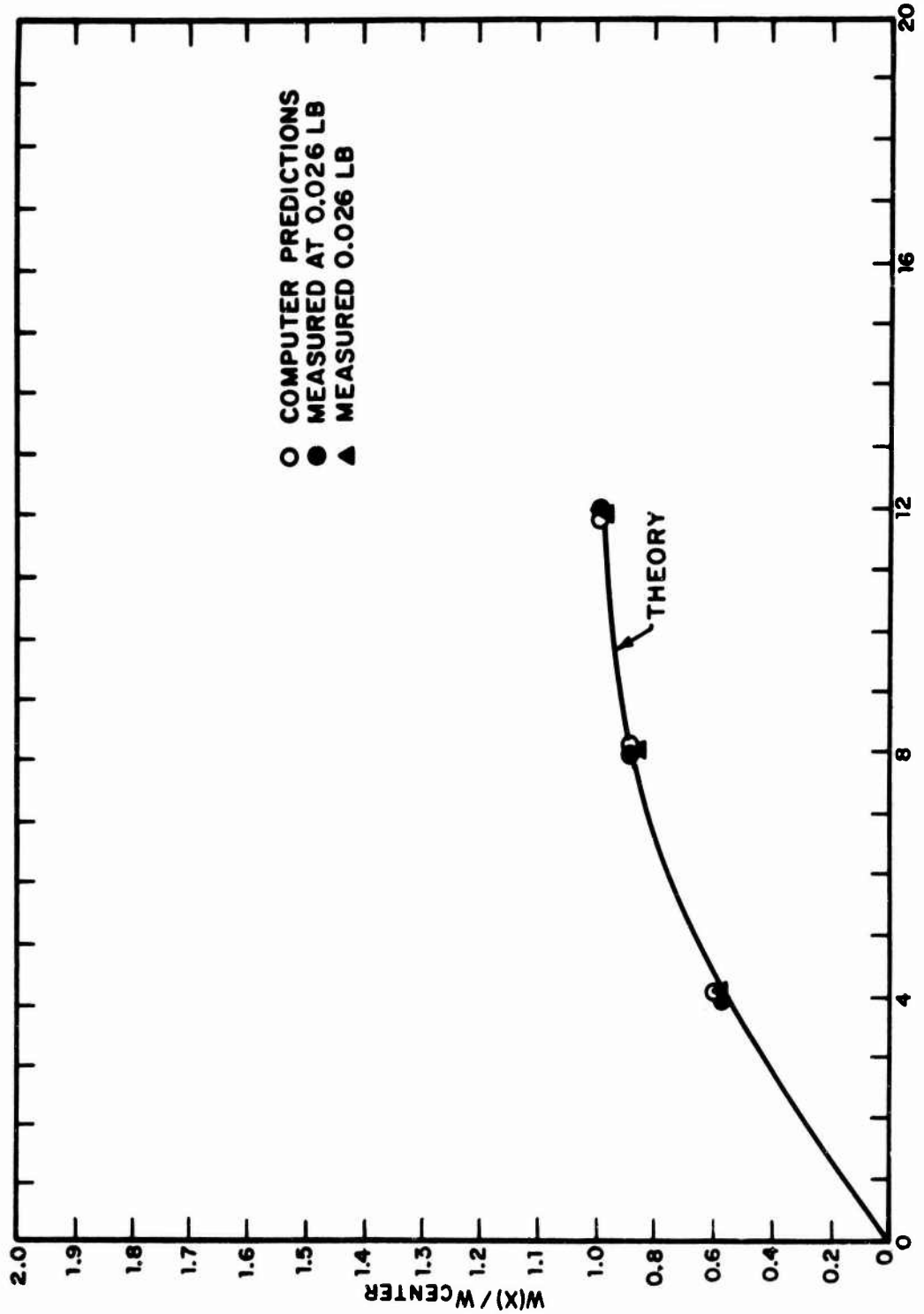

FIG. 6.5. STRIP DEFLECTION AS A FUNCTION OF POSITION.

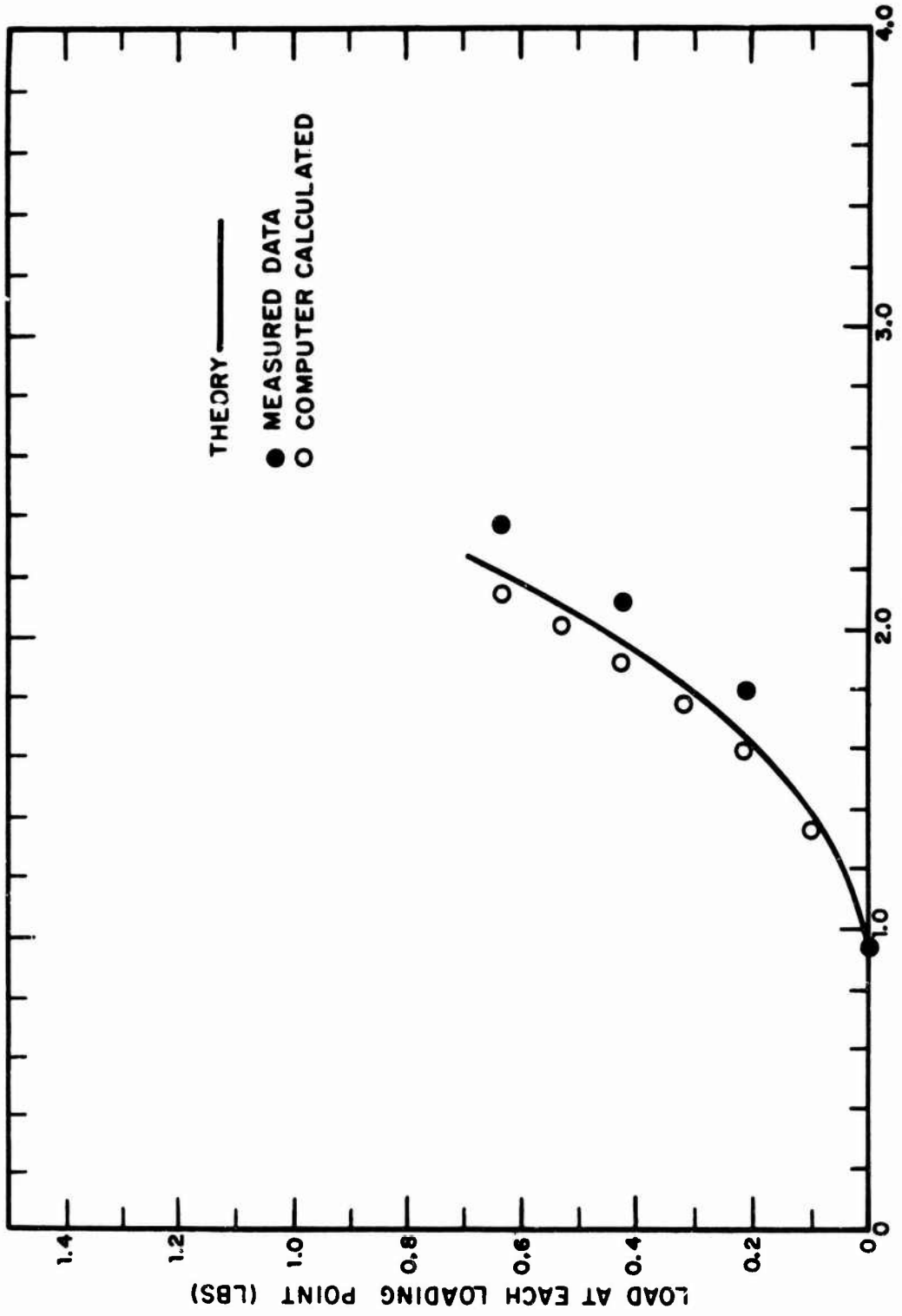

FIG. 6.6. STRIP DEFLECTION WITH AN INITIAL DEFLECTION OF 0.93 IN. AT THE CENTER.

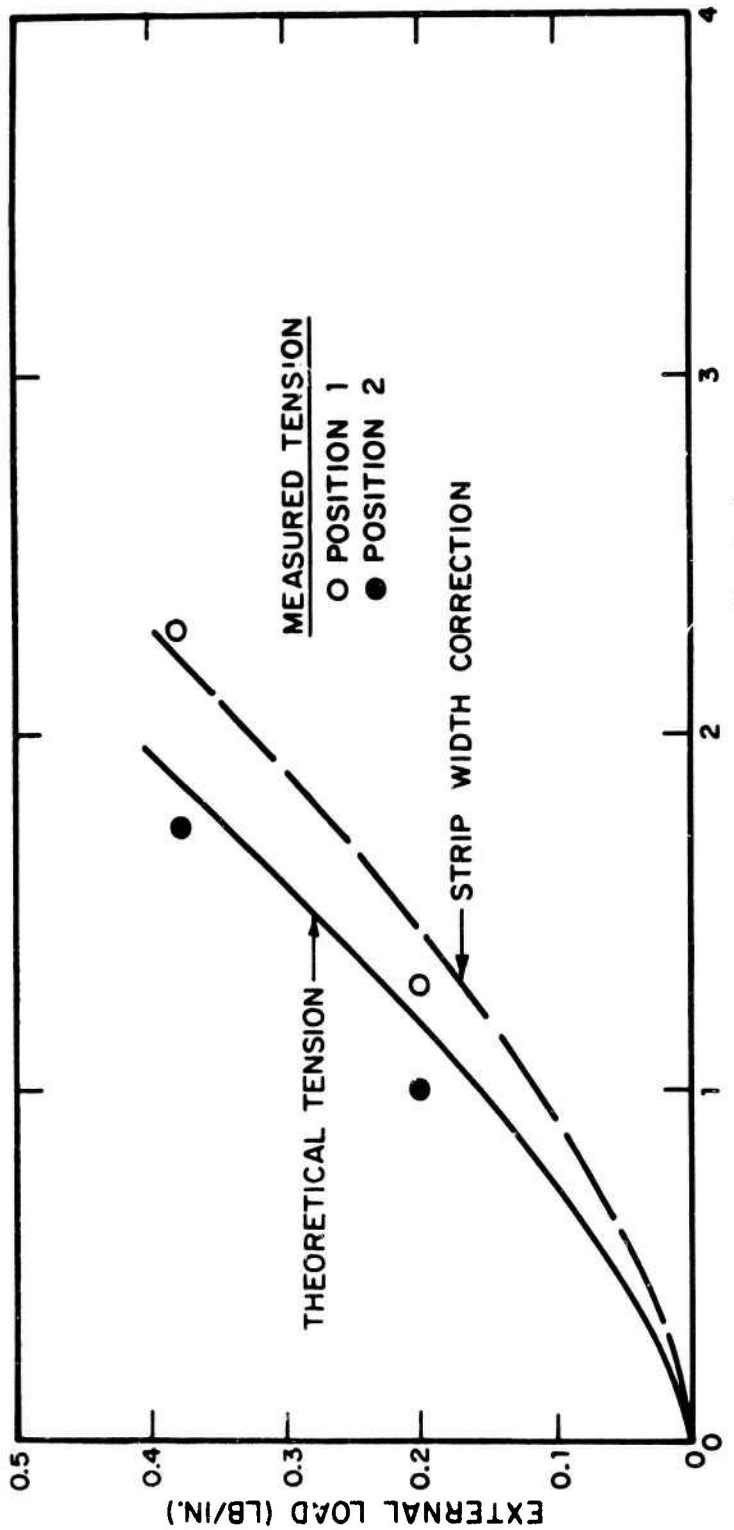

FIG. 6.7. COMPARISON OF THEORETICAL AND MEASURED FABRIC MEMBRANE STRIP TENSIONS.

with the dotted line and the solid circles should coincide with the solid line. We find, in fact, that prediction and measurement agree to within 10 to 20 percent.

6.2 Tent Frame Deflections

To check the ability of the computer code to deal with the deflections of the model tent frames, we performed a very simple test in which point loads were applied to both the slant-roof and the arch frames and the deflections were measured at the point of loading. The computer code was then exercised, and its predictions were compared with the measurements. In the following sections, we describe the computer code and the deflection measurements.

6.2.1 Slant-roof frame computer model

The detailed dimensions of the slant-roof model frame are described in Sec. 5. Figure 6.8 illustrates the computer model used. The dots represent the nodes of the structure and the adjoining number represents the node or joint number. Node 7 defines the point of load application. The boxed numbers are the beam element numbers.

Four computer models of the frame were set up to study the effect of beam-end conditions. In Model 1, it is assumed that the structure is completely built-in and that all joints can support torsional and bending moments. Model 2 differs from Model 1 in that Model 2 is assumed to be pin-jointed in the global z-direction at the base of the four column supports. In the actual scaled tent model, the joints that are screwed together are probably not 100% efficient.* Therefore, Model 3 was designed to simulate the frame behavior when screwed joints cannot support torsional or bending moments. Hence, beam elements 5 and 6 are truss elements and beam elements 11 and 12 have been moment-end released at nodes 5 and 6. Model 4 was developed to simulate a very flexible structure. It was assumed that the base of the columns were built-in and that all other beam joints were ball joints. This model can only support a global x and y load. The material properties for all models were $E = 10^7$ psi and $\nu = 0.333$. All beams in the frame have the same relevant geometric properties:

---

*This implies that the joints are not rigid; i.e., the angle between adjoining beams is not constant under load.

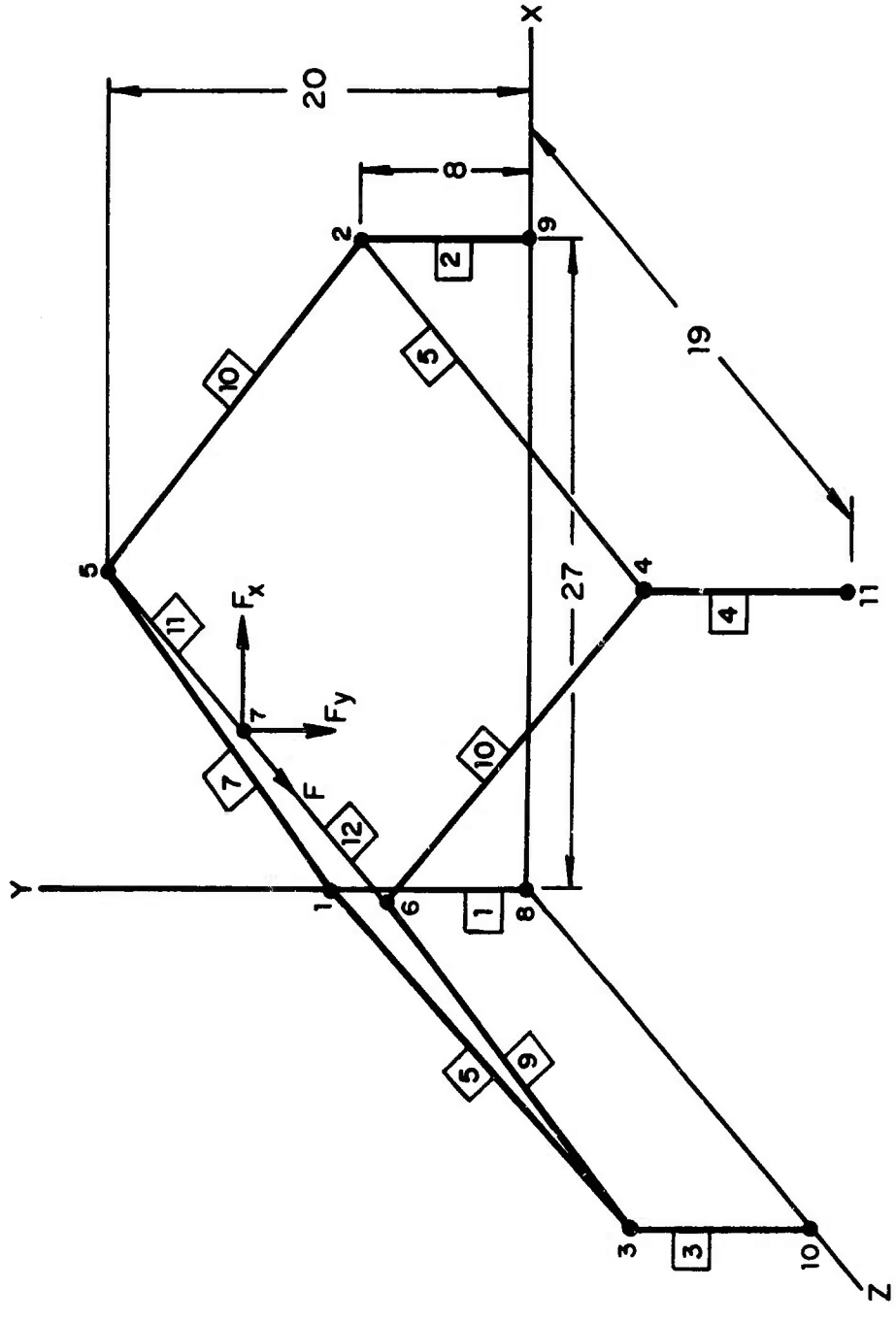

FIG. 6.8. SLANT-ROOF FRAME COMPUTER MODEL.

cross-sectional area	0.0625 in.^{4}
cross-sectional dimension	0.25 in. × 0.25 in.
bending moment of inertia	3.26 × 10^{-4} in.^{4}

6.2.2 Arch-roof frame computer model

The detailed dimensions of the arch-roof model frame are given in Sec. 5. Figure 6.9 illustrates the computer model used to predict the frame deflections. Note that we can make use of symmetry and thus model only one half of the frame. The numbers at each node are the node designations, and the numbers in boxes at each beam represent the beam designation.

We consider three different models to study the effects of joint efficiencies. Model 1 has all joints built in. Model 2 is similar to Model 1 except that joints 1 and 16 are pin-released about the global y-axis; i.e., these joints cannot support a bending moment about the y-axis. Model 3 is similar to Model 2 except that node 8 is "ball-jointed"; i.e., it cannot support a moment in the x, y, or z direction.

The material properties are the same as for the slant roof model. Different geometric properties are required for the arches and purlins:

arch cross-sectional areas	.045 in.^{2}
purlin cross-sectional areas	.035 in.^{2}
arch cross-sectional dimensions	0.34 in. × 0.187 in.
purlin cross-sectional dimensions	0.187 in. × 0.187 in.
arch bending moment of inertia	6.12 × 10^{-4} in.^{4} and 1.87 × 10^{-4} in.^{4}
purlin bending moment of inertia	1.03 × 10^{-4} in.^{4}

The thinnest dimension of the arch cross section is in the y-direction. For this case only two loads were applied in the computer model (in the x- and z-direction), as shown in Fig. 6.9.

6.2.3 Model tests

The tests performed on the scale model frames were quite simple. A weight was hung by a wire from the point on the model frames corresponding to the loading point in the

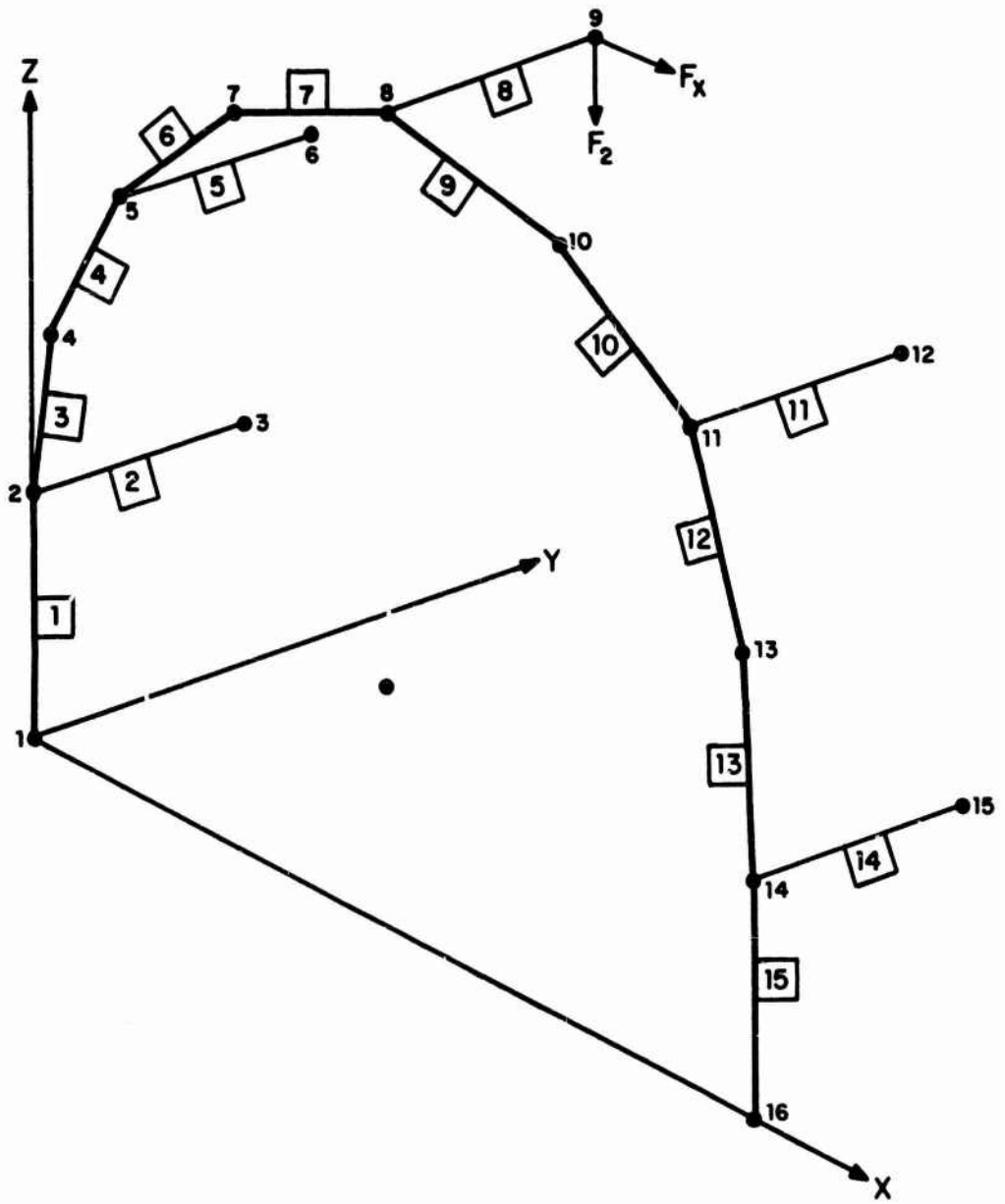

FIG. 6.9. ARCH ROOF FRAME COMPUTER MODEL.

computer calculations. By changing the orientation of the frame, we could vary the direction of application of the load to correspond with that in the computer simulation. A scale was used to measure the deflections relative to a fixed reference in the direction of load application. Loads up to 6 lb were applied to the frames and since the deflections were linearly related to the loads, all deflections were normalized to a 1-lb load. The results normalized to a 1-lb load for the slant roof frame in the x, y, and z directions of Fig. 6.8 were

$$\delta_x = 22 \text{ mils}$$

$$\delta_y = -25 \text{ mils}$$

$$\delta_z = 100 \text{ mils} .$$

The same results for the arch roof frame were

$$\delta_x = 22 \text{ mils}$$

$$\delta_y = 20 \text{ mils} .$$

Comparison with computer predictions is shown in Figs. 6.10 and 6.11. Although we tried to make the feet of the frames appear pinned, the x-direction loads in Figs. 6.10 and 6.11 indicate that they are somewhere between pinned and built-in. The y-direction deflections in Fig. 6.10 and the z-direction deflections in Fig. 6.11 indicate that the arch-to-purlin connections for both frames are somewhere between rigid and pinned. At the present time, the computer code has no provision for dealing with this problem. Clearly, then an extension of the present code is needed to allow for "joint efficiencies",* since real tent frames will probably present similar modeling difficulties.

---

*A joint with an efficiency of 1 is rigid; i.e., a rotation of one beam at the joint produces an equal rotation in the adjoining beam at that joint. A joint with an efficiency of zero is pinned and can transmit no moment.

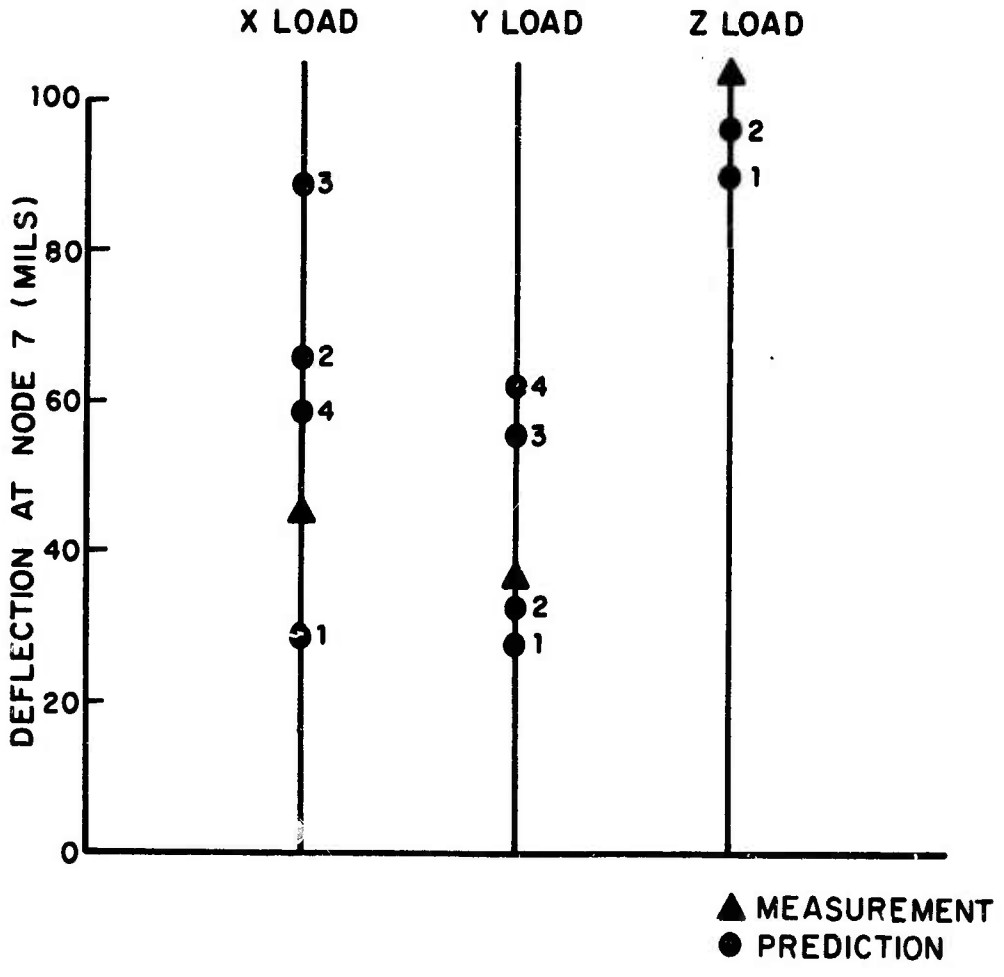

FIG. 6.10. SLANT ROOF FRAME DEFLECTIONS.

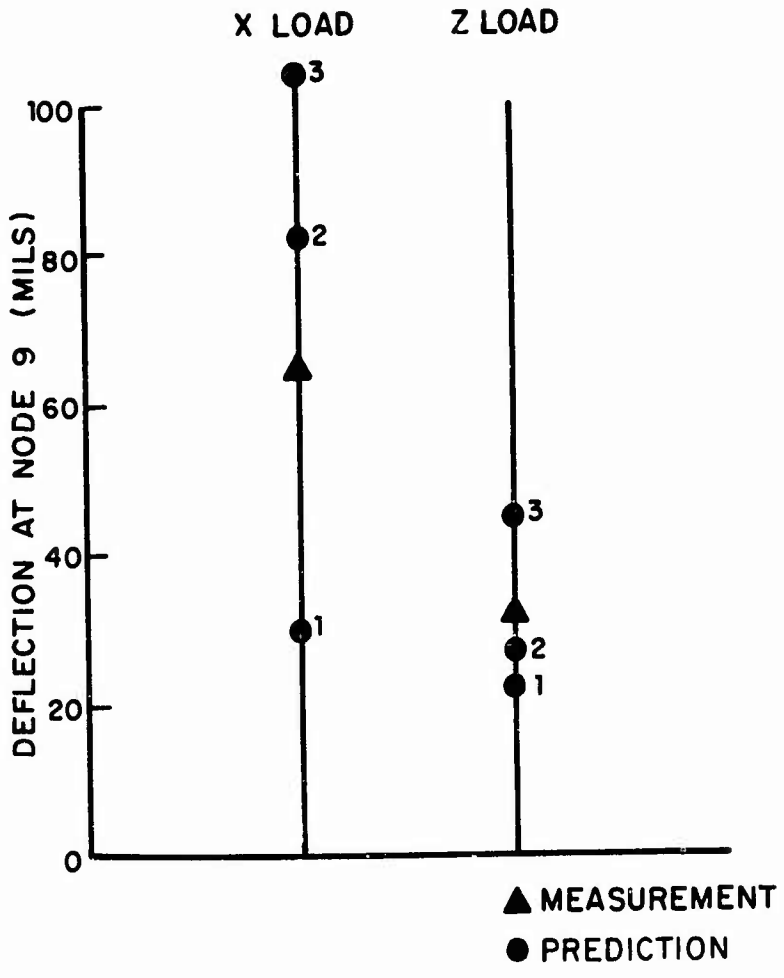

FIG. 6.11. ARCH ROOF FRAME DEFLECTION.

6.3 Two-Dimensional Fabric Membrane

To assess the effectiveness of the computer code in dealing with the mechanics of the fabric (including the nonlinear biaxial stress/strain formulas of Sec. 4.2), we devised a test in which a rectangle of the 2.6-oz cotton typewriter ribbon cloth was suspended from a rigid frame. The fabric was then loaded with a distributed load perpendicular to its plane, and the resulting stresses and deflections were compared with the computer code predictions. In this section, we discuss the results of that comparison.

6.3.1 Testing procedure

The test used a membrane of 2.6-oz typewriter ribbon cloth suspended from a rigid rectangular (17 in. × 20 in.) frame constructed from 2 × 4 lumber as shown in Fig. 6.12. To clamp the fabric to the frame, we screwed a wooden strip to the top of the frame at all four sides and compressed the fabric between the strip and two lengths of 1/8-in. drill rod laid along the full length of the frame on all four sides.

We applied load by laying bags containing lead shot on the fabric. The bags were approximately 4 in. × 20 in. long and were sewn together so that they contained many small compartments for maintaining an even distribution of the shot along the length of the bag. Each bag weighed ~2.5 lb; four bags were required to cover the entire surface of the fabric. One, two, and three layers of bags were used, resulting in total loads of 10, 20, and 30 lb (a maximum load of 13 lb/ ft^2).

The fabric was suspended from the frame in such a way that there was an unloaded center deflection of ~1.3 in. The computer code requires the initial (unloaded) shape of the membrane in order to predict its deflection under load. Before measuring this quantity, we fully loaded the fabric a number of times to obtain a repeatable initial shape. This initial shape was measured with a depth gauge from an aluminum rod (1 in. sq) laid across the frame. We defined the initial deflection by measuring the depth from the rod to the fabric at points interior to the fabric and appropriately subtracting the depth from the rod to the fabric where the fabric joins the frame (see Sec. 6.3.2).

The same procedure was used for measuring the deflection under load. Deflections were recorded at each of the three load levels (10, 20, and 30 lb). In addition, the

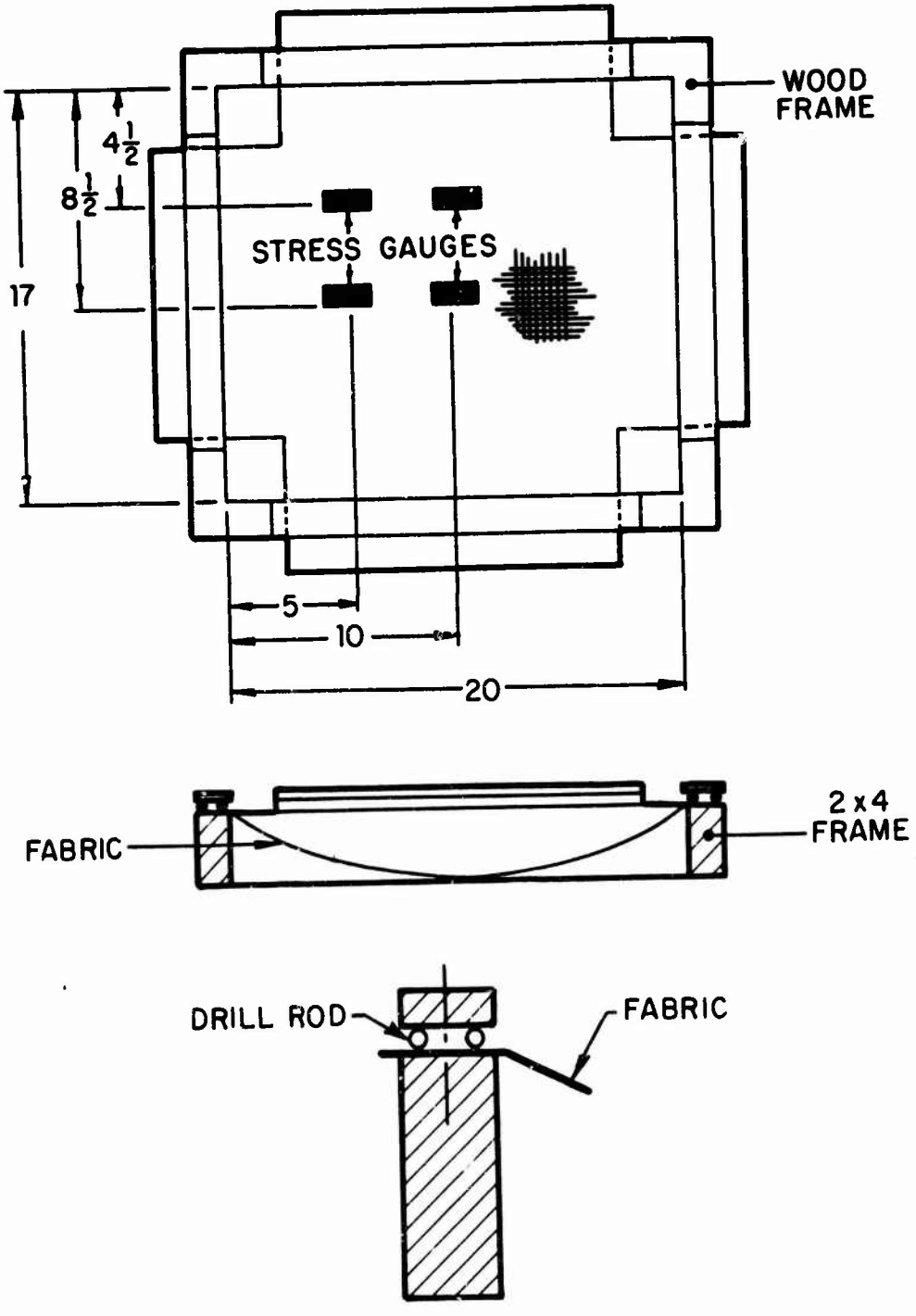

FIG. 6.12. FABRIC FRAME TEST ARRANGEMENT.

stress gauges described in Sec. 4.3 were attached to the fabric at the 4 locations shown in Fig. 6.12. The gauges were oriented in the warp direction (measuring warp stress only) and the lead shot bags were laid between them. The computer model and the results of these measurements are discussed below.

6.3.2 Computer model

The grid for the finite element computer code is shown in Fig. 6.13. The numbers in circles at the center of each triangle designate the element number. The numbers at the junction of the triangles designate the node numbers. Note that only one-quarter of the membrane has been modeled. The symmetry of the initial membrane shape during the testing described above makes this simplification possible. The warp direction of the fabric corresponds to the x axis in Fig. 6.13. The x and y axes define the rigid boundary of the membrane where all deflections are defined as zero. At the other two boundaries of the membrane, symmetry determines the boundary conditions; i.e., for

nodes 2, 3, 4 – the y deflection is zero,

nodes 10, 15, 20 – the x deflection is zero,

node 5 – both x and y deflections are zero.

In order to apply the distributed load to the membrane, the computer applies point loads at each node interior to the membrane. No loads are applied to the nodes at the rigid boundary. If the entire membrane had been modeled, there would have been 49 interior nodes. As a result, at the full load of 30 lb, 1/49 × 30 is applied to each of nodes 2, 3, 4, 5, 7, ··· 18, 19, 20.

One difficulty was encountered in interpreting the computer predictions. The computer code outputs deflections at each node. During the testing, deflections were measured at positions corresponding to nodes 3, 5, and 15. This arrangement makes comparison of measurements and predictions quite convenient. Stresses are referred to an element, and the membrane element is such that the stress throughout the element is constant. Thus, there can be step changes in stress at each element boundary. The stress gauges described in the previous section were attached to the fabric at positions that correspond to nodes 3, 5, 13, and 15. Relating these measurements to computer predictions requires averaging the stress in each computer element contiguous to those nodes.

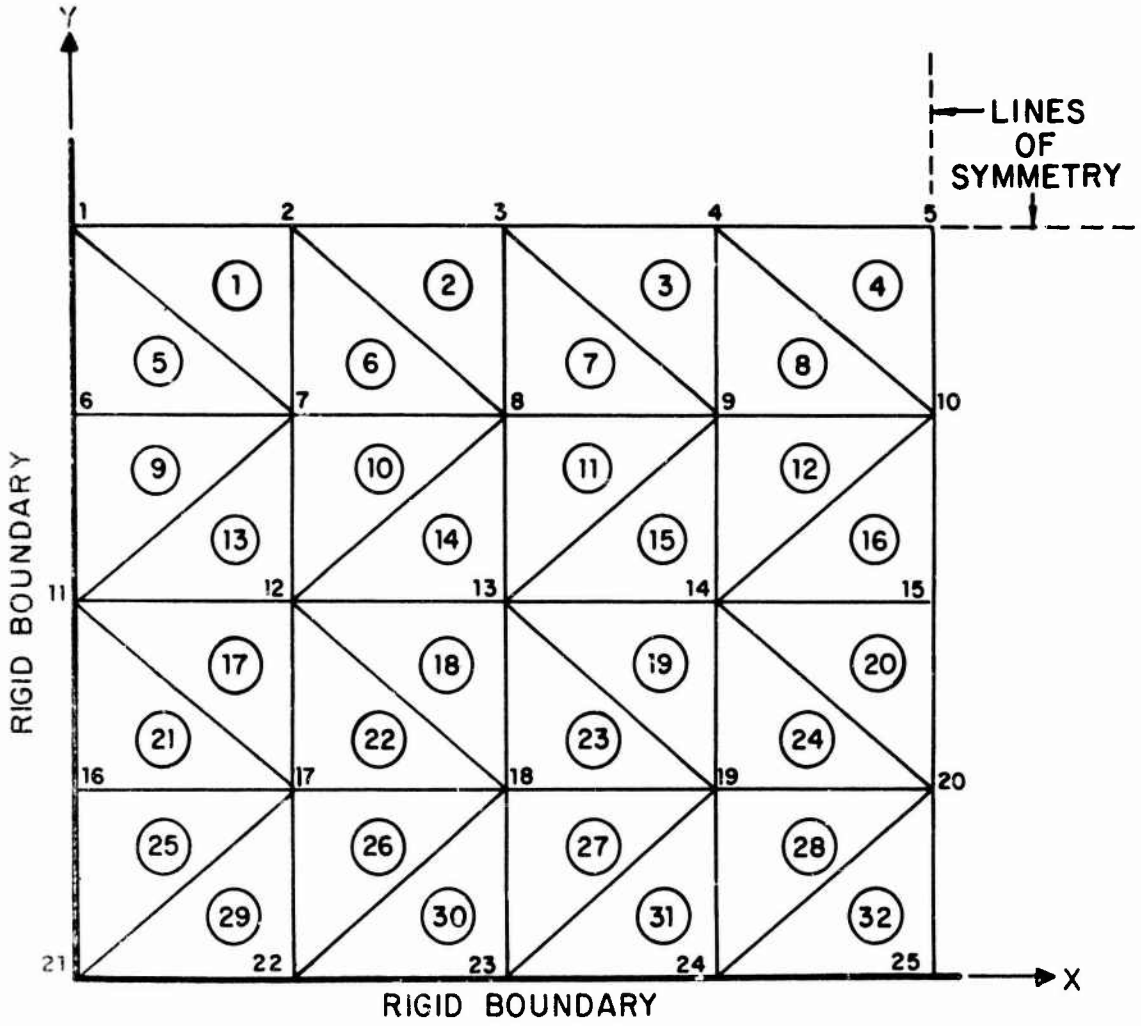

FIG. 6.13. COMPUTER MODEL OF THE 2-D FABRIC MEMBRANE.

Discrepancies can result, if there are large changes in stress across an element boundary.

A further difficulty was encountered in inputting the initial deflections of the membrane. With the measurements used to define the initial shape, the computer code had difficulty in converging. By smoothing this data, we were able to obtain good convergence, although the error in the initial deflections of the membrane introduced by this procedure resulted in deflection errors under load. The initial shape of the membrane is given in Table 6.1, where the nodes refer to Fig. 6.13. The measured data from which these values were derived are given in Table 6.2. All the z positions are referenced to node 1.

6.3.3 Results

In general, the deflections measured during the tests described above agree well with computer code predictions, as is shown in Figs. 6.14 and 6.15. For the three positions shown in Fig. 6.14, the computer code consistently underestimates the measured deflections – primarily because of the smoothing procedure applied to the initial deflections. Figure 6.15 indicates that the code adequately predicts the shape of the fabric membrane at the centerline of the fabric.

The predicition of stresses is considerably less reliable. The measured and predicted stresses at node 5 in the center of the membrane agree quite well, but, unfortunately, this is the only place where the agreement is good. It is apparent that after smoothing the initial unloaded shape of the membrane, we should have expected this result. For example, suppose that in the unloaded state there is a dimple in the fabric and, unknowingly, we place a stress sensor in this dimple. Since we do not place the lead shot-filled bags directly on top of the sensor, it is conceivable that the dimple will not have much load applied to it: Yarns surrounding the dimple must be stretched considerably before the yarns running through the dimple can develop any stress. It is therefore to be expected that under such conditions our sensor will (initially at least) measure very little stress.

In setting up the computer program, we used a fairly coarse grid and smoothed measurements of the initial unloaded shape of the membrane at the nodes of that grid. The coarseness of the grid and the smoothing process would probably prevent any such dimple being entered into the computer calculations, thereby making it impossible for the code to

TABLE 6.1. NODAL POINT INPUT DATA.

Node No.	Boundary Condition Codes						Nodal Point Coordinates			
	X	Y	Z	XX	YY	ZZ	X	Y	Z	
1	1	1	1	1	1	1	0.000	8.875	0.000	-0
2	0	1	0	1	1	1	2.500	8.875	- .850	-0
3	0	1	0	1	1	1	5.000	8.875	-1.200	-0
4	0	1	0	1	1	1	7.500	8.875	-1.270	-0
5	1	1	0	1	1	1	10.000	8.875	-1.290	-0
6	1	1	1	1	1	1	0.000	6.656	0.000	-0
7	0	0	0	1	1	1	2.500	6.656	- .800	-0
8	0	0	0	1	1	1	5.000	6.656	-1.100	-0
9	0	0	0	1	1	1	7.500	6.656	-1.190	-0
10	1	0	0	1	1	1	10.000	6.656	-1.210	-0
11	1	1	1	1	1	1	0.000	4.438	0.000	-0
12	0	0	0	1	1	1	2.500	4.438	- .650	-0
13	0	0	0	1	1	1	5.000	4.438	- .920	-0
14	0	0	0	1	1	1	7.500	4.438	- .980	-0
15	1	0	0	1	1	1	10.000	4.438	-1.000	-0
16	1	1	1	1	1	1	0.000	2.219	0.000	-0
17	0	0	0	1	1	1	2.500	2.219	- .500	-0
18	0	0	0	1	1	1	5.000	2.219	- .600	-0
19	0	0	0	1	1	1	7.500	2.219	- .650	-0
20	1	0	0	1	1	1	10.000	2.219	- .680	-0
21	1	1	1	1	1	1	0.000	0.000	0.000	-0
22	1	1	1	1	1	1	2.500	0.000	0.000	-0
23	1	1	1	1	1	1	5.000	0.000	0.000	-0
24	1	1	1	1	1	1	7.500	0.000	0.000	-0
25	1	1	1	1	1	1	10.000	0.000	0.000	-0

TABLE 6.2. MEASURED UNLOADED INITIAL FABRIC SHAPE.

Node No.	z Location of Node (in.)
1	0
2	-0.80
3	-1.24
4	-1.27
5	-1.29
6	+0.01
7	-0.84
8	-1.19
9	-1.20
10	-1.21
11	+0.06
12	-0.80
13	-1.03
14	-0.98
15	-1.00
16	-0.01
17	-0.65
18	-0.67
19	-0.61
20	-0.58
21	-
22	+0.01
23	-0.01
24	0
25	-0.01

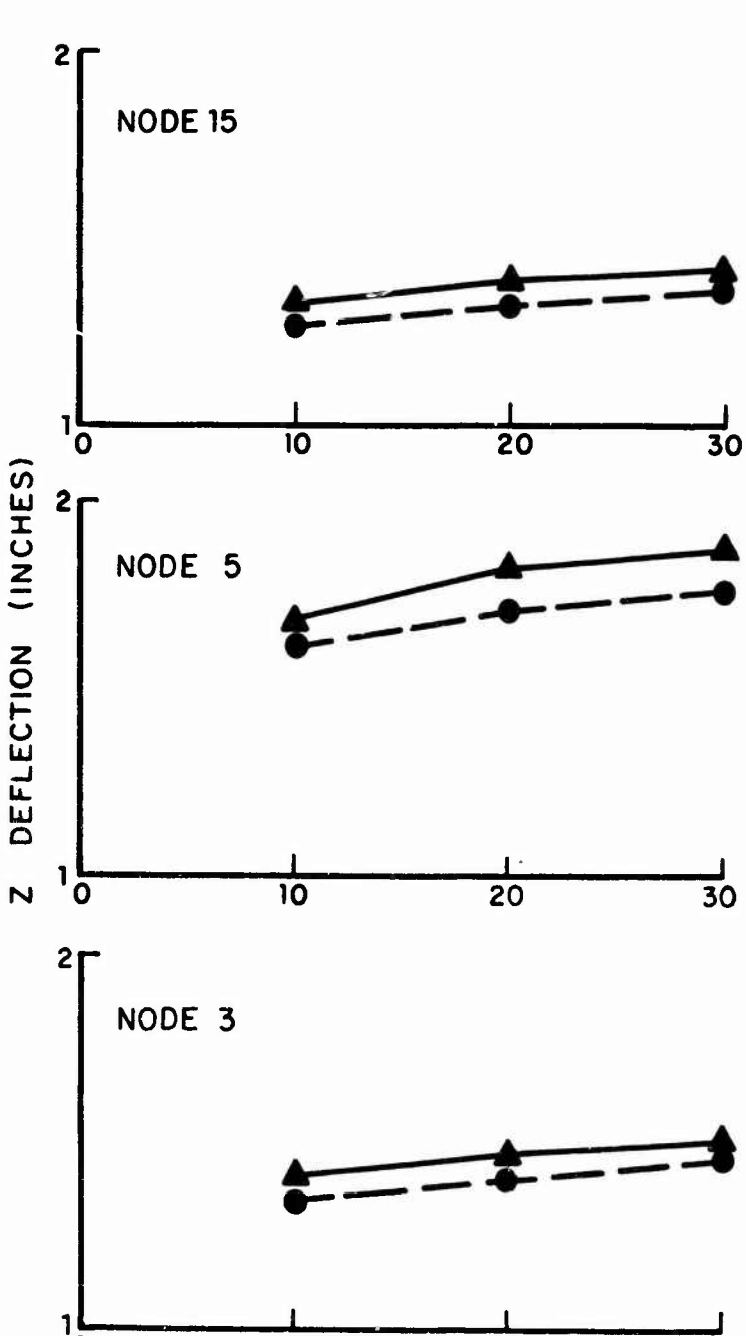

FIG. 6.14. COMPARISON OF PREDICTED AND MEASURED DEFLECTIONS.

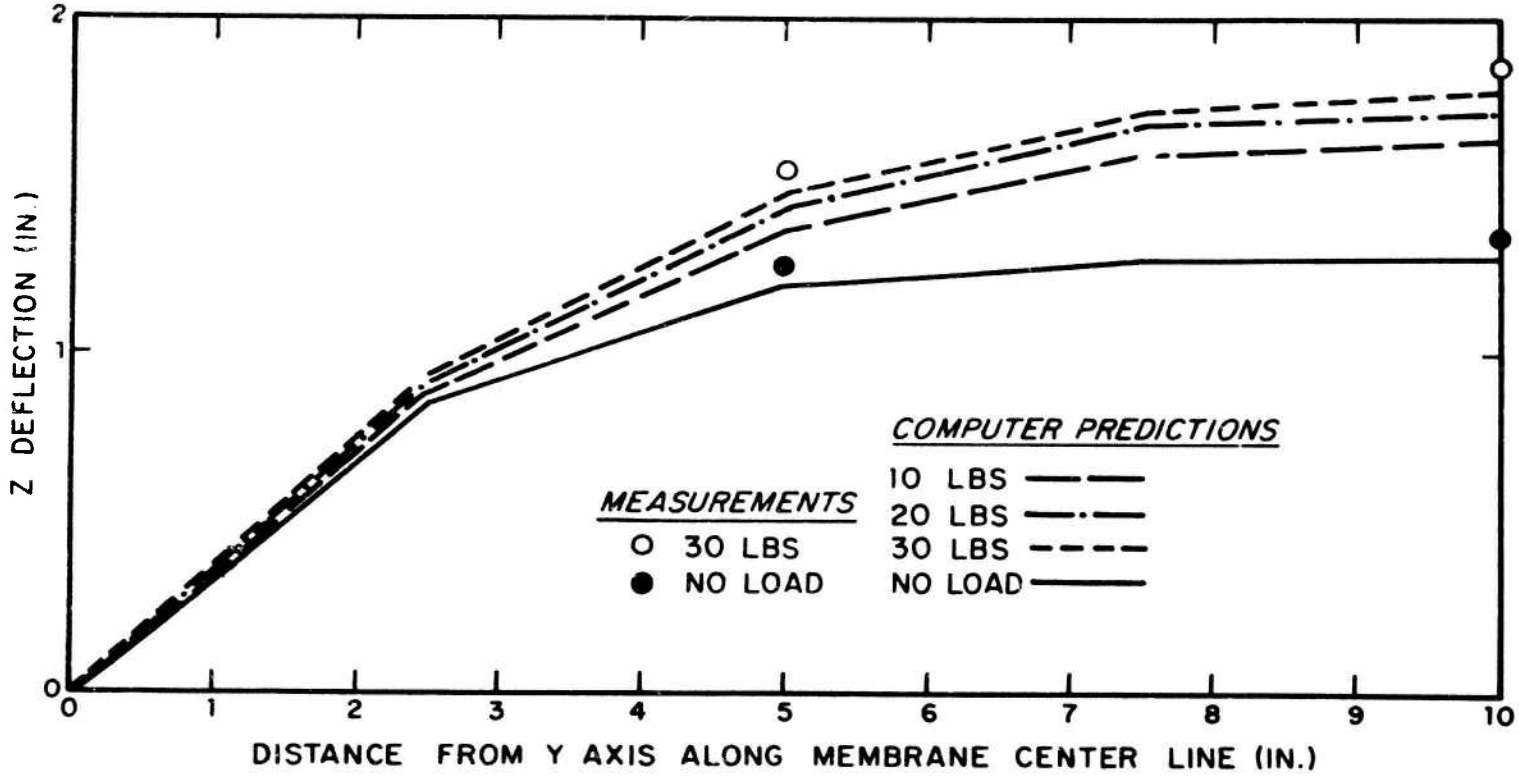

FIG. 6.15. COMPARISON OF MEASURED AND PREDICTED DEFLECTIONS ALONG THE CENTER LINE OF THE FABRIC NODE 1, 2, 3, 4, 5.

predict local regions of low stress in the dimple or possible high stress on the periphery of the dimple. These arguments have considerable implications for using computer codes for the design of frame-supported tents. Clearly, a detailed knowledge of the unloaded shape of the fabric is necessary if stress concentrations in the fabric are to be predicted. Since this detailed shape is extremely difficult, if not impossible, to predict *a priori*, some sort of a safety factor must be introduced for sizing a fabric based on the computer predicted stresses.

Finally, a brief word about the stress measurements at node 13 is in order. Note that Fig. 6.16 says that very low (essentially zero) stresses were measured there. If we carefully examine the computer predictions, we find (see Fig. 6.13) that the stresses in elements 21, 22, 23, and 24 (4 membrane elements in a row beside node 13) are also very low. This result provides considerable confidence in the computer code. By the same token, however, nowhere does the computer code predict the high stresses measured at node 15.

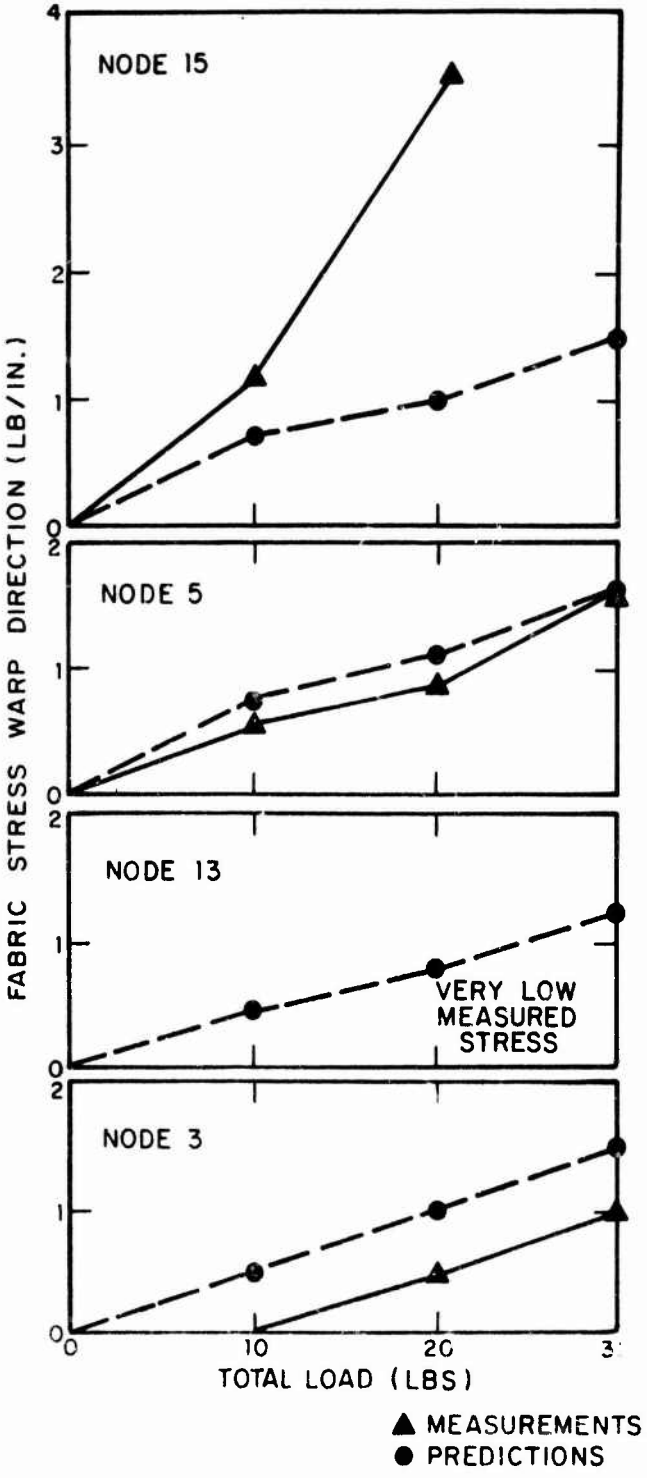

FIG. 6.16. COMPARISON OF MEASURED AND PREDICTED STRESSES.

7. FINAL VERIFICATION OF THE COMPUTER CODE

In this section, we discuss a number of deflection measurements made on the frame and fabric of the model frame-supported tents described in previous sections and compare those measurements with computer code predictions. Initially, we planned to make detailed measurements of stress in both the frame and fabric, but the results described in the previous section discouraged us from this approach. In particular, the need for the inclusion of joint efficiencies in the computer code to obtain adequate agreement of measured and predicted frame deflections indicated that detailed measurements are not justified at this time.

7.1 Computer Models

The grids for the computer models of the slant-roof and arch-roof test models are shown in Figs. 7.1 and 7.2, respectively. Because the tents are symmetrical, only one-half of each was modeled. The numbers at each dot are the node designations, the numbers in the boxes are the beam element designations, and the numbers in the circles are the membrane (fabric) element designations. In both models, fabric was attached to only a small portion of the frame. Only one-half of the roof of the slant-roof frame was covered with fabric, and only about 45° of the arch of the arch-roof frame. In both cases, the fabric was assumed to be attached to the centroids of the beams. In the tests described below, the loading, which is applied vertically (z direction) and is distributed over the fabric, is modeled as a number of equal discrete vertical loads applied to all fabric nodes.

In the slant-roof frame model, all joints are rigid with the exception of the feet of the model, nodes 18 and 19; these are allowed to freely rotate about the Y axis (pinned joints). Also the beam 4 connection to node 3 is taken as pinned about the Y axis. The arch-roof frame model is similar, with pinned joints about the Y axis at nodes 1 and 21. The geometric properties of the beams in both models are the same as used in Sec. 6.2. The fabric is modeled as having the biaxial stress/strain equation of state developed in Sec. 4.2.

7.2 Model Tent Tests

To test the model tents, we attached fabric to the two model frames, as described in Sec. 5. (Note that a number of purlins were removed from the arch-roof frame, Fig. 7.2,

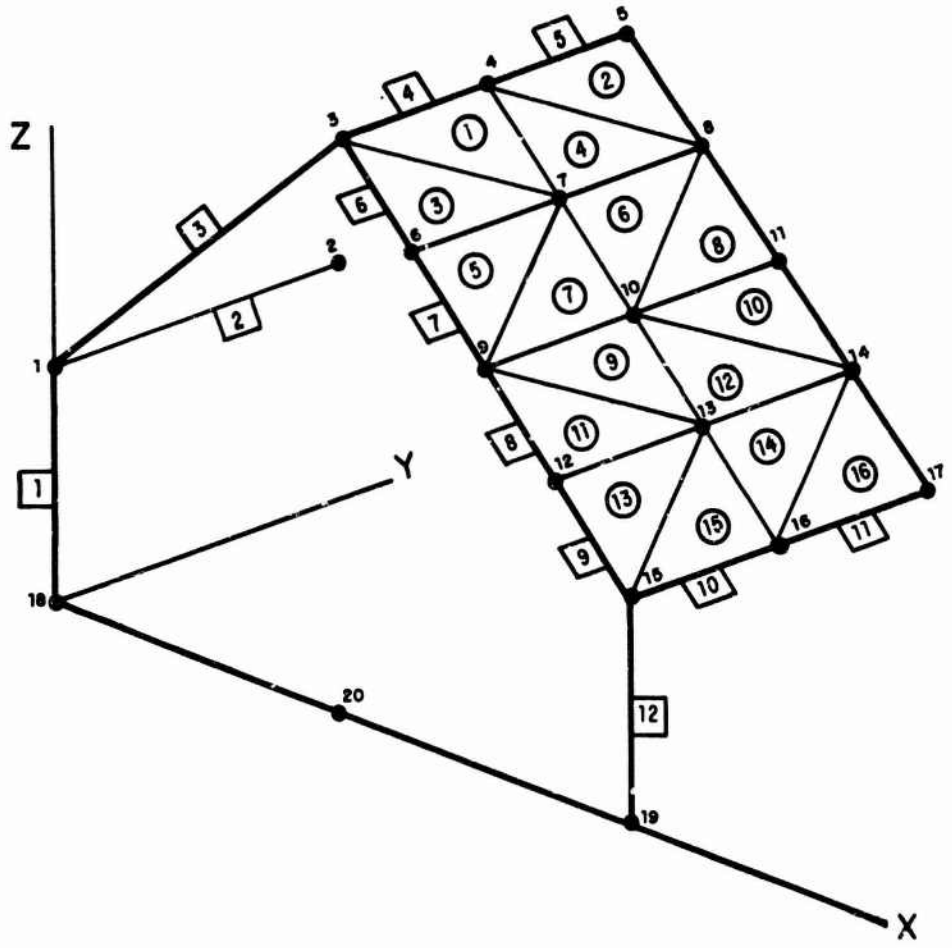

FIG. 7.1. SLANT ROOF TENT COMPUTER MODEL.

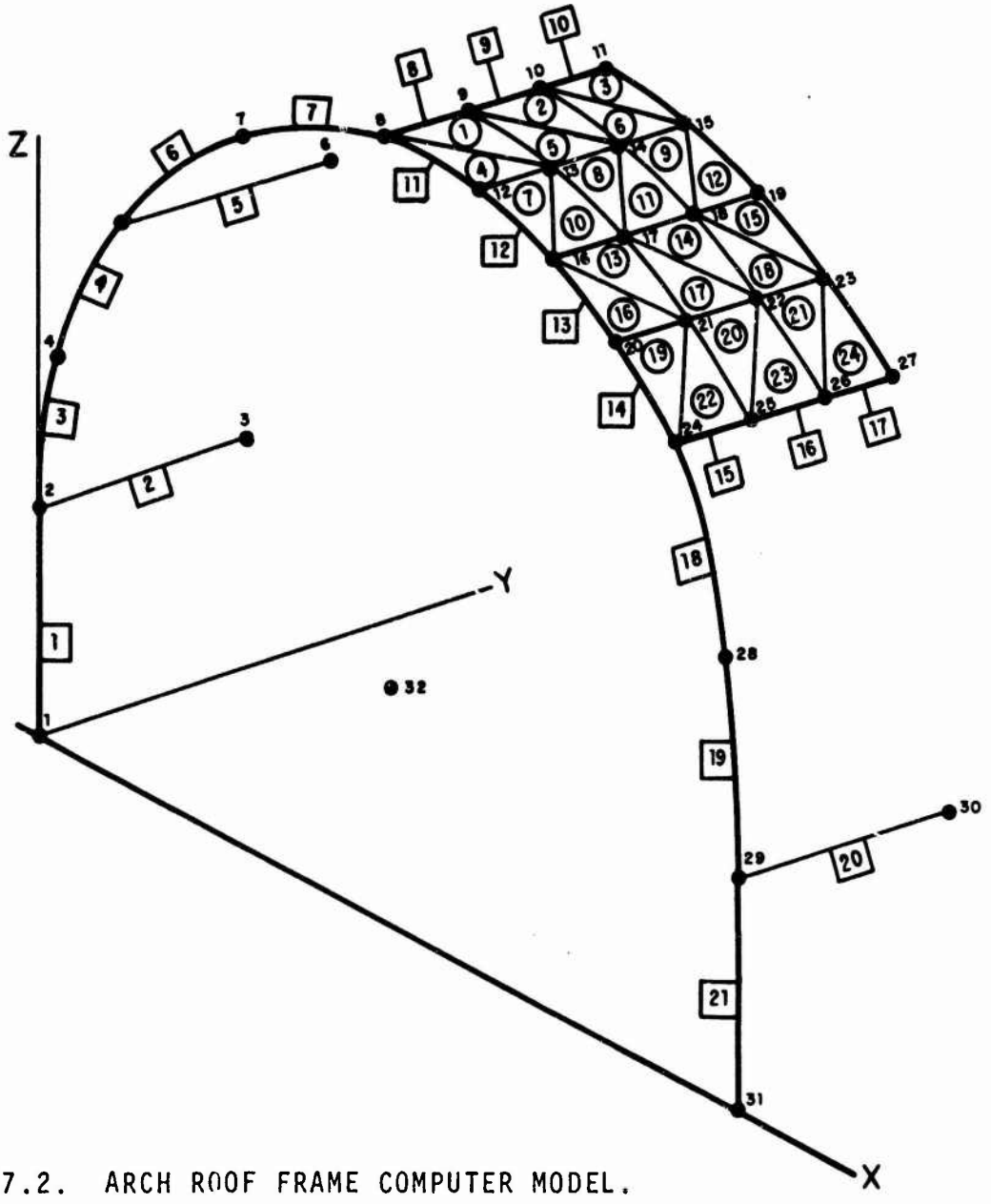

FIG. 7.2. ARCH ROOF FRAME COMPUTER MODEL.

to make it easier to measure frame and fabric deflections.) The computer models illustrated Figs. 7.1* and 7.2 show where the fabric was attached to each model. Each of the four edges of the fabric was folded over and sewn to form a narrow tube. Notches approximately 1 in. square were then cut out of the corners of the fabric to facilitate attachment at the corners and to minimize wrinkling. By disassembling the frame, we could insert the appropriate beams of the frame into these tubes and then reassemble the frame. This method of attaching fabric to frame resulted in the fabric loading the beams approximately through their centroids.

The fabric in both frames was sized so that it would lie slack in the frame. As a result, it was necessary, for input to the computer program, to measure the position of the fabric relative to the frame, as described in Sec. 6.3. We determined the initial unloaded fabric position at each of the fabric grid points shown in Figs. 7.1 and 7.2 after loading the fabric a number of times to take out any slack. The loading was accomplished, as in Sec. 6.3, by laying long bags filled with lead shot on the fabric. The slant-roof fabric initial unloaded position at, say, node 7 (see Fig. 7.1) was measured by laying a straight edge on the frame along the line 6-7-8 and measuring, with a depth gauge at node 7, perpendicular to the plane of the frame (the plane defined by nodes 5-3-15). These measurements are given in Table 7.1. A simple computer program transformed the measurements to the global coordinates of Fig. 7.1. Similar measurements were performed on the arch-roof frame, except that we measured the distance to the fabric at the node of interest in the radial direction (toward the center of the circle that forms the arch), using a straight edge resting on the two arches of the frame. These measurements are given in Table 7.2. Again, a simple computer program transformed these measurements to the global coordinates of Fig. 7.2. These data were smoothed to facilitate convergence of the computer code. The initial fabric position for the two tents used in the code is given in Tables 7.3 and 7.4.

The frames were then each placed on the bed of a milling machine and the fabric was loaded. By attaching a pointer to the head of the milling machine, placing the pointer on the frame or fabric with no load, applying the load, and moving the bed of the milling machine until the

*Fig. 7.1 shows loads applied to nodes 3 through 17. The load at each node is the total load divided by 25.

TABLE 7.1. MEASURED UNLOADED INITIAL FABRIC SHAPE IN THE SLANT-ROOF FRAME.

Node No.	Distance to the Fabric in Inches Perpendicular to the Plane Formed by Nodes (5-3-15) in Fig. 7.1
7	0.52
8	0.51
10	0.73
11	0.69
13	0.62
14	0.64

TABLE 7.2. MEASURED UNLOADED INITIAL FABRIC SHAPE IN THE ARCH-ROOF FRAME.

Node No.	Distance to the Fabric in Inches in the Radial Direction From the Cylindrical Surface Formed by the Two Arches
13	0.59
14	0.75
15	0.88
17	0.63
18	0.78
19	0.82
21	0.73
22	0.98
23	1.04

TABLE 7.3. INITIAL FABRIC POSITION IN SLANT-ROOF FRAME.

Node No.	Boundary Condition Codes						Nodal Point Coordinates			
	X	Y	Z	XX	YY	ZZ	X	Y	Z	
1	0	0	0	0	0	0	0.000	0.000	7.750	-0
2	0	1	0	1	0	1	0.000	9.500	7.750	-0
3	0	0	0	0	0	0	13.500	0.000	19.750	-0
4	0	0	0	0	0	0	13.500	4.750	19.750	-0
5	0	1	0	1	0	1	13.500	9.500	19.750	-0
6	0	0	0	0	0	0	16.863	0.000	16.760	-0
7	0	0	0	1	1	1	16.631	4.750	16.499	-0
8	0	1	0	1	1	1	16.581	9.500	16.443	-0
9	0	0	0	0	0	0	20.227	0.000	13.771	-0
10	0	0	0	1	1	1	19.871	4.750	13.370	-0
11	0	1	0	1	1	1	19.828	9.500	13.322	-0
12	0	0	0	0	0	0	23.590	0.000	10.781	-0
13	0	0	0	1	1	1	23.258	4.750	10.407	-0
14	0	1	0	1	1	1	23.241	9.500	10.389	-0
15	0	0	0	0	0	0	27.000	0.000	7.750	-0
16	0	0	0	0	0	0	27.000	4.750	7.750	-0
17	0	1	0	1	0	1	27.000	9.500	7.750	-0
18	1	1	1	1	1	1	0.000	0.000	0.000	-0
19	1	1	1	1	1	1	27.000	0.000	0.000	-0
20	1	1	1	1	1	1	13.500	0.000	0.000	-0

TABLE 7.4. INITIAL FABRIC POSITION IN ARCH-ROOF FRAME.

Node No.	Boundary Condition Codes						Nodal Point Coordinates		
	X	Y	Z	XX	YY	ZZ	X	Y	Z
1	1	1	1	1	1	1	0.000	0.000	0.000
2	0	0	0	0	0	0	0.000	0.000	6.250
3	0	1	0	1	0	1	0.000	6.000	6.250
4	0	0	0	0	0	0	.915	0.000	11.438
5	0	0	0	0	0	0	3.549	0.000	16.001
6	0	1	0	1	0	1	3.549	6.000	16.001
7	0	0	0	0	0	0	8.759	0.000	19.999
8	0	0	0	0	0	0	15.170	0.000	21.420
9	0	0	0	0	0	0	15.170	2.000	21.420
10	0	0	0	0	0	0	15.170	4.000	21.420
11	0	1	0	1	0	1	15.170	6.000	21.420
12	0	0	0	0	0	0	18.453	0.000	21.061
13	0	0	0	1	1	1	18.362	2.000	20.649
14	0	0	0	1	1	1	18.322	4.000	20.470
15	0	1	0	1	1	1	18.299	6.000	20.364
16	0	0	0	0	0	0	21.581	0.000	19.999
17	0	0	0	1	1	1	21.389	2.000	19.586
18	0	0	0	1	1	1	21.322	4.000	19.443
19	0	1	0	1	1	1	21.308	6.000	19.413
20	0	0	0	0	0	0	24.405	0.000	18.285
21	0	0	0	1	1	1	24.063	2.000	17.840
22	0	0	0	1	1	1	23.915	4.000	17.646
23	0	1	0	1	1	1	23.878	6.000	17.598
24	0	0	0	0	0	0	26.791	0.000	16.001
25	0	0	0	0	0	0	26.791	2.000	16.001
26	0	0	0	0	0	0	26.791	4.000	16.001
27	0	1	0	1	0	1	26.791	6.000	16.001
28	0	0	0	0	0	0	29.425	0.000	11.438
29	0	0	0	0	0	0	30.340	0.000	6.250
30	0	1	0	1	0	1	30.340	6.000	6.250
31	1	1	1	1	1	1	30.340	0.000	0.000
32	1	1	1	1	1	1	15.170	0.000	0.000

pointer touched the point of interest again, we could determine the X-Y-Z deflection of a given point under load.

Each of the bags of lead shot weighed ~2.5 lb; four were required to cover the surface of the slant roof frame fabric, giving 10 lb per layer. At most, three layers were used, for a total maximum load of 30 lb or approximately 16.5 lb/ft^2.* Using the scaling laws of Sec. 3, we find that this load corresponds to a full-scale load of

$$P_{FS} = \frac{L_m}{L_{FS}} \frac{K_{FS}}{K_m} P_m .$$

Since the model is 1/8 scale and since the model fabric is approximately 1/5 as stiff as cotton duck (see Sec. 4.1),

$$P_{FS} = 1/8 \cdot 5 \cdot 16.5 \simeq 10 \text{ lb/ft}^2 .$$

For the arch-roof frame, three bags will cover the fabric surface, giving 7.5 lb or ~7.5 lb/ft^2 per layer of bags. Two layers of bags then correspond to a full-scale load of

$$P_{FS} = 1/8 \cdot 5 \cdot 15 \simeq 9.4 \text{ lb/ft}^2 .$$

7.3 Results

Computer model predictions of frame and fabric deflection of the slant-roof tent frame are compared with measurements on the model tents in Figs. 7.3 to 7.10. Figures 7.3 to 7.6 show deflections of the fabric under the three load increments in the X and Z directions. In general, agreement of measurement and prediction is good, with the exceptions of the X deflection at node 8 in Fig. 7.3 and the Z deflection at node 10 in Fig. 7.4. We believe that these discrepancies would be reduced (1) if a finer mesh were used in the computer code, especially for modeling the fabric, and (2) if a more accurate means of measuring the initial

*Based on the projected area of the slant roof on the X-Y plane.

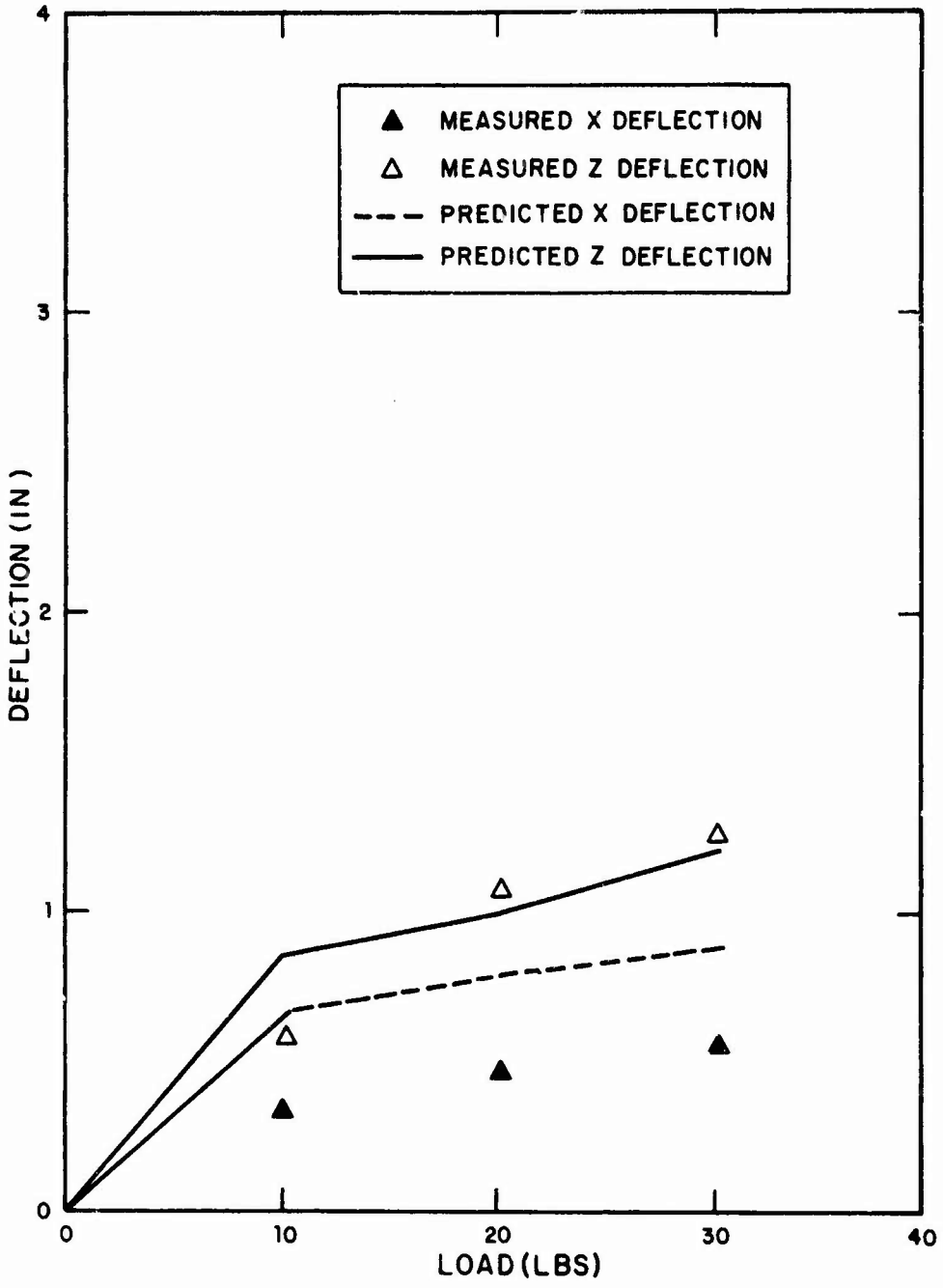

FIG. 7.3. COMPARISON OF MEASURED AND PREDICTED DEFLECTIONS IN THE SLANT-ROOF TENT AT NODE 8.

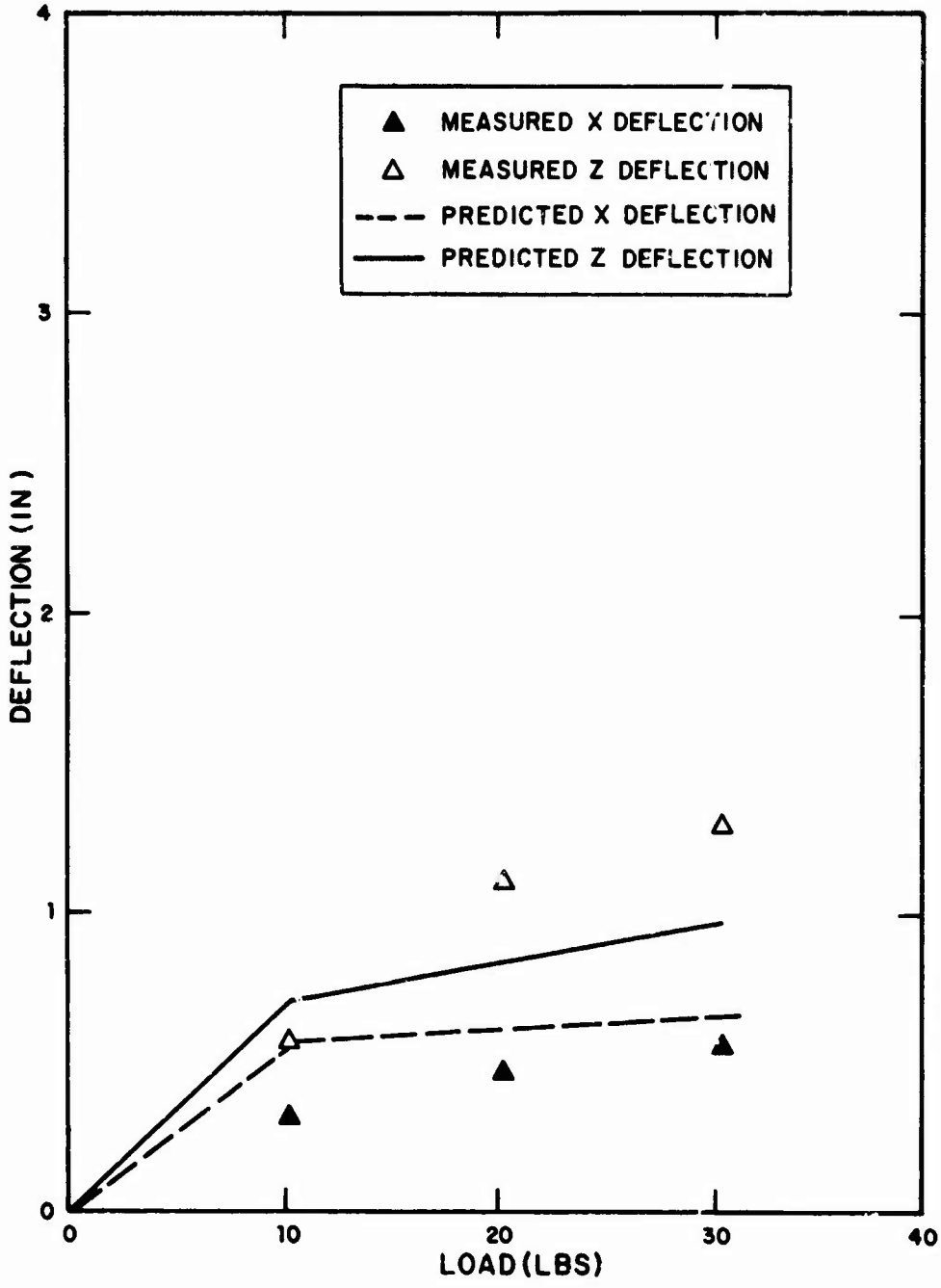

FIG. 7.4. COMPARISON OF MEASURED AND PREDICTED DEFLECTIONS IN THE SLANT-ROOF TENT AT NODE 10.

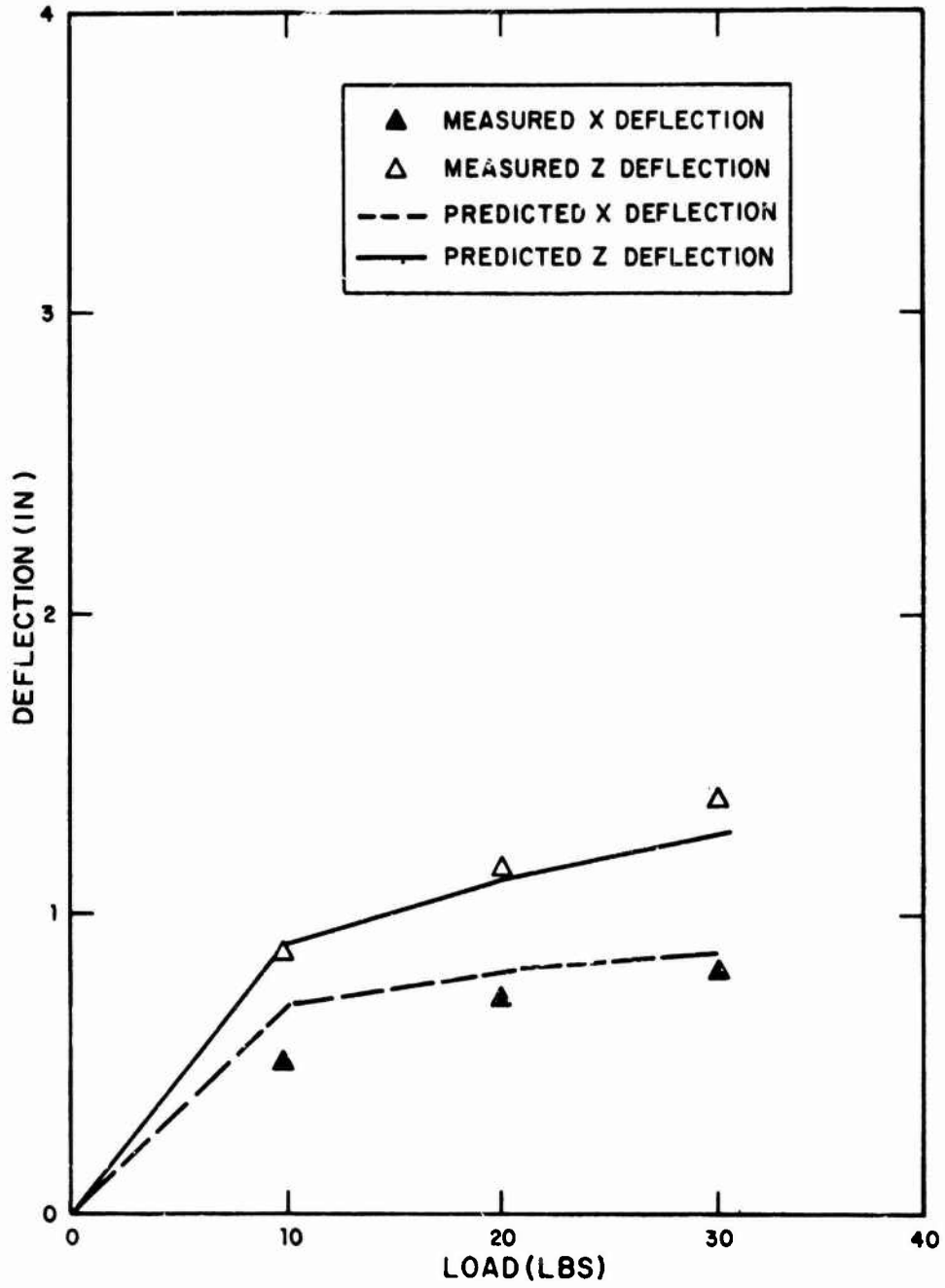

FIG. 7.5. COMPARISON OF MEASURED AND PREDICTED DEFLECTIONS IN THE SLANT-ROOF TENT AT NODE 11.

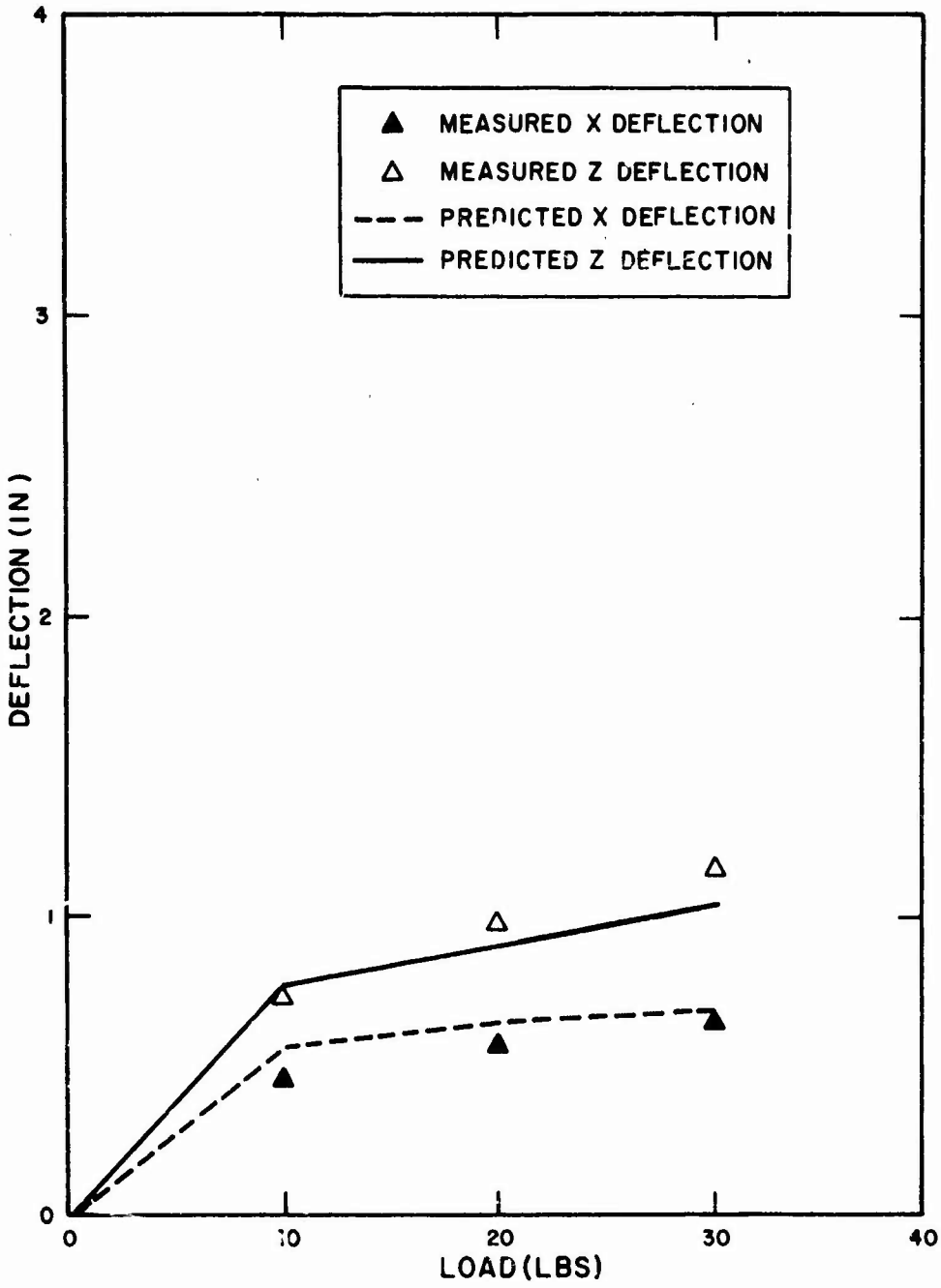

FIG. 7.6. COMPARISON OF MEASURED AND PREDICTED DEFLECTIONS IN THE SLANT-ROOF TENT AT NODE 14.

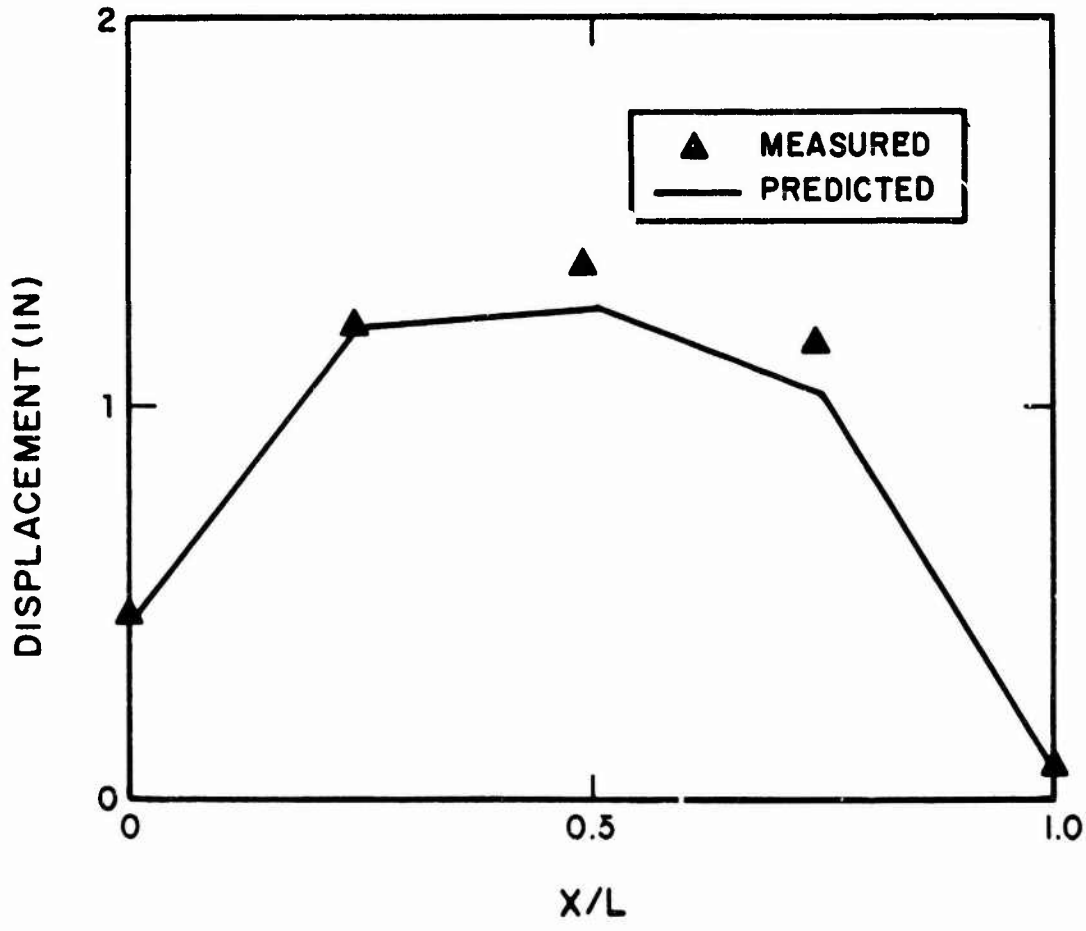

FIG. 7.7. Z DEFLECTION IN THE SLANT-ROOF TENT ALONG NODES 5-8-11-14-17 WITH 30-LB LOAD.

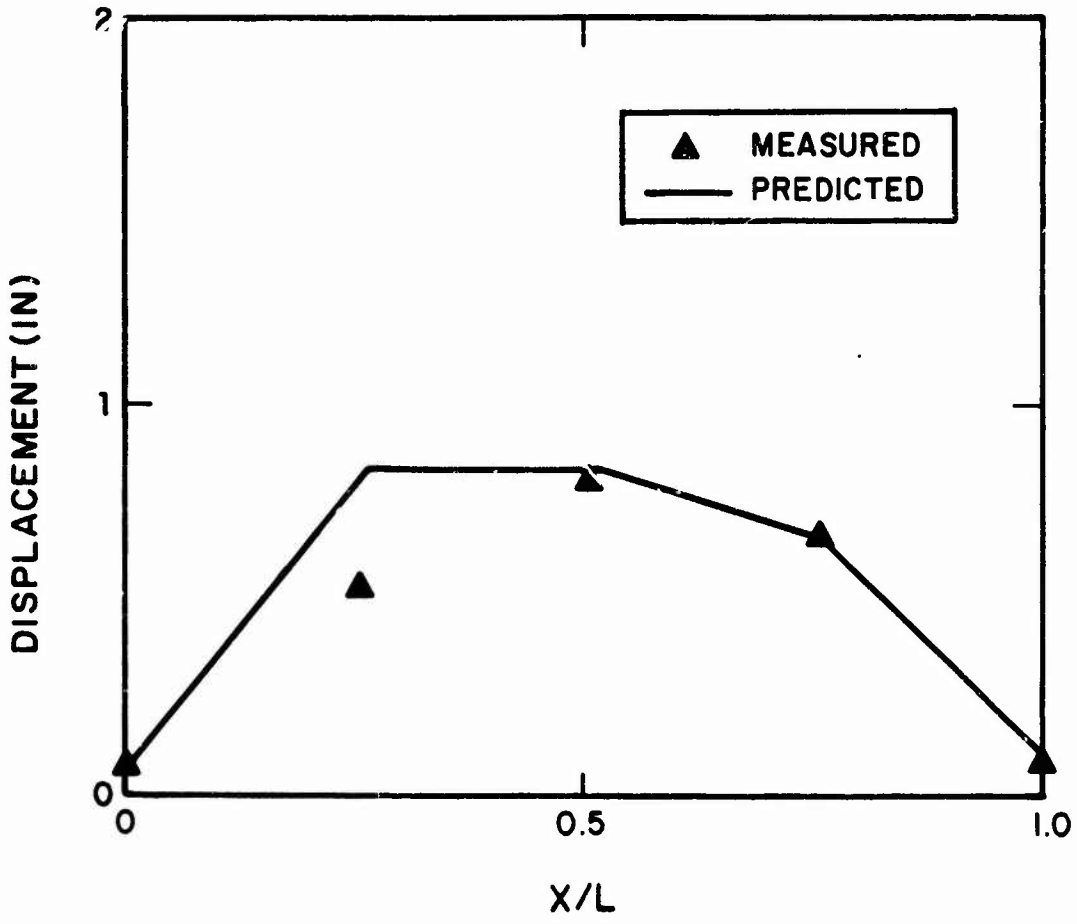

FIG. 7.8. X DEFLECTION WITH SLANT-ROOF TENT ALONG NODES 5-8-11-14-17 WITH 30-LB LOAD.

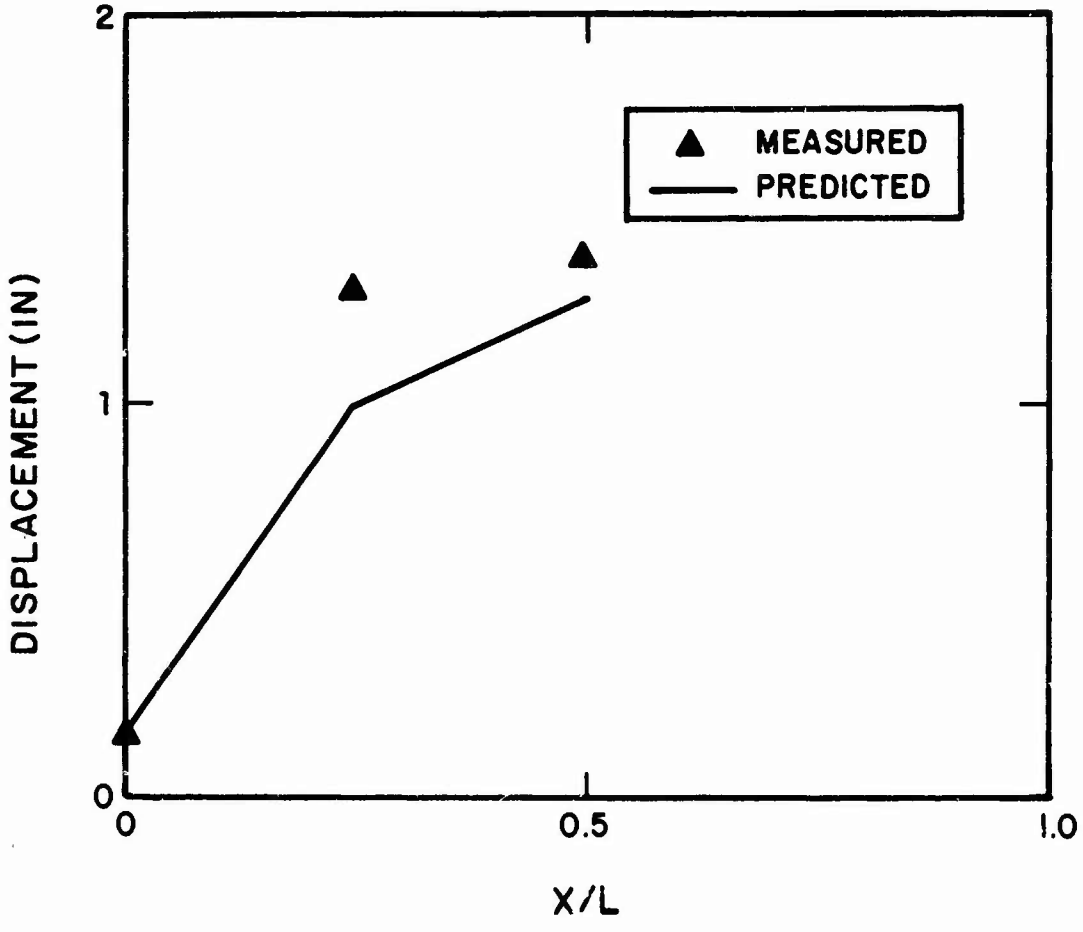

FIG. 7.9. Z DEFLECTION IN THE SLANT-ROOF FRAME ALONG NODES 9-10-11 WITH 30-LB LOAD.

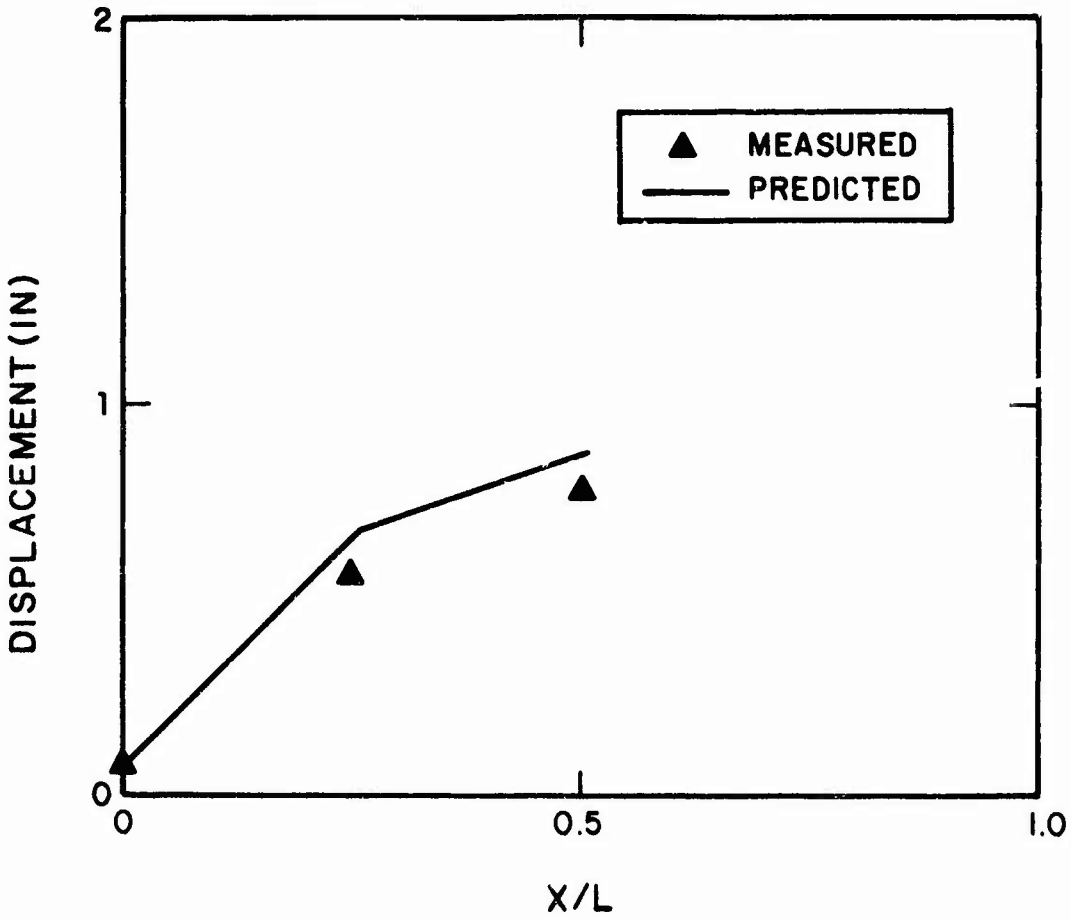

FIG. 7.10. X DEFLECTION IN THE SLANT-ROOF FRAME ALONG NODES 9-10-11 WITH 30-LB LOAD.

unloaded fabric shape could be found. A third source of error is the modeling of the joints in the frame. Note that the pinning of beam 4 about the Z axis at node 3 (see Sec. 7.1) is somewhat artificial, as the ridge pole of the tent is simply bolted to the arch at the peak. Experimentation with the frame suggested that we do this and. In fact, if beam 4 is modeled as built-in rather than pinned, the agreement is less satisfactory. Figures 7.7 through 7.10 show the deflection on the beams and fabric as a function of position in the model. Figures 7.7 and 7.8 show the Z and X deflections along the line defined by nodes 5-8-11-14-17* and Figs. 7.9 and 7.10 give the same information along the line defined by nodes 9-10-11† for the full load of 30 lbs. In all cases, deflection in the Y direction was quite small.

Figures 7.11 through 7.17 compare computer model predictions and measurements on the arch-roof tent model. Figures 7.11 through 7.13 show the X and Z deflections at points interior to the fabric as a function of load. Agreement of predictions and measurements is less satisfactory than was obtained for the slant-roof frame, although at the higher loads the agreement is generally pretty good. The discrepancies in this case are due, in part, to the coarseness of the grid in the computer model, especially in the fabric. This result was particularly noticeable when we measured the unloaded initial shape of the fabric. Because of the curved geometry, this initial shape is too complicated to be adequately modeled by the coarse grid of Fig. 7.2. In addition, some minor discrepancies between predicted and measured frame deflections are probably traceable to inadequately modeled joints. Errors in frame deflection are particularly bad because they are amplified in the fabric. This problem is discussed in some detail in the appendix, where it is shown that a small horizontal deflection in one of the end supports of a fabric strip leads to large vertical deflections at the center of the fabric.

Figures 7.14 through 7.17 show the X and Z deflections of the fabric and frame as a function of position at the full load. Figures 7.14 and 7.15 show the X and Z deflection along the line of nodes 11-15-19-23-27, where X/L = 0 corresponds to node 11, X/L = 1.0 corresponds to node 27,

---

*In these figures, the position X/L = 0 corresponds to node 5, X/L = 0.5 corresponds to node 11, X/L = 1.0 corresponds to node 17, etc.

†As in the previous figures, X/L = 0 corresponds to node 9, X/L = 0.5 corresponds to node 11, etc.

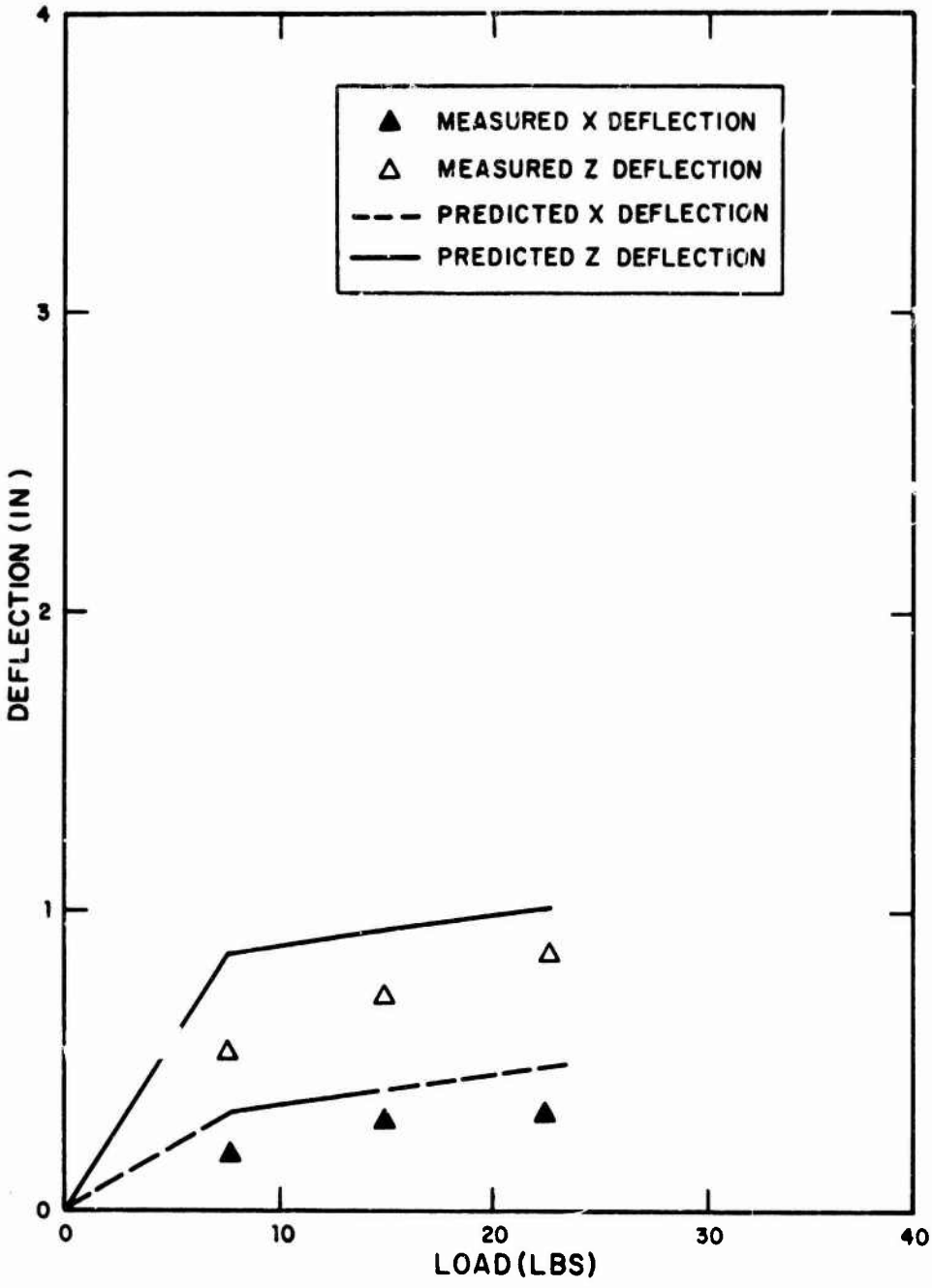

FIG. 7.11. COMPARISON OF MEASURED AND PREDICTED DEFLECTIONS IN THE ARCH-ROOF TENT AT NODE 15.

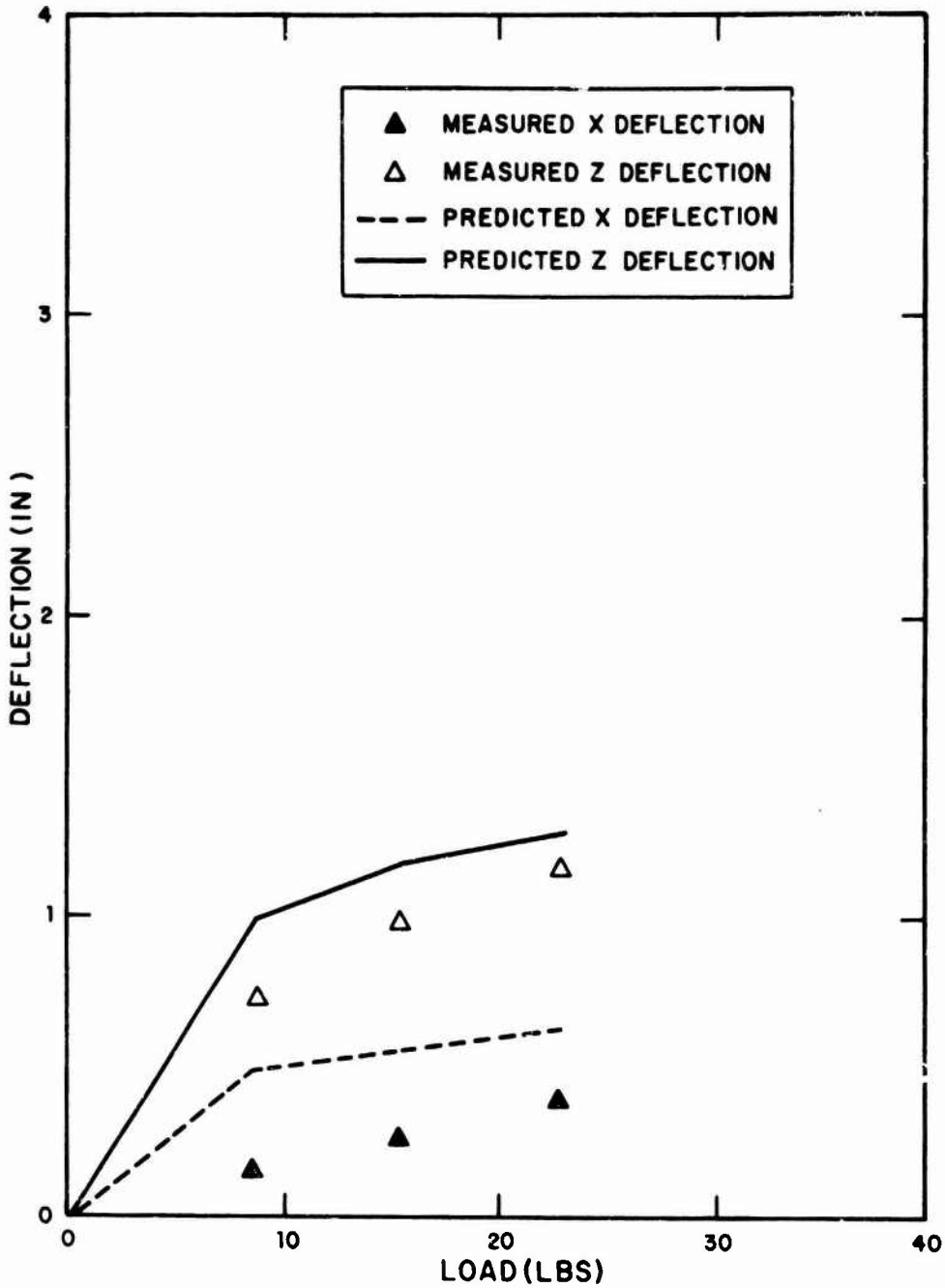

FIG. 7.12. COMPARISON OF MEASURED AND PREDICTED DEFLECTIONS IN THE ARCH-ROOF TENT AT NODE 19.

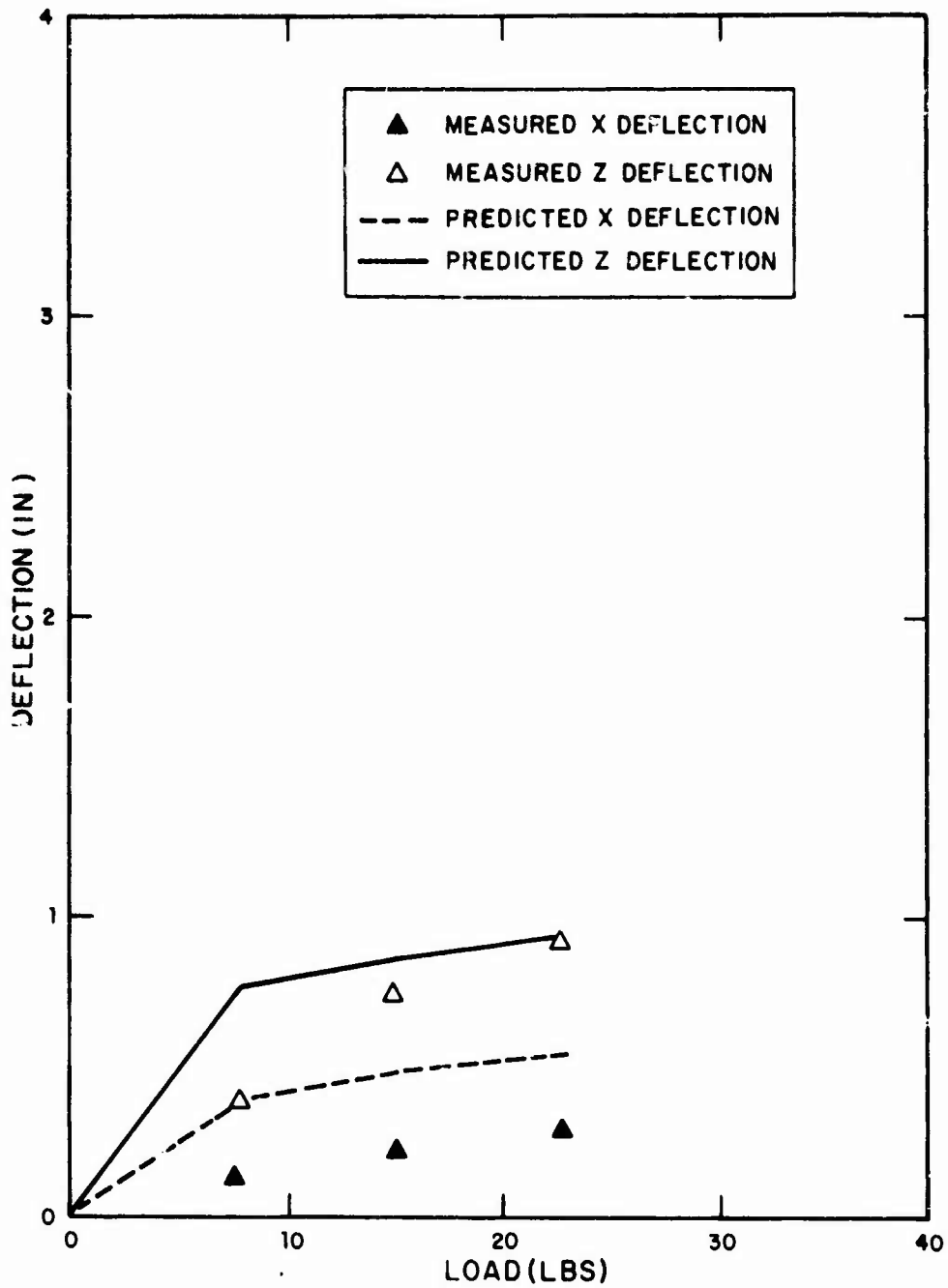

FIG. 7.13. COMPARISON OF MEASURED AND PREDICTED DEFLECTIONS IN THE ARCH-ROOF TENT AT NODE 23.

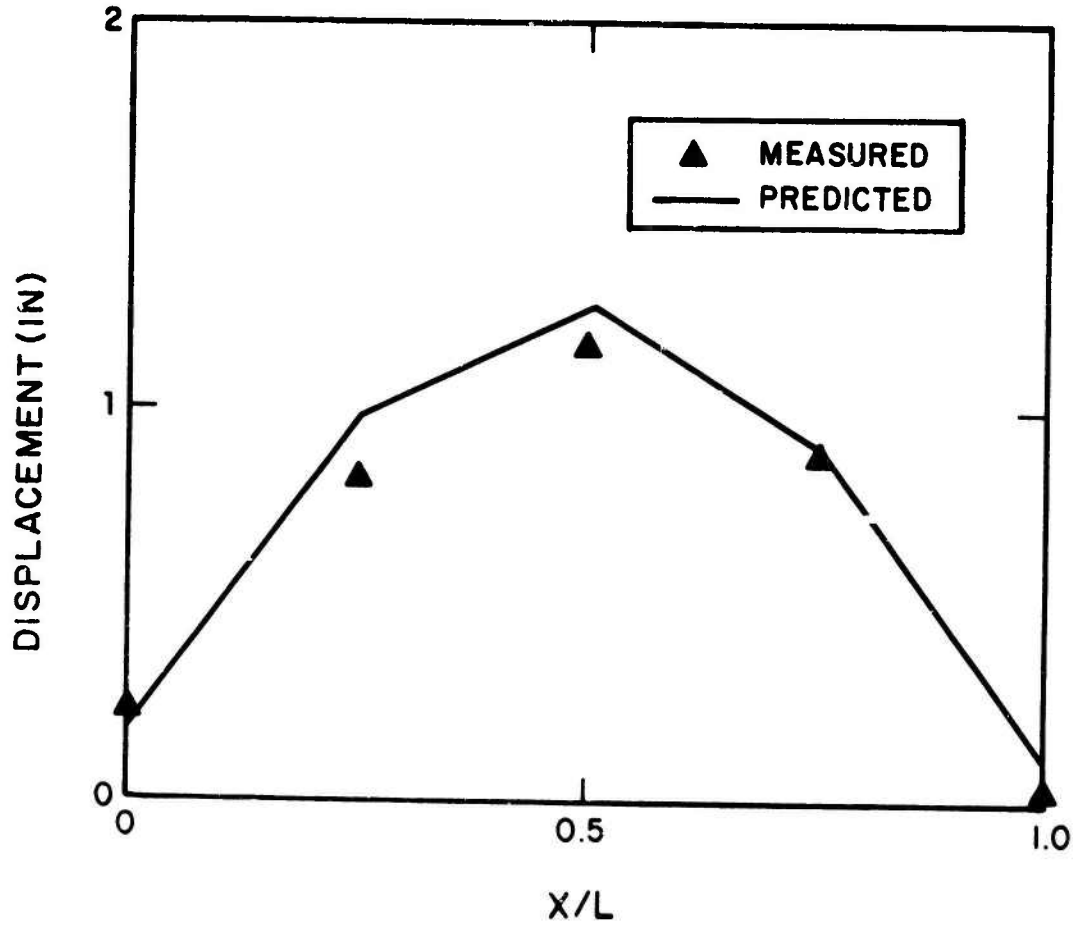

FIG. 7.14. Z DEFLECTION IN THE ARCH-ROOF TENT ALONG NODES 11-15-19-23-27 WITH 21-LB LOAD.

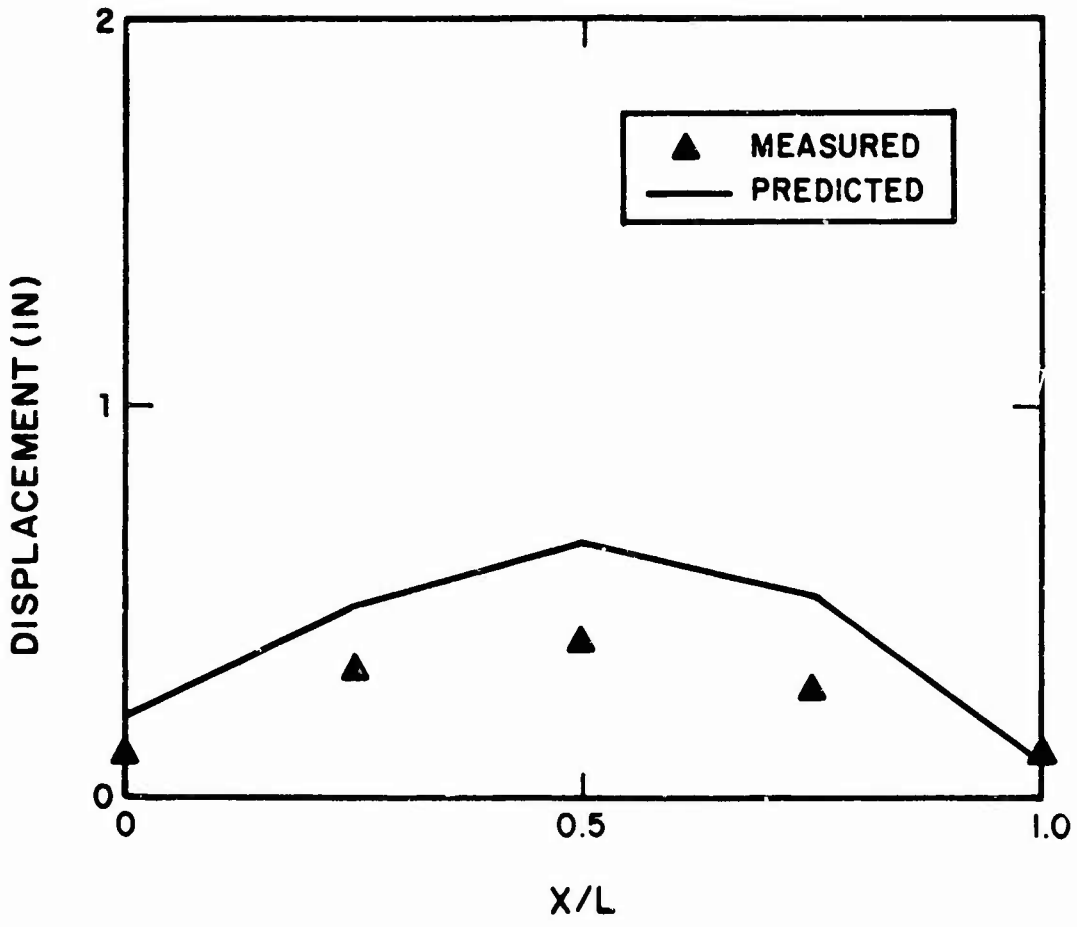

FIG. 7.15. X DEFLECTION IN THE ARCH-ROOF TENT ALONG NODES 11-15-19-23-27 WITH 21-LB LOAD.

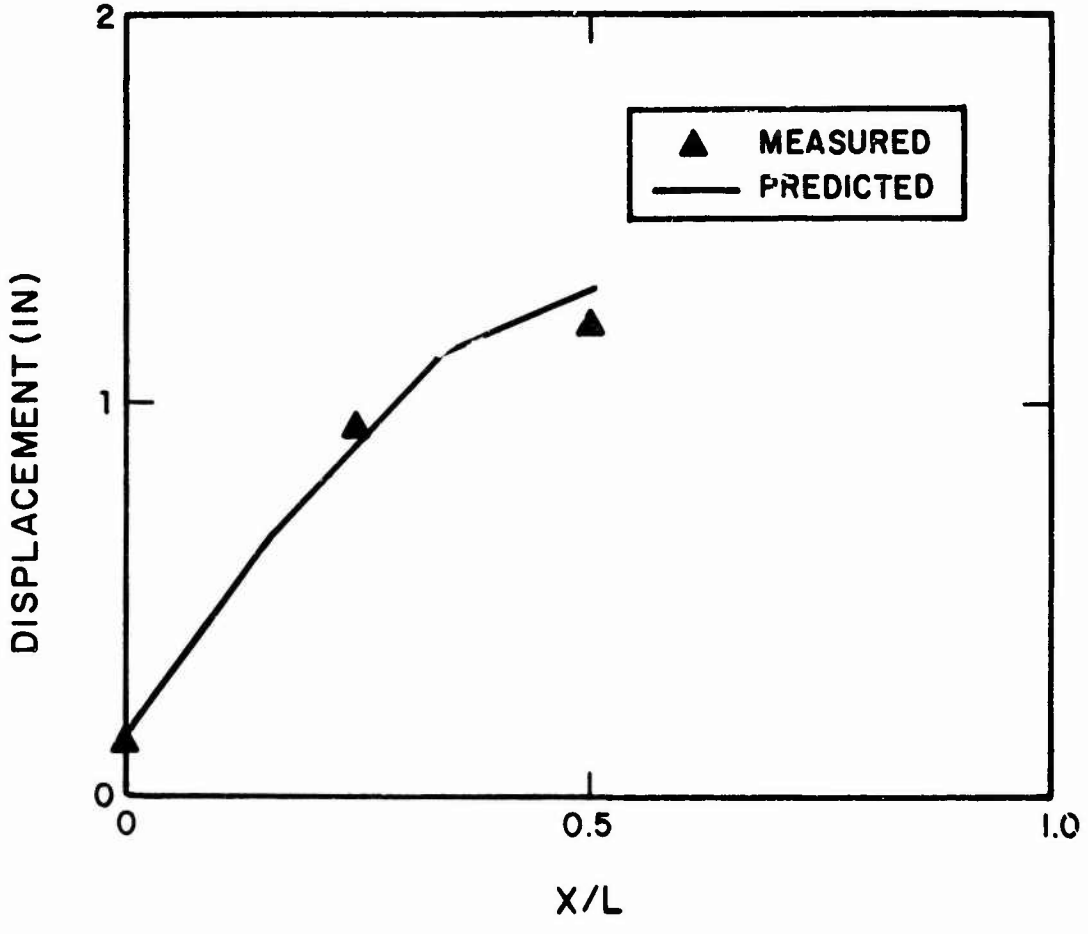

FIG. 7.16. Z DEFLECTION IN THE ARCH-ROOF TENT ALONG NODES 16-17-18-19 WITH 21-LB LOAD.

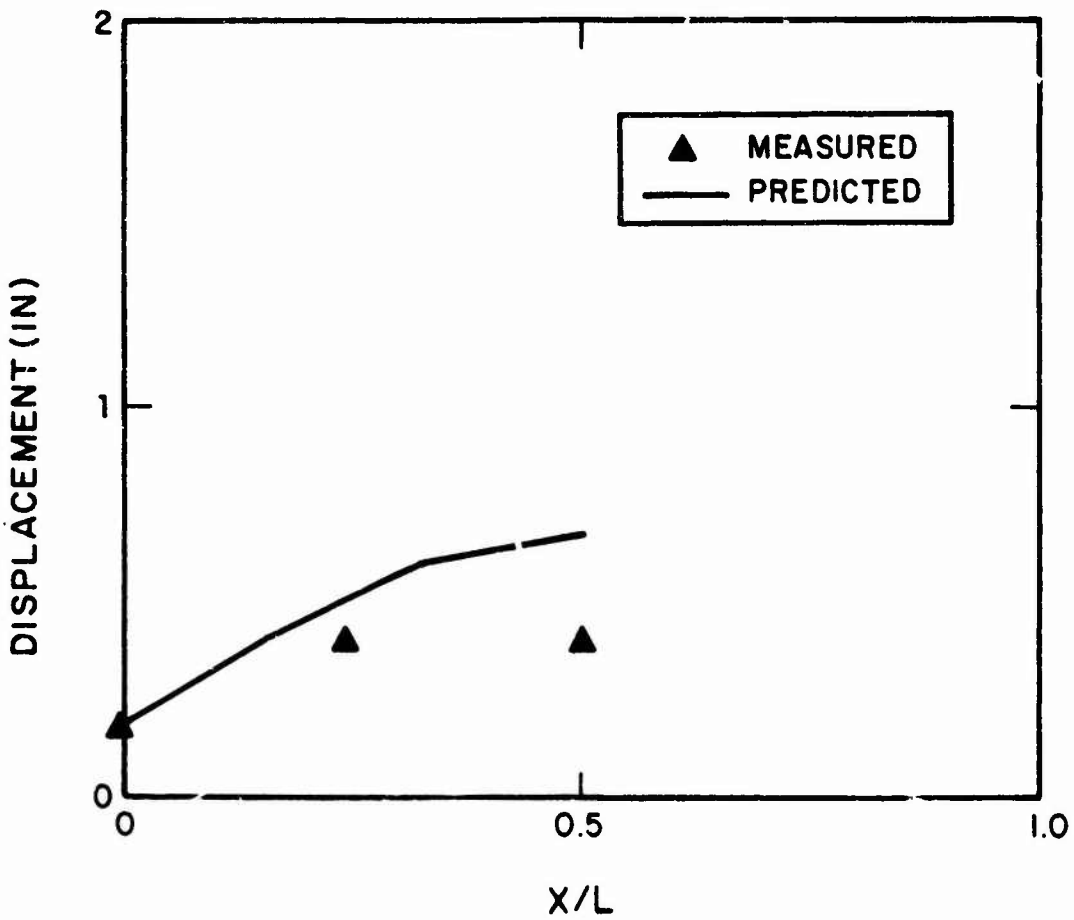

FIG. 7.17. X DEFLECTION IN THE ARCH-ROOF TENT ALONG NODES 16-17-18-19 WITH 21-LB LOAD.

etc. Figures 7.16 and 7.17 present the same information for the line of nodes 16-17-18-19, where X/L = 0 corresponds to node 16, X/L = 0.5 corresponds to node 19, etc.

8. CONCLUSIONS

It has been demonstrated during this program that the stress strain behavior of fabrics can be measured and used to predict the stresses and deflections in these fabrics when they are used as membrane structural components. Measured uniaxial properties of a dacron fabric were used successfully to predict the stresses and deflections in a strip of that fabric when it was loaded normal to its plane. The measured biaxial stress strain properties of cotton typewriter ribbon cloth were used with some success in a computer code to predict the stresses and deflections in a rectangular piece of that fabric mounted in a rigid frame and loaded normal to its plane. These same biaxial properties were again used successfully in the same computer code to predict the deflections in the fabric when it is mounted in small scale metal frames designed to simulate the slant-roof and arch-roof frame-supported tents used by the Army. Discrepancies between computer code predictions and measurements on the model tents are traceable partly to too coarse a mesh in the computer model but primarily to inadequate modeling of the joints between members in the model frames. Further efforts should concentrate on building into the computer code a better capability for modeling these frame joints.

APPENDIX A: SIMPLIFIED MEMBRANE ANALYSIS

To evaluate results obtained from the computer program and fabric tests and to develop some insight into the geometrically nonlinear deflections of membranes, we derived an approximate solution of a one-dimensional membrane strip. The following sections contain brief derivations of a membrane (string) with and without initial displacements.

A.1 Analysis of an Initially Flat Membrane

The membrane is assumed to be initially flat with linear elastic material properties. Figure A.1 shows the initial and deformed configurations of a portion of the membrane. Summing forces in the x-direction will produce the x-coordinate equilibrium equation as

$$\frac{\partial}{\partial x}(T\cos\phi)dx = 0 \qquad (A.1)$$

where T is the total membrane tension and ϕ is the angle between the x coordinate and the deformed membrane. Similarly, the y-coordinate equilibrium equation becomes

$$\frac{\partial}{\partial x}(T\sin\phi)dx + PdS_x = 0 \ , \qquad (A.2)$$

where P is the distributed loading in the global y-direction and dS_x is the projection of the deformed elemental portion of the membrane onto the x-coordinate. The dS quantity is a measure of strain and may be written as (see Fig. A.2)

$$dS = \lambda dx = [(1+u_{,x})^2 + w_{,x}^2]^{\frac{1}{2}}\, dx \qquad (A.3)$$

where u, w are the displacements in the x and y directions, respectively, the comma represents differentiation, and λ becomes the extension parameter. Also,

$$dS_x = (1+u_{,x})dx \ , \qquad (A.4)$$

which may be used in Eq. A.2 to produce

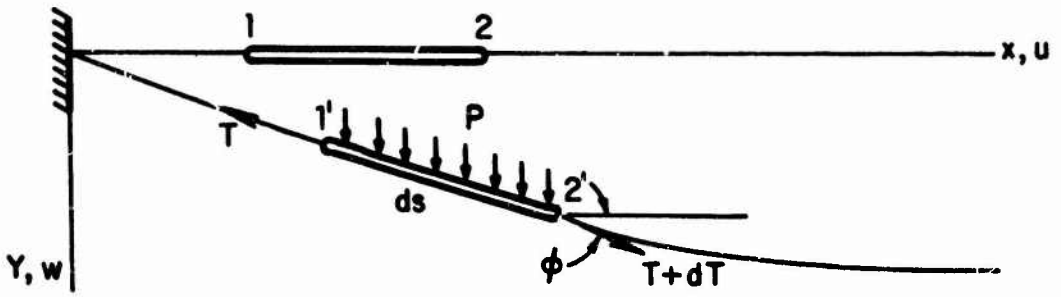

FIG. A.1. COORDINATE SYSTEM FOR INITIALLY FLAT MEMBRANE STRIP.

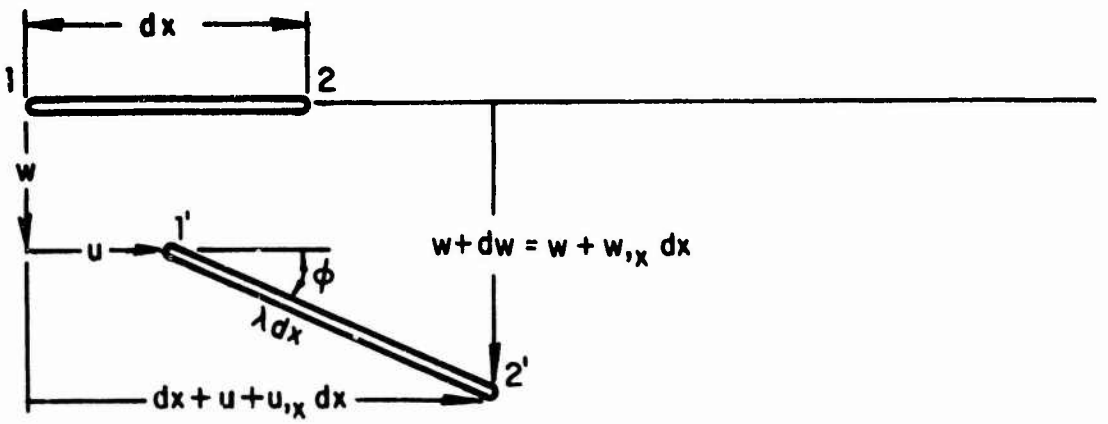

FIG. A.2. DISPLACEMENTS OF ELEMENTAL PORTION OF MEMBRANE.

$$(T \sin\phi)_{,x} + P(1+u_{,x}) = 0 \ . \qquad (A.5)$$

From Fig. A.2, it can be shown that the sine and cosine functions of ϕ may be expressed in terms of λ and displacement derivatives as

$$\sin\phi = \frac{w_{,x}}{\lambda} \ , \qquad (A.6)$$

$$\cos\phi = \frac{1+u_{,x}}{\lambda} \ . \qquad (A.7)$$

The equilibrium equations may now be written as

$$T\left[\frac{(1+u_{,x})}{\lambda}\right]_{,x} = 0 \qquad (A.8)$$

$$T\left[\frac{w_{,x}}{\lambda}\right]_{,x} + P(1+u_{,x}) = 0 \qquad (A.9)$$

with boundary conditions as

$$w(0) = w(L) = 0$$

$$u(0) = u(L/2) = u(L) = 0 \ . \qquad (A.10)$$

The load strain relationship for the membrane is

$$T \approx K\varepsilon_x \ , \qquad (A.11)$$

where K is the stiffness parameter with units in pounds and ε_x is the strain in the x-direction. The strain can be expressed as

$$\varepsilon_x = \frac{\lambda dx - dx}{dx} = \lambda - 1 \ . \qquad (A.12)$$

If we assume that the components of strain are small compared to unity, then

$$\lambda \simeq 1 + u_{,x} + \frac{1}{2} w^2_{,x} \qquad (A.13)$$

and Eq. A.11 becomes

$$T = K\left(u_{,x} + \frac{1}{2} w^2_{,x}\right) . \qquad (A.14)$$

To obtain an approximate solution of Eqs. A.9 and A.10, we assume that

$$\lambda \simeq 1 ; \qquad 1 + u_{,x} \simeq 1$$

in Eq. A.9 to give

$$T_{,x} = K(u_{,xx} + w_{,x}w_{,xx}) = 0 . \qquad (A.15)$$

The above relation implies

$$T = \text{constant} , \qquad (A.16)$$

which may be used in Eq. A.10 to give

$$Tw_{,xx} + P = 0 . \qquad (A.17)$$

Integrating Eq. A.17 twice and applying the appropriate boundary conditions produces

$$w = \frac{Px}{2T} (L-x) , \qquad (A.18)$$

where L is the distance between membrane supports. Note that the vertical displacement is a parabolic function of position.

The u displacement is obtained by using Eq. A.18 in Eq. A.15, integrating twice and applying boundary conditions

$$u = -\left(\frac{P}{T}\right)^2 \left[\frac{x^3}{6} - \frac{Lx^2}{4} + \frac{L^2x}{12}\right] . \qquad (A.19)$$

Performing the appropriate differentiation of u and w and substituting into Eq. A.14 gives

$$T = \left(\frac{KP^2L^2}{24}\right)^{\frac{1}{3}} . \qquad (A.20)$$

This equation can be used to express the displacements as a function of the loading:

$$\frac{w(x)}{L} = \left(\frac{3PL}{K}\right)^{\frac{1}{3}} \left(\frac{x}{L}\right) \left(1 - \frac{x}{L}\right) \qquad (A.21)$$

$$\frac{u(x)}{L} = -\frac{2}{3} \left(\frac{3PL}{K}\right)^{\frac{2}{3}} \left(\frac{x}{L}\right) \left[\left(\frac{x}{L}\right)^2 - \frac{3}{2}\left(\frac{x}{L}\right) + \frac{1}{2}\right] . \qquad (A.22)$$

Equation A.21 can be modified to account for any initial tention T_0 in the membrane

$$T = T_0 + \left(\frac{KP^2L^2}{24}\right)^{\frac{1}{3}} \qquad (A.23)$$

and Eq. A.21 becomes

$$\frac{w}{L} = \frac{3PL/K}{\left[6\,\frac{T_0}{K} + \left(\frac{3PL}{K}\right)^{\frac{2}{3}}\right]} \left(\frac{x}{L}\right) \left(1 - \frac{x}{L}\right) . \qquad (A.24)$$

Equations A.23 and A.24 are used to solve for the tension and displacement of the initially flat membrane with a pretension.

A.2 Analysis of a Membrane With an Initial Deflection

The development of the deflection equations of an initially deflected membrane is similar to the derivation performed in Sec. A.1, except that the strain relations must be modified to account for the initial displacement.

From Figs. A.3 and A.4 we see that the λ parameter is

$$\lambda = [(1+u_{,x} + u^0_{,x})^2 + (w_{,x} + w^0_{,x})^2]^{\frac{1}{2}} , \tag{A.25}$$

where the superscript zero on the displacements refers to the initial displacement. The parameter λ may be simplified by expanding Eq. A.25 and assuming the strains to be small compared to unity:

$$\lambda \simeq 1 + u_{,x} + u^0_{,x} + \frac{1}{2} (w_{,x} + w^0_{,x})^2 . \tag{A.26}$$

The load-displacement relationship as described in the previous section becomes

$$T = K\left[u_{,x} + u^0_{,x} + \frac{1}{2} (w_{,x} + w^0_{,x})^2\right] . \tag{A.27}$$

The equilibrium equations become

$$T_{,x} = 0 \tag{A.28}$$

$$Tw'_{,xx} = -P \tag{A.29}$$

$$w' = w + w^0 , \tag{A.30}$$

where w' is the total displacement of a point on the membrane relative to the flat unstrained, undeflected position of the membrane and w is the incremental displacement.

The vertical free-hanging shape of the membrane is assumed to be parabolic as

$$w^0 = 4w_0 \left(\frac{x}{L}\right) \left(1 - \frac{x}{L}\right) , \tag{A.31}$$

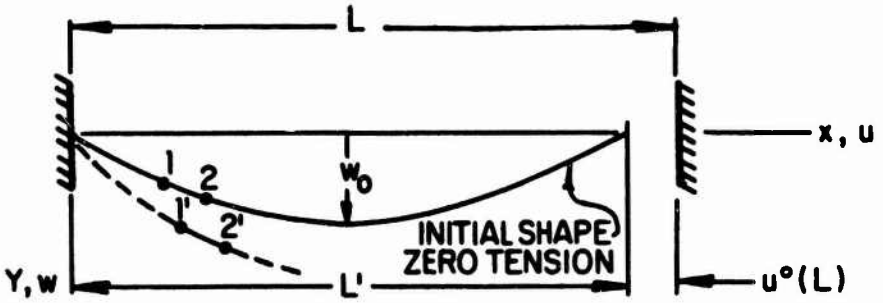

FIG. A.3. COORDINATE SYSTEM FOR INITIALLY DISPLACED MEMBRANE STRIP.

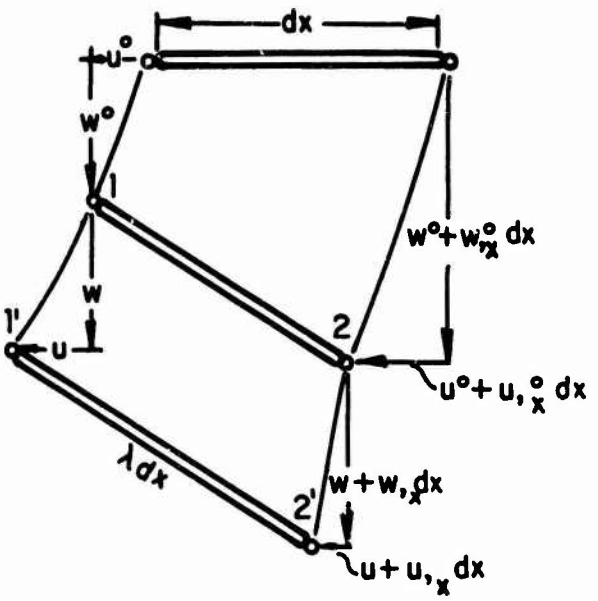

FIG. A.4. DISPLACEMENTS OF MEMBRANE WITH INITIAL DEFLECTION.

where w_0 is the initial center displacement of the membrane. Using Eqs. A.6 and A.7 in Eq. A.5 and integrating as before produces

$$\frac{w}{L} = \frac{1}{2}\left(\frac{PL}{T} - \frac{8w_0}{L}\right)\left(\frac{x}{L}\right)\left(1 - \frac{x}{L}\right) \quad . \quad (A.32)$$

The corresponding initial displacement in the x direction is obtained from Eq. A.27 when zero load has been applied to the system. Therefore,

$$u^0_{,x} = -\frac{1}{2}\left(w^0_{,x}\right)^2 \quad . \quad (A.33)$$

Integrating and applying appropriate boundary conditions gives

$$u^0 = -\frac{8w_0^2}{L}\left(\frac{x}{L}\right)\left[1 - 2\left(\frac{x}{L}\right) + \frac{4}{3}\left(\frac{x}{L}\right)^2\right] \quad . \quad (A.34)$$

The amount of extra material used to create the initial displacement of the membrane (see Fig. A.3) is determined by substituting the length of membrane into Eq. A.34. Therefore

$$u^0(L) = -\frac{8}{3}\frac{w_0^2}{L} \quad . \quad (A.35)$$

The actual initial distance between membrane supports when there is no initial deflection can be approximated by

$$L = l'\left[1 + \frac{8}{3}\left(\frac{w_0}{L'}\right)^2\right] \quad , \quad (A.36)$$

where L' is the new distance between end supports that results in the initial deflection w^0 in Eq. A.31.*

The u-displacement function is obtained by using Eqs. A.28 and A.33:

$$u_{,xx} = -[w_{,x}(w_{,xx}+w^0_{,xx}) + w^0_{,x}w_{,xx}] \ . \qquad (A.37)$$

The u displacement as a function of membrane parameters is determined by substituting the appropriate terms in Eq. A.37 using Eqs. A.31 and A.32, integrating twice, and applying the boundary conditions to give

$$\frac{u}{L} = -\frac{1}{6}\left[\left(\frac{PL}{T}\right)^2 - \left(\frac{8w_0}{L}\right)^2\right]\left[\left(\frac{x}{L}\right)^3 - \frac{3}{2}\left(\frac{x}{L}\right)^2 + \frac{1}{2}\left(\frac{x}{L}\right)\right] \ . \qquad (A.38)$$

The relationship between the tension and the applied load is obtained from Eq. A.27 using Eqs. A.31, A.32, A.34, and A.38:

$$\frac{T}{K} = \frac{1}{24}\left[\left(\frac{PL}{T}\right)^2 - \left(\frac{8w_0}{L}\right)^2\right] . \qquad (A.39)$$

Using this equation in the equation for the membrane incremental displacement, we obtain

$$\frac{w}{L} = \frac{12T/K}{\left(\frac{PL}{T} + \frac{8w_0}{L}\right)}\frac{x}{L}\left(1 - \frac{x}{L}\right) \qquad (A.40)$$

as an alternative expression for Eq. A.32.

---

*Note that in the model the initial deflection is envisioned as being produced by moving the membrane end support at x = L a distance $u^0(L)$ (see Eq. A.33) closer to the other membrane support. Thus, the distance between end supports that one measures in an actual experiment with initial deflection w^0 is L'.

Equations A.39 and A.40 are used to determine the tensions and incremental displacements of an initially displaced membrane.

LIST OF SYMBOLS

B_{WW}, B_{WF}, B_{FW}, B_{FF}	Material constants in the fabric stress strain model each of which is a function of the fabric tension.
C_W, C_F	Warp and fill biaxial stress strain model constants respectively.
E	Young's modulus of the frame material.
f	Load per unit area.
$G_W(\alpha)$ $G_F(\alpha)$	Warp and fill biaxial stress strain model functions, respectively.
I	Frame beam moment of inertia.
K	Fabric stiffness constant (in Appendix).
L	Characteristic length, distance between supports.
P_W, P_F	Exponents in the biaxial fabric stress strain model.
P	Load per unit length (in Appendix).
T_W, T_F	Warp and fill tension/unit length, respectively.
T	Tension/unit length (in text).
T	Total tension in a fabric strip (in Appendix).
T_0	Initial total tension (in Appendix).
u, w	x and y fabric strip deflections (in Appendix).
u, w_F	In plane and out of plane fabric deflections.
w_B	Frame beam deflections.
w_0	Initial center deflection of the fabric strip (in Appendix).

LIST OF SYMBOLS *(Cont'd.)*

w^0	Initial free hanging fabric strip shape (in Appendix).
w'	Total fabric strip deflection initial plus incremental (in Appendix).
X, Y, Z	Global coordinates.
α	Ratio of warp to fill stress.
ε, ε_W, ε_F	Fabric strain, warp and fill strain, respectively.
κ	Fabric stiffness – slope of the uniaxial stress strain curve.
λ	Fabric elongation including rotational effects (in Appendix).
ν	Poisson's ratio.
ϕ	Rotation of the fabric strip (in Appendix).
$( )_{,x}$	$\frac{\partial}{\partial x}$
$( )_{,xx}$	$\frac{\partial^2}{\partial x^2}$
$( )_m$	Refers to scale model.
$( )_{FS}$	Refers to full scale.
$( )_W$	Refers to fabric warp direction.
$( )_F$	Refers to fabric fill direction.